Computational Modeling of Flow in a 10MW$_e$ Natural Convection Molten Salt Reactor

A Dissertation
Presented in Partial Fulfillment of the Requirements for the
Degree of Doctor of Philosophy
with a
Major in Mechanical Engineering
in the
College of Graduate Studies
University of Idaho
by
G. M. Strombach

Major Professor: Richard Christensen, Ph.D.
Committee Members: Ralph Budwig, Ph.D.; John Crepeau, Ph.D.; Tao Xing, Ph.D.
Department Administrator: Steven Beyerlein, Ph.D.

May 2020

Authorization to Submit Dissertation

This dissertation of G. M. Strombach, submitted for the degree of Doctor of Philosophy with a Major in Mechanical Engineering and titled "Computational Modeling of Flow in a 10MW$_e$ Natural Convection Molten Salt Reactor," has been reviewed in final form. Permission, as indicated by the signatures and dates below, is now granted to submit final copies to the College of Graduate Studies for approval.

Major Professor: _____ Date: _____

Richard Christensen, Ph.D.

Committee Members: _____ Date: _____

Ralph Budwig, Ph.D.

_____ Date: _____

John Crepeau, Ph.D.

_____ Date: _____

Tao Xing, Ph.D.

Department Administrator: _____ Date: _____

Steven Beyerlein, Ph.D.

Abstract

This research investigates the use of computational fluid dynamics (CFD) to simulate flow in a practical power system that includes a natural-convection molten salt reactor (MSR). Included herein are five sets of simulations, which start simply and build in complexity.

Unique aspects of this research:

- Each simulation explores realistic design aspects of practical MSRs; i.e., those used for electric power generation, etc.
- Each simulation uses internal heat generation (instead of surface/external heat flux) to reflect energy released in the reactor vessel.
- An actual fuel salt was used for three of the five simulation sets. It is based on a mixture of lithium & beryllium fluoride salt, known as FLiBe.
- Simulations that use FLiBe as the working fluid include a newly developed relation – variable energy source/power density – for energy released in the reactor vessel. This unique approach is based on operational data from actual MSRs. It reflects changes in reactivity (and thus power density) as a function of salt temperature and thus captures the negative temperature coefficient effect.

First is a series of 16 cases, using simple cylinders for the reactor and heat exchanger, with water as the working fluid. These determine the size, shape & elevation difference between the reactor vessel and heat exchanger. To achieve natural convection flow within a specified temperature range, the minimum relative elevation difference between the reactor and heat exchanger is 12 feet. CFD results in the range of interest match analytic values within 4.4%.

Next is a series of 10 cases, using baffled cylinders for the reactor and heat exchanger, with FLiBe salt as the working fluid. These determine the elevation difference between the reactor vessel & heat exchanger. To achieve natural convection flow within a specified temperature range, the minimum relative elevation difference between the reactor and heat exchanger is also 12 feet. CFD results in the range of interest match analytic values within 0.55%.

The third set is a benchmarking template for a test rig built at the University of Idaho campus in Idaho Falls. At the point of incipient natural convection flow, the temperature difference from the simulation is within 2.45% of the value predicted by analytic means.

Next is simulation of a realistic MSR system. It includes a reactor vessel with complex internal structure, to model an array of graphite moderator bars. This confirms that a relative difference in elevation of 12 feet meets the design criteria for the specified temperature range.

Finally, a simulation of a different realistic MSR system which uses an external reflector rather than internal moderator bars. The original design has a difference in elevation of 4 feet. Simulations show that this does not meet the design criteria of achieving the recommended temperature range.

These results suggest that it is possible to simulate a realistic natural convection molten salt reactor. Using the techniques herein, one can obtain valuable engineering information to assist in the design of practical power systems.

Acknowledgements

Without the contribution of many people & companies, my course of study (including this research) would not have been possible.

Thanks to Denise Engebrecht and Paula Peterman, at the Boise Water center, for proctoring exams. Thanks to Lana Unger and Alice Allen, at Idaho Falls, for guidance through various administrative processes, as well as helpful folks at the College of Graduate Studies (COGS).

The University of Idaho has many knowledgeable & talented professors who made the courses interesting and memorable. Many thanks to the members of my dissertation committee, for their inspiration and guidance through these processes.

A list of acknowledgements would not be complete without recognizing the groups and companies who offer analysis software that was critical in the completion of this research:

- Autodesk Inventor Professional 2016™ and 2020™, both of which are available under a student license.
- ANSYS™ Workbench 2019 R1™, including SpaceClaim™, Design Modeler™, Meshing Module™, Fluent™ CFD and solution viewing applications.

I'm also thankful to have a well-built Dell Precision T7700 workstation, with dual quad-core processors and 90GB memory, whose internal cooling fans ran on overdrive for several years without fail.

Thanks to countless students, scientists & researchers who came before. People of all genders, races, ethnicities & creeds put in countless hours forming the basis of today's research; the unsung heroes, giants & geniuses upon whose shoulders we humbly stand.

Dedication

To my wife Sara, for graciously putting up with my self-indulgence over the years.

To my children, grandchildren, my sister Cathy, my brother Matthew, and their families.

To my parents, who taught me the value of knowledge and hard work.

To many wonderful friends who provided support and encouragement. Their kind words, pats on the shoulder, and knowing expressions mean more than they will ever know.

Even our pets gave their support, including the late “Professor Pooh.”

Many thanks.

Table of Contents

List of Tables

List of Figures

1 Introduction

1.1 Abstract

This chapter provides:

- A brief introduction to nuclear power's practical uses.
- A review of national & international partnerships researching nuclear energy; their thoughts, recommendations, and focus of their efforts.
- The system selected for this work – the Molten Salt Reactor (MSR); its advantages, history, systems built, a summary of work done to date, and remaining work needed.
- The specific focus for this dissertation; objectives, methods and tasks.

1.2 A Brief Introduction to Nuclear Power's Practical Uses

Investigation and research into uses for nuclear energy began in the 1940's. The first applications were military in nature; ship & aircraft propulsion. Since then, hundreds of reactors were constructed; some for use as power plants, and others to conduct experiments & research. Decades of operation provided much knowledge and experience, although some lessons were learned the hard way; i.e., through accidents and disasters.

There are several different reactor types, which vary in three basic aspects; fuel, moderator, and heat transfer medium. There are pros & cons for each type, in terms of safety, cost of operation and fuel, disposal of waste and the potential for proliferation of harmful materials. Due to the characteristics of cites available for construction, it's possible that no one type is be the "best" in all circumstances or applications.

1.3 National & International Partnerships – Nuclear Energy Research

1.3.1 The Generation IV International Forum (GIF)

The GIF is an international collective of countries that consider nuclear power to be significant now, as well as vital for their future. It was created in January of 2000 by nine countries, and formally chartered in July of 2001. There are currently 13 member countries.

The GIF identifies key R&D challenges and possibilities for overcoming them. A summary of this information is presented in a "technology roadmap," the first of which was issued in 2002. Every few years, the GIF updates the roadmaps, to help guide ongoing research efforts.

The 2014 technology roadmap provided a timeline of reactor development, with examples of each.

- Generation I: Early prototype reactors, from 1948 to 1967.
- Generation II: Early commercial power reactors, from 1967 to 1992.
- Generation III: Advanced Light Water Reactors (LWRs), from 1992 to 2008.
- Generation III+: Evolutionary designs, from 2008 to 2027.
- Generation IV: Revolutionary designs, from 2027 and thereafter.

The GIF defined four essential criteria for advancing nuclear energy to the next (fourth) generation:

- Sustainability,
- Safety & Reliability,
- Economic Competitiveness, and
- Proliferation Resistance and Physical Protection

In 2002, GIF reviewed nearly 100 concepts and selected the following six reactor system types as being the most promising:

1) The Sodium-Cooled Fast Reactor (SFR), including pool-type, loop and modular configurations.
2) The Supercritical Water Cooled Reactor (SCWR), which is a high-temperature, high-pressure light-water reactor.
3) The Very-High Temperature Reactor (VHTR), which is graphite moderated and helium cooled.
4) The Gas-Cooled Fast Reactor (GFR), which is also helium cooled, but without a moderator, its fuel can use fast neutrons.
5) The Lead-Cooled Fast Reactor (LFR), which uses lead or lead-bismuth eutectic liquid metal as a coolant, with a natural convection circulation system that doesn't require pumps.
6) The Molten-Salt Reactor (MSR), which uses a Lithium-Beryllium-Fluoride (or other) salt as coolant. Fuel can be in the form of coated spheres (pebble bed) or dissolved in the coolant salt.

With each update, the technology roadmap summarizes significant events, and presents the current readiness for each system, based on viability, performance, demonstration & commercialization phase. A table in the 2014 technology roadmap gave the following readiness ranking, in terms of viability and performance:

Table 1-1 – 2014 GIF Technology Roadmap Readiness Ranking

Rank	Viability	Performance
1	VHTR	LFR
2	SFR	SFR
3	LFR	VHTR & SCWR
4	SCWR	
5	GFR	GFR & MSR
6	MSR	

1.3.2 The International Thorium Energy Committee (IThEC)

This organization was founded in late 2012 at CERN (Geneva, Switzerland) by scientists, engineers, political figures and industrialists, to promote the use of thorium as a means of reducing existing and future nuclear waste, as well as generate electricity. Their first conference, ThEC13, was held in Geneva, Switzerland. It lasted four days and included numerous participants. The proceedings were compiled into a book; *Thorium Energy for the World*. The second conference, ThEC15, was held in Mumbai, India. It grew considerably, featuring 300 participants, 127 papers, and 46 speakers from 30 countries.

1.3.3 Safety Assessment of the Molten Salt Fast Reactor (SAMOFAR)

As part of the European Union's research program – Horizon 2020, the SAMOFAR project was started in 2015, with a kick-off meeting in August, at the Delft University of Technology. It is a 4-year research program, initially including 11 partners. Their goal is to prove the innovative safety concepts of the MSFR, using advanced experimental and numerical techniques, to deliver a breakthrough in nuclear safety, optimal waste management, and to create a group of stakeholder to demonstrate the MSFR beyond SAMOFAR.

1.3.4 U.S. Department of Energy – Nuclear Energy University Programs (NEUP)

The USDoE's Office of Nuclear Energy created NEUP in 2009, to consolidate its university support under one program. In 2013, NEUP issued four white papers, which are the proceedings from Integrated Research Project (IRP) workshops. Topics include:

- The six safety design criteria for fluoride-salt-cooled, high-temperature reactors (FHRs), based on the Nuclear Regulatory Commission (NRC) licensing framework.
- FHR Methods and Experiments Program, which presents requirements for CFD codes and validation.

- Materials, Fuels and Components, which address use of American Society of Testing and Materials (ASTM) test procedures, structural materials and corrosion control.
- Development Roadmap and Test Reactor Performance, which presents a path forward to the design and building of an FHR, including different types of fuel elements; particles, pins, pebbles, prisms, plates, etc.

The MSR chosen by USDoE/NEUP uses molten fluoride salts for the coolant only. Fuel is in the form of pellets, coated in a graphite-ceramic matrix. The pellets are roughly spherical in shape, and are evenly distributed in a pebble bed configuration in the reactor vessel. The molten cooling salts circulate through spaces between fuel pellets. To simulate this reactor's performance, the pebble bed is modeled as a porous media.

In 2010, NEUP issued a Nuclear Energy Roadmap; a broad description of past, present and future plans. Future work focuses on small modular reactors (SMRs) and high-temperature reactors (HTR), as previously described. NEUP is separate from previous large-scale demonstrations, such as the Next Generation Nuclear Plant (NGNP). The Energy Policy Act of 2005 allowed the US Department of Energy and Idaho National Laboratory to establish the Next Generation Nuclear Project (NGNP). Its mission was to develop, license, build and operate a prototype modular high-temperature gas-cooled reactor. This would move away from the use of water as a moderator, and provide higher process heat to produce various products. However, the Department of Energy elected to not move into the design & licensing phase, and the NGNP project was suspended in 2013.

1.3.5 The Multinational Design Evaluation Program (MDEP)

MDEP was started in 2006 by the US Nuclear Regulatory Commission (NRC) and the French Nuclear Safety Authority (ASN). Its focus is to find expedite Gen-III opportunities.

1.4 The System Selected for this Work

Of these, the MSR seems to need the most work, and thus provides the most opportunity for research. It is the particular type of reactor type/system selected for this study.

1.4.1 Molten Salts – the "MS" in MSR

Two basic types of fluorine-lithium salts have been used in MSRs:

- "FLiBe" – a binary mixture of LiF and BeF_2, and
- "FLiNaK" – a trinary mixture of LiF, NaF and KF.

Below 460 °C (850 °F), both are white solids, which can be cast in various shapes (Figure 1–1, left). From 460 °C (850 °F) to 1460 °C (2670 °F), both are clear liquids that look and behave somewhat like water (Figure 1–1, right).

Figure 1–1 – FliNaK Solid Castings (Left) - Molten Liquid (Right)

Compatible fissile & fertile fuel salts can be added to either of these; i.e., UF_4, PuF_3, ThF_4, CeF_3, et al.

1.4.2 The First Liquid Fuels in the Laboratory

A year after the discovery of fission, researchers in England started experimenting with liquid fuels, using a U_3O_8-D_2O slurry[1]. A slurry fuel was also used at the University of Chicago in 1943. In 1944, Clinton Laboratories used a slurry to explore ^{233}U breeding potential. That same year, Los Alamos National Laboratory (LANL) built the LOPO water boiler, which used an aqueous solution of enriched uranium.

The first instance of liquid fuel circulating outside the core was the $1MW_t$ Homogeneous Reactor Experiment (HRE), built at the Oak Ridge National Laboratory (ORNL) and operated from 1952 to 1953[2]. A second experimental reactor – the $5MW_t$ Homogeneous Reactor Test (referred to as the HRE-2, or HRT in other literature) was built at ORNL and operated from 1957 to 1961[3].

1.4.3 The MSR's Military History: The Aircraft Reactor Experiment (ARE)

The very first MSR was built for a nuclear powered aircraft. The design started designed shortly after WWII, by Ed Bettis and Ray Briant at ORNL. In 1954, the ARE achieved a power of 2.5 MW_t. It used graphite for a moderator, molten sodium for a primary coolant, and the circulating fuel was NaF-ZrF_4-UF_4. Note that, due to the intended use (aircraft propulsion), some choices were motivated by space & weight considerations. However, molten sodium & fuel salts provided higher operating temperatures, and thus offered better thermal efficiency.

Figure 1–2 shows a section view of the ARE reactor vessel[4].

---

1 Haubenreich, PN, 1973. A Catalog of Dynamics Analyses for Circulating-Fuel Reactors, ORNL-MSR-73-7

2 IBID

3 IBID

4 The Aircraft Reactor Experiment – Design and Construction. Nucl. Sci. Eng. 2, 804, Bettis, E.S., Schroeder, R.W., Cristy, G.A., Savage, H.W., Affel, R.G., Hemphill, L.F. (1957)

Figure 1–3 shows a top view of the ARE reactor core, with the top thermal shield and header removed[5]. The hexagonal pieces with flow passages down the center are blocks of graphite. The U-shaped, stainless-steel tubes extending up out of the core are for fuel circulation.

Figure 1–4 shows the NB-36 experimental aircraft[6]. It made numerous flights carrying an operating nuclear reactor that provided power. The flight crew worked from a lead-shielded cockpit.

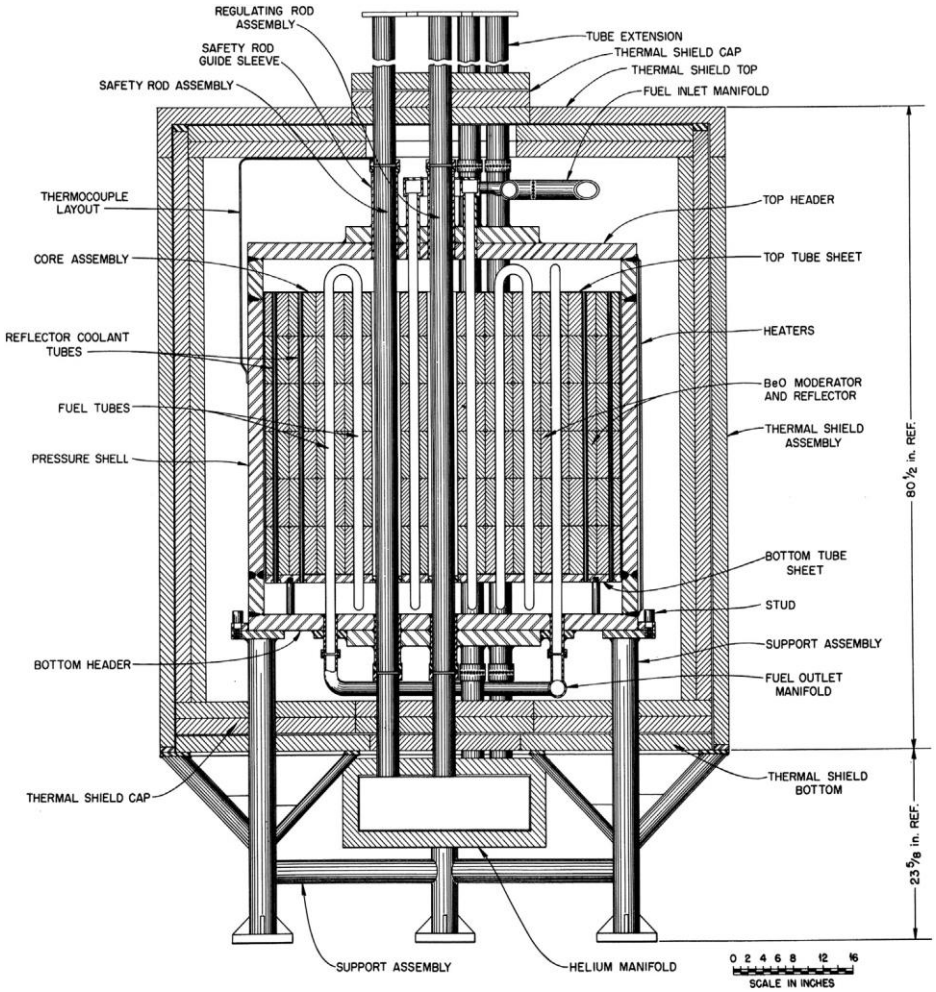

Figure 1–2 – The Aircraft Reactor Experiment (ARE) Core, Section View

5 IBID

6 ASME Photo Archives

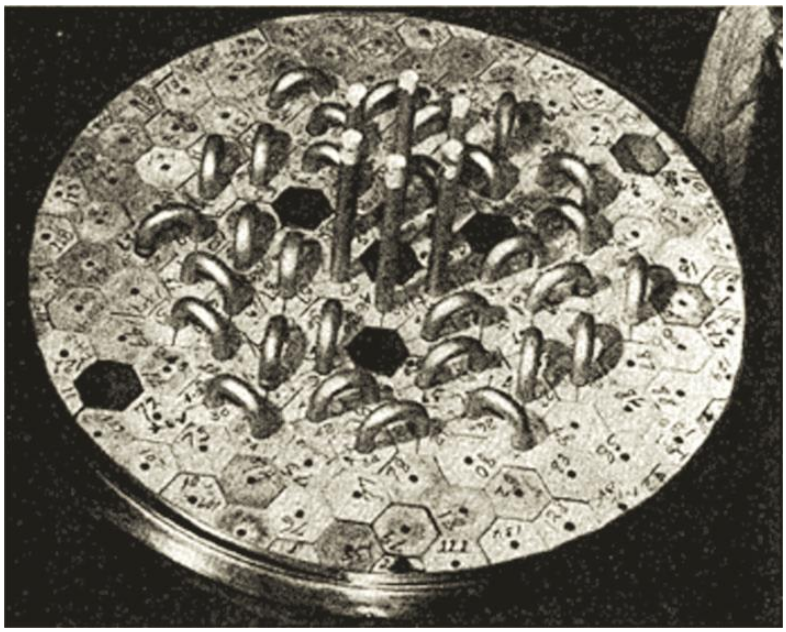

Figure 1–3 – Top View of ARE Core with Covers Removed

Figure 1–4 – The NB-36 – Nuclear Aircraft Powered by the ARE MSR

1.4.4 The MSR's Civilian History: The 7.5 MW_t Molten Salt Reactor Experiment (MSRE)

In 1956, Alvin Weinberg wanted to adapt an MSR for use as a civilian power plant, which resulted in the MSRE[7]. It started at ORNL as a design study, with several configurations

[7] Scarlat, et al, "Design and Licensing Strategies for the Fluoride Salt-Cooled, High-Temperature Reactor (FHR) Technology, Progress in Nuclear Energy, 77 (2014) 406-420

proposed; Figure 1–5 shows a top & side view of a two-fluid design. Note the five, equally-spaced fuel-salt pumps on top, with two additional (outrigged) cooling blanket-salt pumps[8].

In July 1957, the MSR design study was expanded to conduct material studies. In October 1957, it was expanded further to include additional testing & experiments. Construction was completed in 1964 and the reactor was taken critical in 1965. It was initially fueled with LiF-BeF_2-ZrF_4-$^{235}UF_4$, with a secondary cooling salt of LiF-(2)BeF_2 (FLiBe). It operated several years, including long continuous periods of time. In 1968, the fuel was replaced by $^{233}UF_4$.[9]

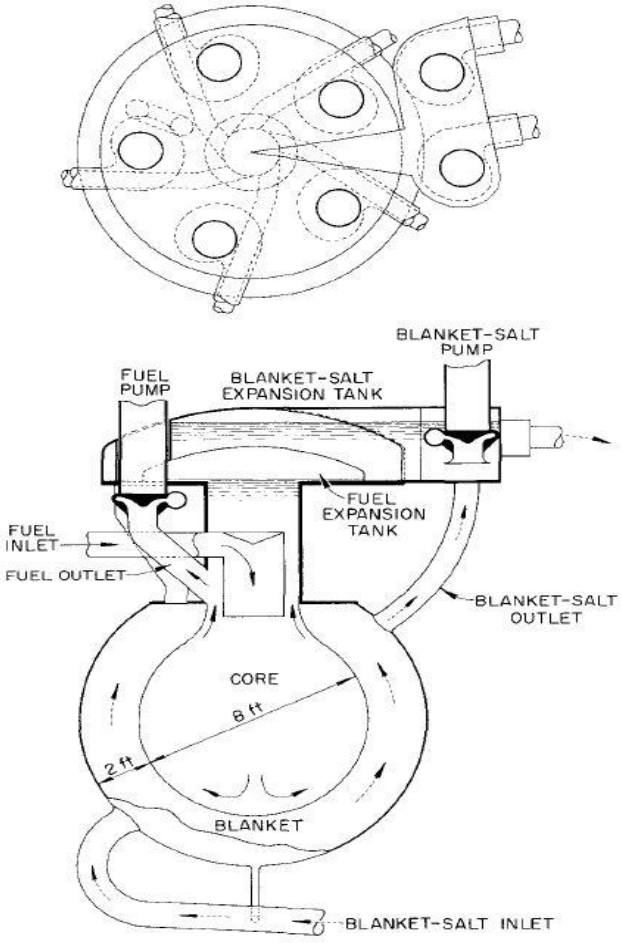

Figure 1–5 – An Early MSR Layout with (Inner) Fuel-Salt & (Outer) Blanket-Salt Pumps

[8] ORNL-2474, MSR Program Quarterly Progress Report for Period Ending January 31, 1958

[9] Scarlat, et al, "Design and Licensing Strategies for the Fluoride Salt-Cooled, High-Temperature Reactor (FHR) Technology, Progress in Nuclear Energy, 77 (2014) 406-420

Figure 1–6[10] shows a cutaway view of the MSRE facility. The fuel salt path (with storage & flushing vessels) is shown in red (the reactor is item #1). The blanket salt path is shown in yellow. It includes a heat exchanger (item #7), which is air-cooled via large fans (item #9).

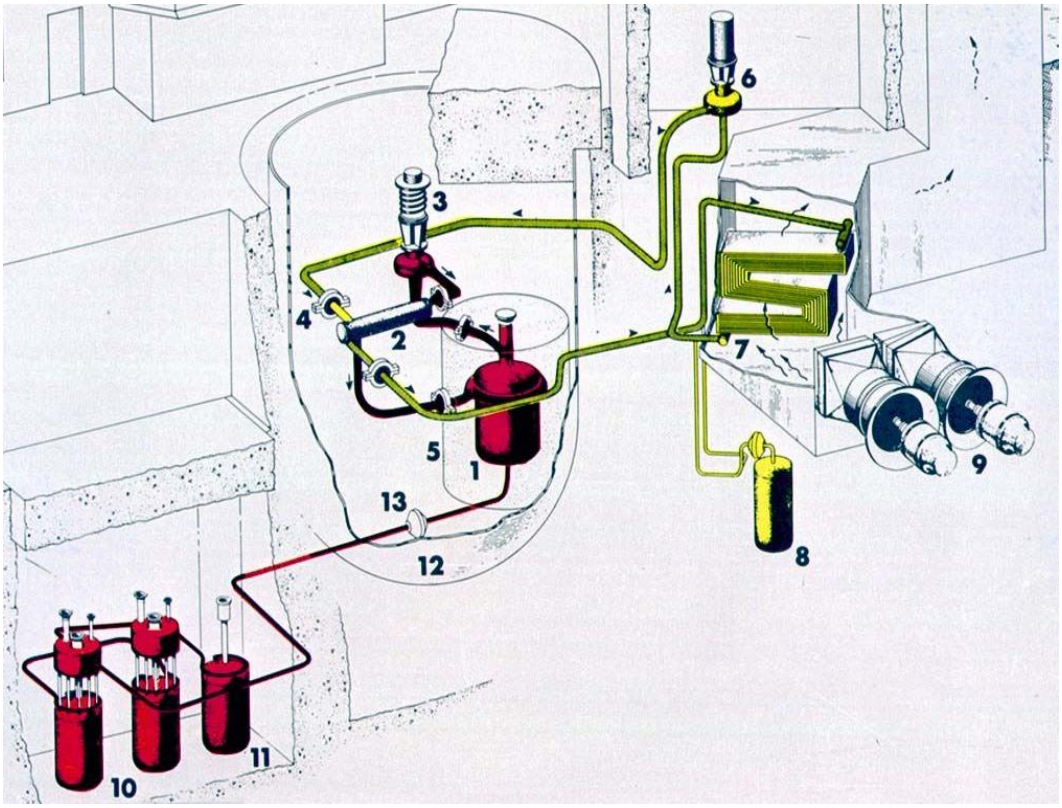

Figure 1–6 – Cutaway View of MSRE Facility

Figure 1–7[11] shows the MSRE's final design core vessel during fabrication. The welder in the photograph gives an idea as to its size & scale.

[10] Molten Fluoride Fuel Salt Chemistry, L.M. Toth, G.D. Del Cul, S. Dai, and D. H. Metcalf (ORNL) – American Institute of Physics Conference Proceedings, 346, 617 (1995)

[11] ORNL Photo, Public Domain

Figure 1–7 – MSRE Reactor Vessel Fabrication

Figure 1–8[12] shows a cutaway view of the MSRE reactor vessel, with circumferential fuel salt inlet distributor/volute.

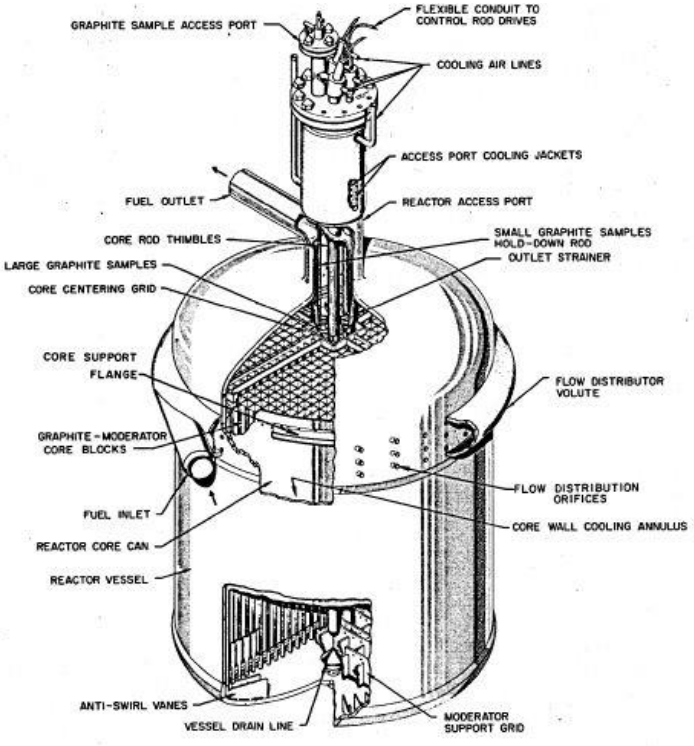

Figure 1–8 – MSRE Vessel Assembly Cutaway

[12] ORNL-LR-DWG 61097R1A

Figure 1–9[13] shows the arrangement of graphite moderator and control rods used in the MSRE. The fuel flow channels are the oval-shaped passages, measuring 0.4 inches x 1.2 inches.

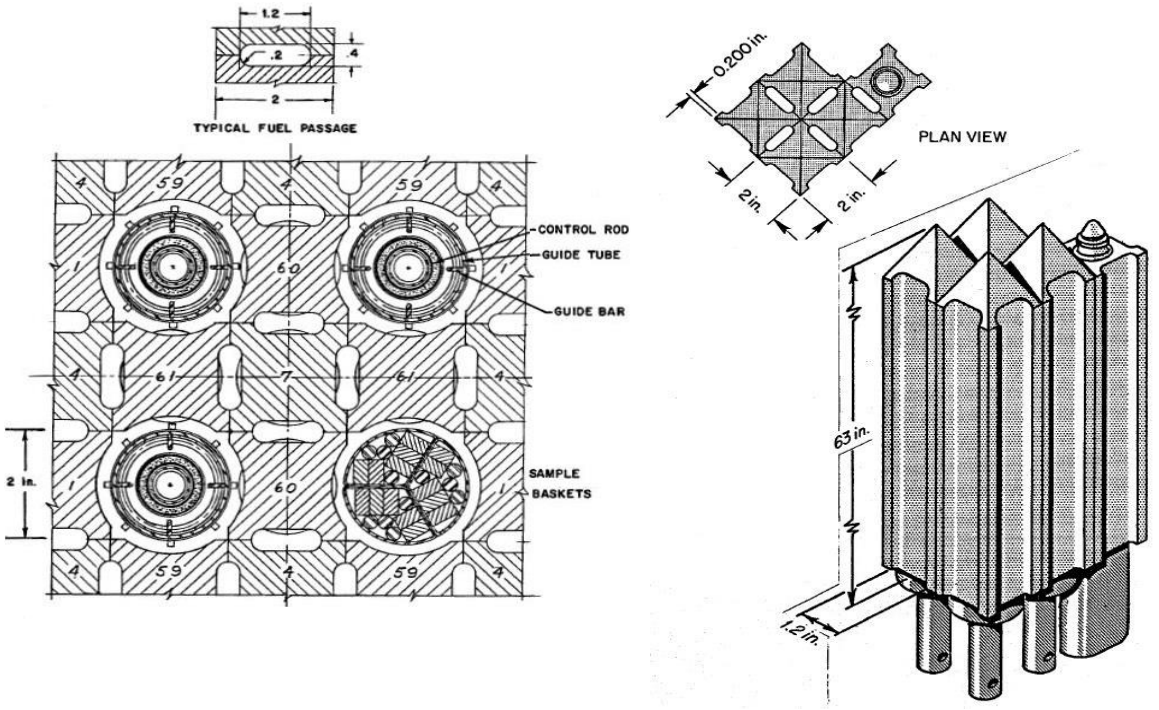

Figure 1–9 – MSRE Control & Moderator Rods

Figure 1–10[14] shows a top view of the MSRE vessel and heat exchanger installed in the containment room. On top of the vessel are the control rod drive mechanisms, a tangle of connecting pipes & wires for the pumps, instrumentation and other equipment. A worker can be seen standing on the reactor vessel, to give a sense of scale.

[13] ORNL-LR-DWG 56874 R (right) and ORNL-DWG 64-8814 (left)

[14] The MSR in Gen-IV: Overview & Perspectives, J. Serp, et al, Progress in Nuclear Energy, 77308 (2014)

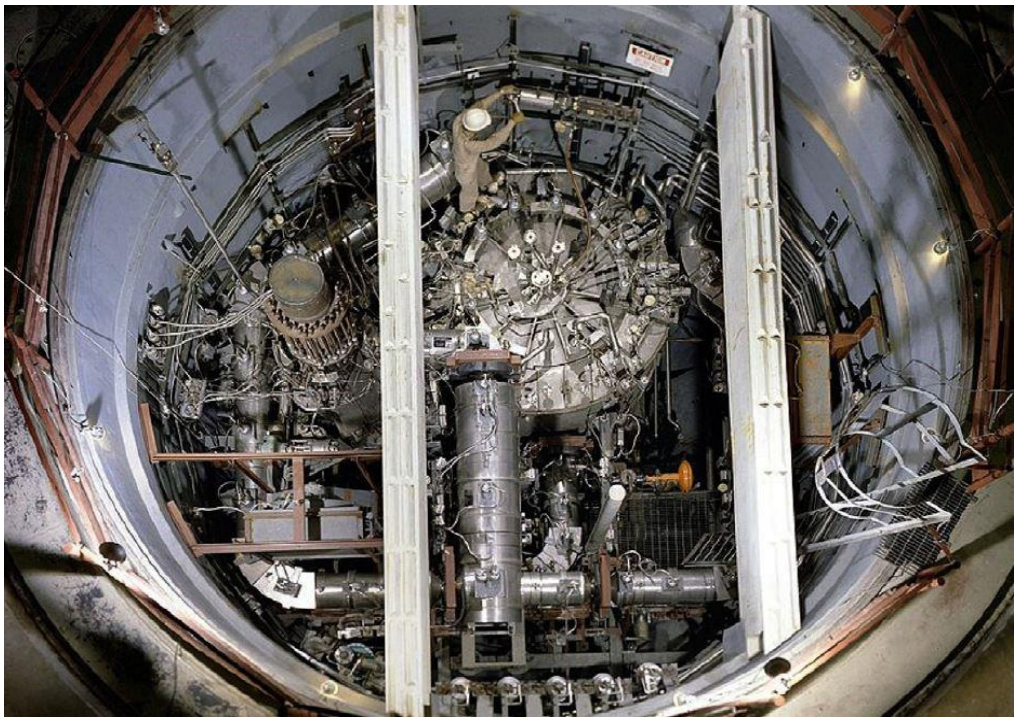

Figure 1–10 – Top View of Completed MSRE Containment Vessel

The MSRE was taken out of service in 1969, after 26,000 hours of operation. Afterwards, interest and research into MSRs waned, due to concerns about safety, security and proliferation of nuclear weapons & materials. Regardless, a wealth of information was obtained from studying the operational history, materials & equipment from the MSRE. These studies continued well into the 1970's; determining thermal & physical properties of various molten salts, examining corrosion of structural & piping materials, etc.

1.4.5 A Renewed Interest in MSRs – One of the GIF's "Most Promising Types"

The new millennium saw renewed interest in MSR research, due to its inclusion in the GIF's six Gen-IV reactor types. In 2002, research began on a liquid salt, very high temperature reactor (LS-VHTR), intended to achieve core temperatures of 950-1000C. It was based on the MSRE and a previous helium-cooled VHTR design. However, the MSR's inherent

advantages are worth a look from a fresh perspective, as opposed to just picking up where previous researchers left off[15].

The 2014 GIF roadmap cites two general subclasses of MSR:

1) Fuel material(s) are dissolved into the molten fluoride salt, which is also the heat transport medium (coolant). Fuel salts enter the core, which has a sufficiently large volume so as to achieve criticality. As the salts move through the core, they collect heat generated. Upon exiting the core, the salts move into heat exchangers. They have a smaller volume, so as to be subcritical. The heat exchangers cool the fuel salts before returning them to the core area. The heat extracted can be used to power turbine generators, provide process heat, etc.

2) Fuel material(s) are in the form of coated solid particles (pellets/pebbles). The pellets always remain in the core, while the coolant (molten salt) flow through them and collect/transfer heat generated. This is similar to the VHTR, and is sometimes referred to as a fluoride salt-cooled, high-temperature reactor (FHR).

1.4.6 MSR Advantages – Meeting the GIF Criteria

a) Sustainability:

Early nuclear power plants required the use of $^{235}U_{92}$. However, this isotope is only 0.72% of the element's natural abundance. At the current rate of consumption, it might last another 80 years[16]. In contrast, the MSR can "burn" Thorium, which is found in soil at about 6 parts per million – three times more abundant than uranium. It's about as common as lead and molybdenum, can be found on all continents, and is

[15] Molten Salt Reactors: A New Beginning for an Old Idea, D. LeBlanc, Nuclear Engineering and Design 240 (2010) 1644-1656

[16] http://phys.org/news/2011-05-nuclear-power-world-energy.html

easier to extract than uranium[17]. Further, other fissile and fertile materials exist (cited later herein), extending a typical MSR power plant's life much longer.

Most nuclear plants are situated near a body of water (lake, river, ocean, etc.), which provides supplemental cooling for condensing steam back into a liquid. In contrast, an MSR operates at temperatures far above the boiling point of water, without any pressurization of the coolant. The molten salts freeze and become solid at even the hottest temperatures on earth. Thus, no additional cooling is needed.

b) Safety & Reliability:

Early nuclear power plants use water as a coolant. In order to prevent boiling in the core (which drastically reduces its ability to provide cooling), it must be under pressure. The vessels & piping carrying the water between components can corrode and/or break. This releases steam, reduces cooling and can spread contamination. A violent release of steam is like an explosion. At higher temperatures, water can dissociate into hydrogen, which also can explode (from ignition). In contrast, MSRs do not use water for cooling. The fuel salts remain liquid for much higher temperatures before boiling, and thus do not even need to be pressurized.

Since the fuel is already molten, previous fears of a reactor meltdown are irrelevant. If the fuel salts exceed a predetermined temperature (determine by structural materials' tolerance), a melt-out plug simply drains out the contents into a holding area, which is sized such that the fuel salts cannot achieve criticality. The mass simply re-solidifies.

c) Economic Competitiveness

Current power plants use fuel elements that are manufactured by complex processes and machined to very close tolerances, all of which add to their expense. These fuel

[17] http://www.livescience.com/39686-facts-about-thorium.html

elements tend to swell during use, due to neutron interaction, which results in additional costs to refuel them. In contrast, MSRs only need to have the fuel combined chemically to form a salt that can be melted and placed in the reactor.

Early power plants are fueled with uranium. The power output and service life depends on the amount of enrichment. As the fuel starts to deplete, it becomes more difficult to burn even the good fuel that remains. When a power plant reaches the end of its service life, there's still a lot of fissile and fertile material in the core. Such material is currently disposed of as radioactive waste. In contrast, an MSR can use several different types of fuel; i.e., $^{242}Am_{95}$, $^{242}Pu_{94}$, $^{244}Pu_{94}$, $^{242}Cm_{96}$, $^{242}Cf_{98}$, $^{233}U_{92}$ $^{235}U_{92}$, $^{238}U_{92}$, $^{242}U_{92}$, $^{232}Th_{90}$, and other trans-uranic (actinide) elements. As the fuel decays, it changes from one element to another, many of which can also be "burned." Since a higher percentage of the fuel can be used, overall plant efficiency is higher.

The MSR is also thermally more efficient than early generation power plants. A measure of the maximum possible thermal efficiency of a reversible cycle is the Carnot equation:

$$\eta_{Thermal} = \eta_{Carnot} = 1 - \frac{T_{Cold}}{T_{Hot}}$$

The T-terms are (absolute) temperatures leaving (Hot) and returning (Cold) to the reactor.

A typical steam cycle may have an output temperature of 300 °C (573K) and return temperature of 20 °C (293K). Thus, its maximum possible thermal efficiency is:

$$1 - \frac{293}{573} = 0.4887 = 48.87\%$$

It is worthwhile to note that the allowance of a 20 C return temperature depends on a "heat sink" – the aforementioned nearby body of water; lake, river, ocean, etc.

In contrast, an MSR may have an output temperature of 900 °C (1173K) (a limitation of the reactor vessel's structural material). This can be provided to a generating plant (perhaps using an advanced Brayton-cycle turbine using CO_2) with a return temperature of 35 °C (308K). Note that this return temperature allowance does not depend on a nearby body of water, but instead is just an average (conservative) ambient air temperature.

Thus, its maximum possible thermal efficiency is:

$$1 - \frac{308}{1173} = 0.7374 = 73.74\%$$

The MSR's output can also be used for higher-temperature processes, such as gypsum board drying, and production of H_2 from water for fuel cell fabrication.

d) Proliferation Resistance and Physical Protection

As previously mentioned, early reactors are not able to use up all their fuel. Thus, even when a fuel element is "depleted," it still contains materials that could be used for other (including bad) things. Currently, those materials are considered "waste." In contrast, an MSR uses more of the available fissile material, thus reducing the amount disposed of as waste.

Further, it is possible for current (fissile and fertile) waste materials (i.e., spent fuel, etc.) to be reprocessed into useful fuel for an MSR, reducing the volume of materials that need to be disposed.

Finally, MSRs can "burn" existing stockpiles of weapons-grade materials, turning them into electrical power, process heat & manufacture of other needed materials.

1.4.7 Nuclear Alchemy? The Breeder Reactor

This report mentions "burning" of fuel, even though no combustion (oxidation or chemical reaction) occurs. In this context, this refers to a reactor system's ability to make efficient use of the fuel, reducing the amount of waste created in the process. In another, it means MSRs can make use some of the current/existing waste (in processed form), as fuel. It also refers to using stockpiles of weapon materials, by converting one (fertile) element into another (fissile). The latter is what's referred to as a "breeder" reactor, as theorized by Enrico Fermi. Intense exposure to neutrons (such as in a reactor core) causes a "fertile" material (like thorium) to become a "fissile" (fuel) material (specifically uranium), by[18]

$$^{232}Th + n \rightarrow {}^{233}Th + \vec{\beta} \rightarrow {}^{233}Pa + \vec{\beta} \rightarrow {}^{233}U$$

The uranium can then be "burned" for energy. There are other nuclear reaction pathways that describe how other (non-fuel) elements can be converted into suitable fuels for MSRs.

1.4.7.1 EBR-1 & EBR-2

What Enrico Fermi conceived in 1944, Walter Zinn (et al) turned into reality. Experimental Breeder Reactor #1 (EBR-1) was built near Arco, ID. On 12/20/1951, it achieved the first use of nuclear energy to produce electricity[19]. Its basketball-sized core of enriched U-235 was surrounded by numerous annular segments containing U-238 (fertile) fuel, which either absorbed or reflected back neutrons that would have otherwise leaked out and been lost.

The outer blanket also served as a safety feature; upon a reactor SCRAM (emergency shutdown), blanket elements were unlatched from their support structure and dropped into the basement. This reduced the neutron population in the core, curtailing the chain reaction. Even so, on 11/29/1955, it suffered a partial melt-down during a coolant flow test.

---

[18] WASH-1222; An Evaluation of the Molten Salt Breeder Reactor (1972) USAEC

[19] The X-10 Graphite Reactor in Oak Ridge TN generated electricity on 9/3/1948

In 1953, EBR-1 achieved a 1:1 ratio of Pu-239 production to U-235 consumption. The best recorded ratio was about 1.2:1. On 11/27/1962, EBR-1 was then the first facility to generate electricity from a 100% Pu-239 fuel load. EBR-1 was taken out of service in 1963.

In 1952, before successful breeding had been announced, plans were made to build EBR-2, a larger pilot plant. Construction started in 1958 and was completed in 1961. On 7/16/1964, EBR-2 the power level was slowly ramped up, and in August 1964, it achieved a power level of 30 MW_t. In May 1965, EBR-2 used 100% "recycled" fuel for the first time, achieving a power level of 45 MW_t. In September 1965, the power level was increased to the design value of 62.5 MW_t (19 MW_e).

In April 1986, a crucial test was conducted at EBR-2, to show that the plant was inherently safe. All the designed safety systems were taken off line, and the coolant pumps stopped. As the temperature rose, fuel density decreased, which slowed the reaction rate. EBR-2 then self-regulated its temperature and power without the use of any emergency safety operations or operator intervention. This feature became a main pillar of later design intents, such as EBR-3 and the Integrated Fast Reactor (IFR). EBR-2 operated until 9/27/1994[20].

Initially, it was thought that breeder reactors would need to keep the fertile and fissile fuel salts separated, resulting in the need for a two-fluid reactor core. However, once on-site fuel processing became possible, neither a two-fluid or multi-pass system was necessary.

1.4.7.2 Molten Salt Breeder Reactors - MSBE & MSBR

In 1972, ORNL completed a conceptual design[21] for a molten salt breeder reactor experiment (MSBE) core, in preparation for building a larger molten salt breeder reactor (MSBR). Figure 1–11 shows an isometric and cross-section view of the "slab" style moderator element proposed for the MSBE, and how groups of them would be stacked in the core.

---

[20] Vision & Reality: The EBR-II Story, C. Westfall, *Nuclear News* (February 2004)

[21] ORNL-CF-72-11-8

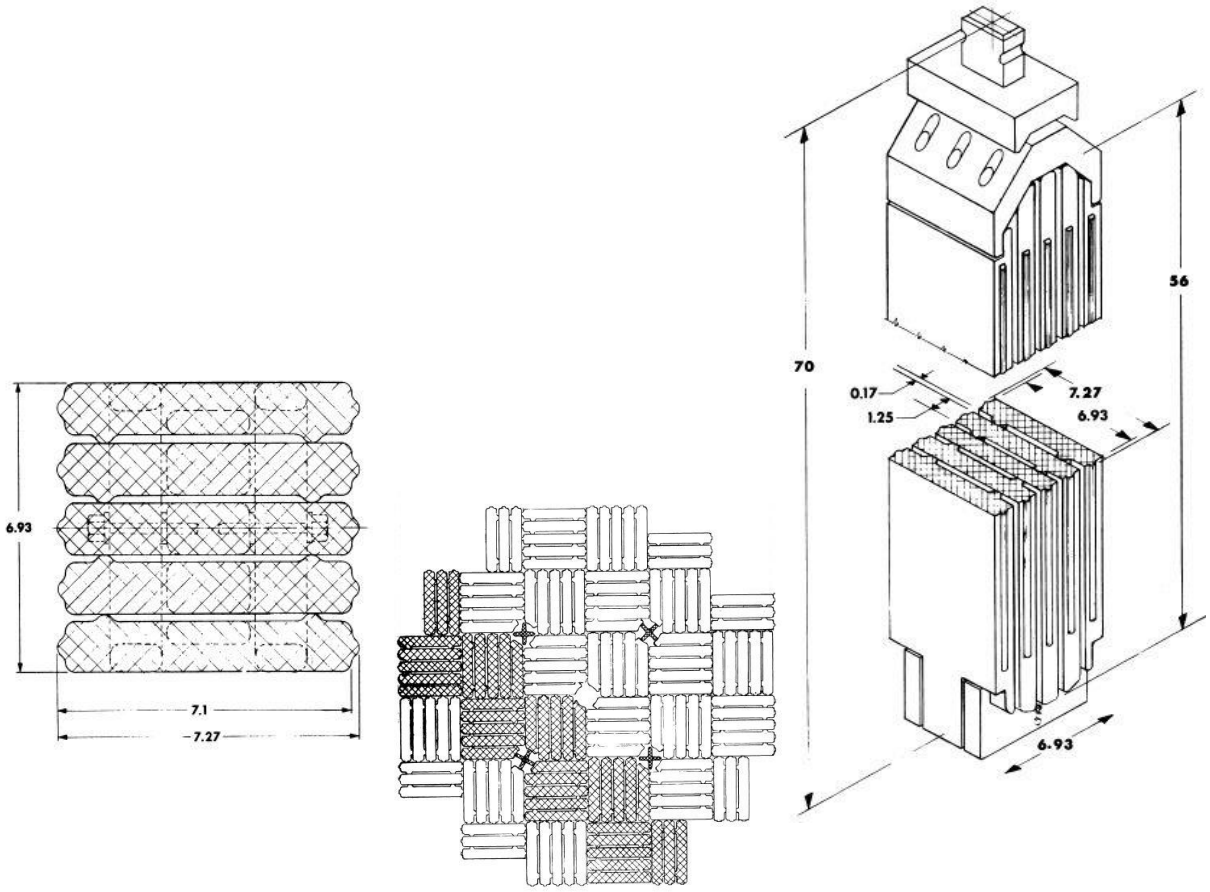

Figure 1–11 – MSBE Moderator Slab Features and Core Stacking

1.4.8 Other MSR Uses

1.4.8.1 Medical Radioisotope Production

Numerous radioisotopes have valuable medical applications, including $^{111}In_{49}$, $^{131}I_{53}$, $^{99}Tc_{43}$, $^{177}Lu_{71}$, $^{213}Bi_{83}$, $^{90}Yb_{70}$, $^{131}Cs_{55}$, $^{103}Pd_{46}$, $^{223}Ra_{88}$, $^{225}Ac_{89}$, et al. Note that $^{213}Bi_{83}$ (for example) comes from the decay chain ^{233}U->^{229}Th->^{225}Ac->^{221}Fr->^{217}At->^{213}Bi, and that the first three of these can be used in an MSR.

Note that $^{99}Tc_{43}$ comes from ^{99}Mo, which can also be extracted from MSRs. It has a half-life of 66 hours, which allows on-site processing of medical isotope $^{99}Tc_m$ (which has a half-life of 6 hours). In 2014, the estimated world-wide demand for $^{99}Tc_m$ was 400-450 TBq per

week. At that time, most of the ^{99}Mo supply was produced by five aging reactors, located in Canada, the European Union and South Africa, all of which used enriched uranium fuels.

There is at least one patent[22] whereby ^{238}U fuel can be used to produce ^{99}Mo -> $^{99}Tc_m$ & ^{131}I.

An MSR's cooling salt components (LiF & BeF_2) have a low molecular weight. Thus, it is possible to bubble helium (an inert gas) upwards through this molten mixture. One of the GIF roadmap milestones mentions bubbling with helium. It has been shown[23] that helium can be bubbled vertically through a mixture of 66% LiF 34% BeF_2 to create medical radioisotopes at a temperature of 900K. The helium gas entrains aerosols in the molten salt, which can be extracted using multilayered, nickel nanofilters. Note that helium is naturally produced during fission reactions, and in normal decay chains of fuel & fission products.

1.4.8.2 Higher Temperature Process Heat

Beyond producing electricity, the higher temperatures produced by an MSR can be used to meet the needs of several industrial processes, such as petrochemical fertilizer production, extracting hydrocarbons from oil sands, converting coal and biomass into higher quality liquid fuels, and the production of hydrogen (for fuel cells, et al) from water[24].

1.4.9 MSR Research Needs – The GIF Roadmap & Milestones

The GIF considers the scoping and screening phase to be complete as of 2011. The timeline for other topics include:

- Management & salt control (2012-2014)
- Confirmation of bubbling efficiency (2014-2015)
- Heat exchanger development and viability (2015-2017)
- Validation of (re)processing flow sheets and laboratory scale

---

22 US Patent #8989335-B2 – Tsang (2010)

23 AV Zagnit'ko, DY Chuvilin – Nanoaerosols Formation During the Bubbling of Lithium and Beryllium Fluoride Molten Salt to Produce Reactor Radioisotopes, Nanotechnol Russia (2009) 4:851

24 US Dept. of Energy Quadrennial Technology Review (2015), Chapter 4 – Technology Assessments

- Definition of safety analysis methodology and specification of accident scenarios.

The 2014 GIF roadmap lists the following 10-year goals for the MSR:

- Develop a baseline concept for the molten salt fast reactor (MSFR).
- Identify and leverage commonalities with other systems using molten salts, such as the fluoride salt-cooled, high-temperature reactor (FHR), with respect to heat transfer systems.
- Further R&D on liquid salt physical chemistry and technology, particularly with respect to corrosion, safety-related issues and treatment of used salts.

Development of a baseline concept MSR includes the following sub-tier goals:

- Structural materials and piping system components, with respect to corrosion (oxidation/reduction) and high operating temperature properties (i.e., creep & fatigue). Materials from the MSRE were tested; Hastelloy N and several other (Ni, W, Cr) materials are being developed and tested.
- Liquid salt physical chemistry, behavior and other properties. This includes development of technology for production, handling and processing. It also includes defining the coupling between neutronic, thermal-hydraulic and chemistry, including fission products, tritium creation & extraction, as well as other (re)processing aspects.
- Fuel and fuel cycle; treatment of used/spent (fuel) salts. There is much experimental data on the fluorination process, due to work carried out in the US. Additional processing steps are being tested at CNRS laboratories (France). This includes various electrochemical steps.
- System design and operation. Study commonalities with other systems using molten salts, such as FHR, heat transfer systems. Note that the use of molten salts is not restricted to the reactor core or fuel transport; secondary systems can use molten fluoride salts as well. This is advantageous because of its high volumetric heat capacity, resulting in reduced equipment size, and use with power cycle coolants.
- Safety and related safety systems. This relates to handling of the salts, whether molten or solid, regardless of whether it does or doesn't have dissolved fuel(s).

- System integration and assessment, including startup, shutdown, freeze handing, instrumentation, control systems, etc.

1.5 Specific Focus: A Match between Research Interests & MSR Needs

It seems clear that computer simulation of fluid flow and/or heat transfer phenomena would help achieve GIF goals for MSR research. This includes heat exchanger development, optimization, component and pipe sizing, development of baseline concepts, etc. Such an undertaking would likely require new theory & modeling techniques, coupling aspects of thermal-hydraulics, chemistry, fluid density differences (due to several fissile & fertile elements), with reactor core physics; i.e., kinetics & neutronics.

It is important to note that MSR & MSBR components & piping are subject to corrosion, due to the fluoride salts commonly used. This includes internal parts of components such pumps. Even unconventional pump types, such as those which employ magneto-hydrodynamic (MHD) effects are susceptible to corrosion & erosion of the electrodes and structural materials. One can't help but wonder whether pumps are necessary.

One of the NEUP white papers[25] includes CFD metrics for determining the time required to establish natural circulation after a loss of forced circulation (pump power). They include providing the expected flow rate & cooling (heat transfer) under steady-state convection flow, and also modeling transient behavior for key events.

An MSR designed to run by natural circulation wouldn't need pumps. This would reduce system complexity & maintenance requirements, and increase reliability.

The idea of a natural-circulation MSR is not new. In 1958, initial (simplified) studies were done for a $5MW_t$[26] and a $60MW_t$[27] natural convection MSR. The latter of these showed that

---

25 IRP Workshop 2; FHR Methods and Experiments (2013)

26 Zasler, J (1958). Experimental 5 MW Thermal Convection Molten Salt Reactor, ORNL-CF-58-6-66

27 Romie, F.E. Kinyon, B.W., A Molten Salt Natural Convection Reactor System, ORNL-CF-58-2-46

the specific power for a natural-convection plant is 900 kW/kg, as opposed to 1275 kW/kg for a forced-convection system. It also states that adding 0.25% thorium (i.e., for a breeder-type reactor, using both fissile & fertile fuel salts) requires an 87% increase in fuel inventory, for a nominal (spherical) core diameter of 8 feet. Figure 1–12 is an excerpt from the 60MW_t study that shows the concept.

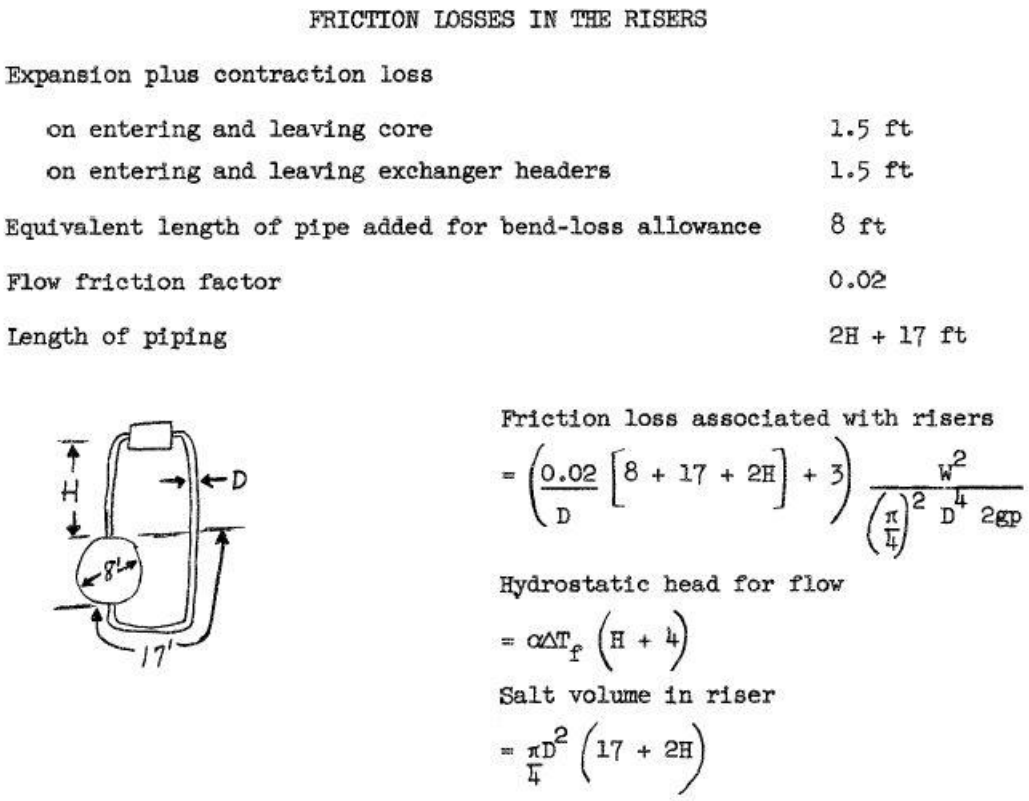

FRICTION LOSSES IN THE RISERS

Expansion plus contraction loss	
on entering and leaving core	1.5 ft
on entering and leaving exchanger headers	1.5 ft
Equivalent length of pipe added for bend-loss allowance	8 ft
Flow friction factor	0.02
Length of piping	2H + 17 ft

Friction loss associated with risers

$$= \left(\frac{0.02}{D}\left[8 + 17 + 2H\right] + 3\right) \frac{W^2}{\left(\frac{\pi}{4}\right)^2 D^4 2g\rho}$$

Hydrostatic head for flow

$$= \alpha \Delta T_f \left(H + 4\right)$$

Salt volume in riser

$$= \frac{\pi D^2}{4}\left(17 + 2H\right)$$

Figure 1–12 – Natural-Convection MSR Concept

In 1962, a simplified study was done for one with a 576MW_t[28] power rating. It concluded that large, natural-convection reactors may not be attractive, since the benefit of eliminating fuel pump(s) was outweighed by the increase in fuel volume. Figure 1–13[29] shows this concept, which is very similar to (scaled up from) the 60MW_t study.

---

28 Zasler, J (1962). 576 MW_t Natural Convection Molten Salt Reactor Study, ORNL-TM-0269

29 IBID

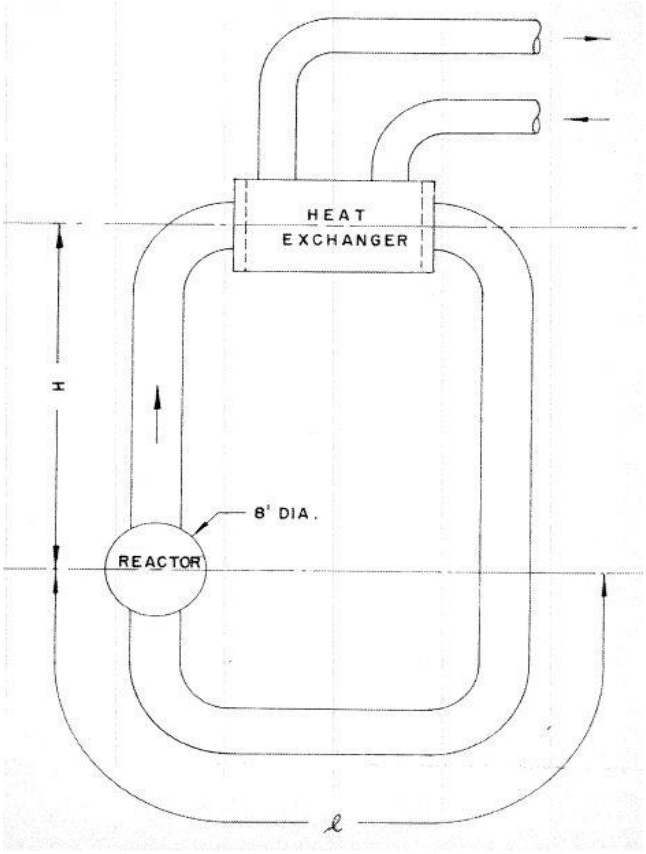

Figure 1–13 – 576MW$_t$ Natural Circulation Reactor Concept

On January 12, 1969, a six-hour test was conducted at the MSRE, to see how much power it would develop under natural convection flow of the fuel salt[30]. The primary salt pump was shut off, but secondary pumps stayed on. The reactor vessel fuel outlet temperature was limited to 1200 degrees F, and the temperature drop across the core was restricted to (a modest) 75 degrees F. The secondary (cooling) salt's minimum temperature was limited to 1010 degrees F, to avoid freezing in the pipes. The reactor power output was changed by opening (throttling) the radiator areas doors (the yellow loop from Figure 1–6). Under these rudimentary and conservative conditions, the maximum power achieved was 354.5 kW at a primary salt flow rate of 31.4 GPM. This is particularly impressive, considering that the design intent of the MSRE did not start with natural-convection flow in mind and that the idle primary fuel-salt pump impeded flow.

[30] Gabbard, C.H. (1969), MSRE Thermal Convection Test – ORNL-MSR-69-25

All of this work dates back to before modern computers and computational methods, such as computational fluid dynamics (CFD) and multi-physics models.

Thus, it is tantalizing to revisit the possibility of a natural-circulation MSR, using modern computer-aided design tools; CFD & multi-physics software. This includes the use of coupled equations for thermal-hydraulics (heat transfer, internal heat generation, fluid dynamics) with neutronics (the study of dynamic motion & interaction of neutrons with other materials). An MSR can use a variety of different fuels, composed of both fissile (can sustain a fission chain reaction) and fertile (not fissionable by thermal neutrons, but can be converted to fissile material by neutron absorption) isotopes.

1.6 Specific Objectives and Task Breakdown for this Dissertation

CFD simulations of natural circulation have been done, but few relate to the operation of MSRs. Verification of CFD codes indicate they provide valid results. Some have provided results that match benchmark tests. This research attempts to simulate basic MSR performance aspects using CFD software to model the behavior of a $10MW_e$ ($33MW_t$) natural-convection MSR.

First, results of a literature search will be presented. Then, the governing equations for mass, momentum and energy conservation will be reviewed. Simplifications such as the use of symmetry and turbulence models will be discussed. Schemes for modeling reactor physics are presented, and their incorporation into the software is described.

1.6.1 Initial Simplified Simulations

Simulations began by using simple shapes (cylinders) for the reactor core & heat exchanger, with water as the initial working fluid. These were used to evaluate & determine the critical size & location aspects. A schematic diagram of the modeled system is shown in Figure 1–14, the details of which are explained later herein.

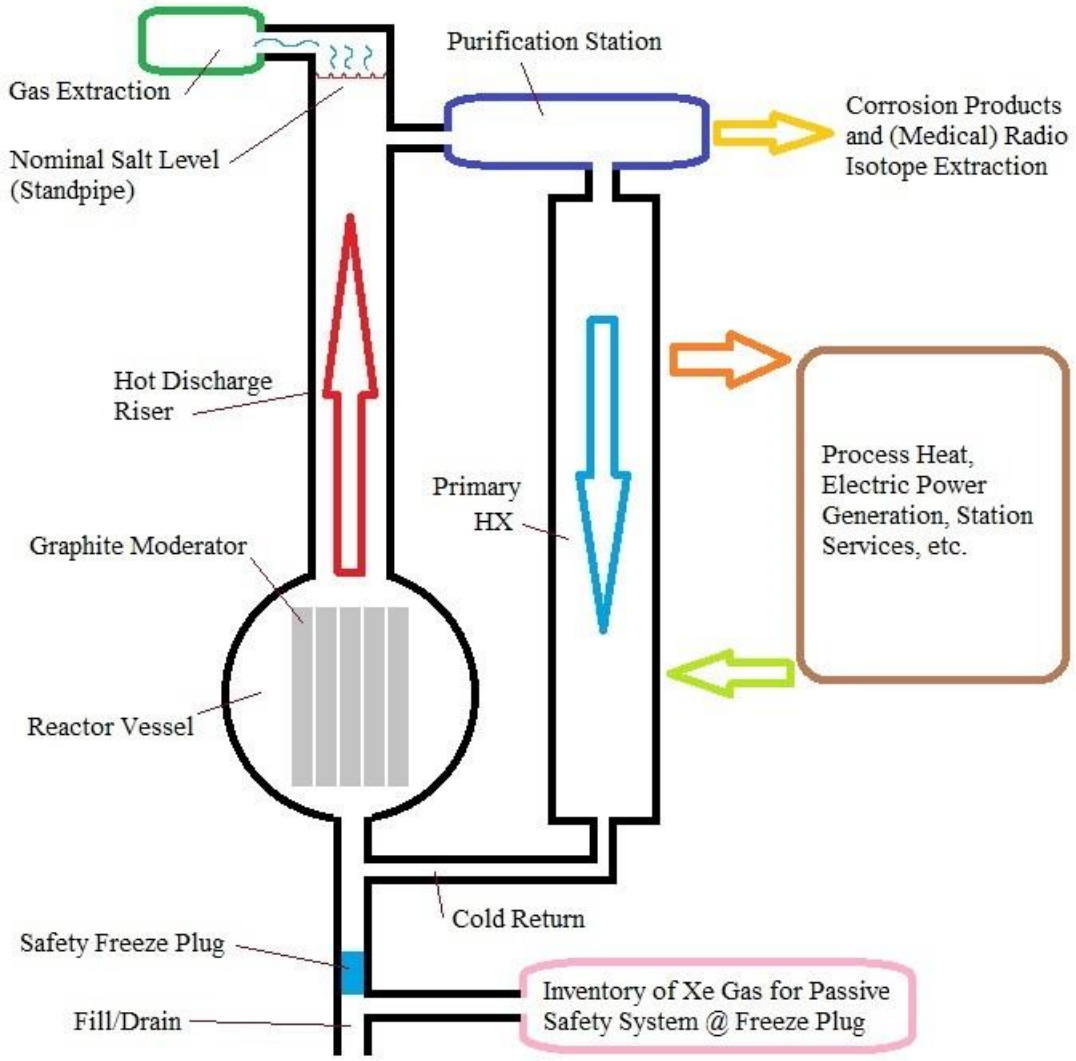

Figure 1–14 – Schematic Diagram of Modeled System

The next level of complexity involves the use FLiBe salt as the working fluid, with a full set of physical characteristics included in the CFD definition.

Water and FLiBe simulation results are compared with those obtained using analytical methods (i.e., from first-principles equations).

1.6.2 Benchmarking Simulations

Students at the University of Idaho campus in in Idaho Falls designed and built a Test Rig to perform experiments with natural circulation flow. The details of the Test Rig are presented herein as the section devoted to the simulation of its flow.

Detailed 2D/3D models were developed for the Test Rig, and CFD simulations were run using water as the test fluid and actual data for the heating and cooling aspects of this setup. A comparison was done between the CFD and analytical results.

1.6.3 Simulating a Realistic Reactor Vessel

The configuration of previous reactor vessel design studies was developed into an accurately-sized vessel with graphite moderator bars that can deliver the desired power output. It was coupled to a simplified heat exchanger, and the operation simulated, using the shapes and configurations shown to be effective in the initial simplified simulations. FLiBe salt was used as the working fluid, with the full set of physical characteristics entered into the CFD software.

1.6.4 Simulating an Actual MSR Reactor System Design

Students at the University of Idaho in Idaho Falls developed a realistic MSR system model. It has a cylindrical reactor core vessel, surrounded by a reflector instead of using a graphite moderator. Thus, the reactor vessel itself is relatively simple. However, the heat exchanger is an outer annular region, with numerous finned tubes extending through the interior. For this research, 2D models were developed to model the details of the designed heat exchanger. These were incorporated into a full reactor system simulation, the results of which are presented herein.

2 Literature Search

2.1 Abstract

This chapter provides the results of a literature search for the specific subject matter of this dissertation – CFD simulation of a natural convection MSR. It describes the unique aspects of the current research as well.

2.2 General Discussion

The previous chapter summarized early MSR concepts, feasibility & design studies, research into cooling & fuel salt physical properties, and the first experimental reactors. This work was carried out by National Laboratories; mention was made about the wealth of information obtained upon taking the MSRE out of service. After 1979, research into nuclear energy waned, due to high-profile accidents, which eroded public trust. In the US, new construction was curtailed and much of the research was devoted to making necessary improvements in reactor safety. Current energy research seems to focus on replacing combustion with renewables (i.e., grid decarbonization), such as solar (photovoltaic & focused boilers) and wind (on-shore & off-shore wind turbines). Many new construction projects are devoted to these technologies.

An up-tick in nuclear energy research took place after the Generation IV International Forum (GIF) issued their first technology roadmap in 2002. The MSR is one of the six most promising types, but ranked last in terms of readiness for implementation. Some MSR systems use TRISO coated fuel pellets arranged in a pebble-bed. The type studied herein uses fuel dissolved in the cooling salt.

Early MSR feasibility & design studies indicated that forced convection types were preferred, as they produced more power for the same fuel/cooling salt inventory. Natural circulation for MSRs was/is mostly studied in the context of passive cooling systems in the event of a loss of pump power event. This is referred to as a Direct Reactor Auxiliary

Cooling System (DRACS). Still, natural circulation systems are simpler overall, and avoid the corrosion problems of pump internal parts.

Computational Fluid Dynamics (CFD) is an indispensable tool in many areas of engineering interest. A summary of just the contributions to the aerospace field would take up many volumes. With the increase in computational speed, use of multiple CPUs, and better turbulence models, CFD results have improved with respect to accuracy, realism and the speed at which results can be obtained.

There is some skepticism as to whether CFD can accurately model natural circulation flow. Thus, many papers on this subject include benchmarking of simulations with experimental results.

2.3 Research on the Specific Subject Matter

Despite the popular trends in energy research and the rather esoteric nature of simulating natural circulation MSR performance, some important papers have been produced.

2.3.1 Theory & Coding

One paper[31] presented a simplified scheme to couple neutronics and thermal-hydraulic behavior of a 1D reactor. It uses the DRAGON code (initially developed in 1998) and multi-group library IAEA172 (2006), for neutronic information. It uses the SIMPLE algorithm for discretizing equations, and a modified QUICK scheme at control volume interfaces. The study used constant values for density, heat capacity and thermal conductivity, based on published values for 0.5% mol fraction UF_4 fuel dissolved in LiF-NaF-BeF_2 solvent. An important result is that flow velocity through the reactor did not appreciably affect neutron flux (fast or thermal). Flow velocity does however affect the concentration of delayed neutron precursors, moving the maximum point further along in the direction of flow.

[31] P Wang, et al, Study on the Coupled Neutronic and Thermal-Hydraulic Characteristics of the New Concept Molten Salt Reactor, Journal of Engineering for Gas Turbines and Power, Vol. 132/102923 (2010)

Another important result is that inlet temperature (within the operating range) did not affect the neutron flux. With a fixed velocity, the temperature increase (ΔT) through the reactor is constant, regardless of the inlet temperature. However, fluid velocity had a marked effect on overall ΔT; i.e., faster flow reduced residence time, which reduced the temperature increase. Finally, this study showed that as the inflow temperature increased, reactivity decreased (k_{eff}). The negative temperature coefficient (discussed later herein) is an important inherent safety feature.

Another paper[32] conducted a 2D computational study of a graphite-moderated (outer reflector) MSR vessel. It used neutron diffusion theory and the HELIOS neutron transport code. It states that neutronic and thermal-hydraulic coupling is stronger in an MSR of the type with dissolved fuel, which makes perfect sense. The study used a thorium-based fuel salt (ThF_4 – to achieve a breeder reactor, discussed herein), with FLiBe salt as the solvent. The conclusions therein match the 1D model in many respects; i.e., that fluid velocity through the reactor vessel does not appreciably affect neutron flux (both fast and thermal). However, delayed neutron maximum concentration moves farther downstream in the core with increased velocity.

There are other tools and codes that are useful for studying neutron kinetics and reactor behavior, such as the Standard Thermal Reactor Analysis Code (SRAC-CITATION) and the JENDL data library.

BISON[33] is a finite-element based nuclear fuel performance code, based on the Multiphysics Object-Oriented Simulation Environment (MOOSE) code[34] developed in 2008 by Idaho National Labs (INL). BISON can perform steady state and transient analysis of solid fuel elements, and is applicable to MSRs that use UO_2 TRISO-coated fuel elements (i.e., pebble-bed types). MOOSE is an open-source, parallel finite element framework, that can run on

[32] J Wang, X Cao, Investigation on Fluctuations in Full-Size Molten Salt Reactor with Coupled Neutronic/Thermal-Hydraulic Model, Annals of Nuclear Energy 92 262-276 (2016)
[33] RL Williamson, SR Novascone, Application of the BISON Fuel Performance Code to the FUMEX-III Coordinated Research Project, INL/EXT-12-25530 (2012)
[34] D Gaston, et al, MOOSE: A Parallel Computational Framework for Coupled Systems of Nonlinear Equations, Nuclear Engineering and Design, Vol. 239, p. 1768 (2009)

MacOS, Windows 10 and Linux platforms. BISON access requires a license agreement between INL and interested parties.

The Simulation of Core Damage Progression/Reactor Excursion & Leak Analysis Program (SCDAP/RELAP5)[35] was originally developed circa 1989 at INL to model operational transients and accidents for light-water reactors (LWRs). The latest release is RELAP5-3D, which includes molten salts[36] (including FLiBe) and compatible substitutes such as DOWNTHERM A[37] and Solar Salt[38] as working fluids. It can model high Prandtl number coolants and natural circulation[39] for passive decay heat removal (i.e., DRACS), and porous media flow, such as pebble bed MSRs. Interested parties may request a license via Battelle Energy Alliance, LLC, for a fee. A proprietary version of this code, RELAP5-MSR[40] has been developed by the Shanghai Institute of Applied Physics (SINAP) specifically for MSR analysis. It has been used to model a thorium-fueled MSBR design concept.

2.3.2 Pure Simulation w/o Experiment

A parametric study of a particular MSR configuration[41] was conducted, using a cylindrical primary vessel containing the fuel salt, which recirculates internally from natural convection. The vessel was modeled in 2D, as an axisymmetric object. The tube (vessel) exterior is in contact with a secondary coolant, nominally at 728K, which removes heat from the primary fuel salt, using a constant value for convective heat transfer coefficient. This study used ANSYS FLUENT, which the author states "does not have a perfect solver setup to obtain an exact solution."

---

[35] NUREG/CR-5535 (1998), CR-6150, EGG-2720 (1993), et al
[36] CB Davis, Implementation of Molten Salt Properties into RELAP5-3D/ATHENA (2005)
[37] RL Moore, Implementation of DOWTHERM A Properties into RELAP5-3D/ATHENA, INL/EXT-10-18651 (2010)
[38] R Ferri, A Cammi, D Mazzei, Molten Salt Mixture Properties in RELAP5 Code for Thermodynamic Solar Applications, International Journal of Thermal Science 47-1676 (2008)
[39] N Zweibaum, RO Scarlat, PF Peterson, Verification and Validation of a Single-Phase Natural Circulation Loop Model in RELAP5-3D (2013)
[40] C Shi, M Cheng, G Liu, Development and Application of a System Analysis Code for Liquid-Fueled Molten Salt Reactors Based on RELAP5 Code, Nuclear Engineering and Design, 305 378-388 (2016)
[41] AM Pauzi, A Cioncolini, H Iacovides, Parametric Study of Natural Circulation Flow in Molten Salt Fuel in MSR, AIP Conference Proceedings 1659, 030004 (2015)

However, there are some problems with this study:

- The claim is made that no published results are available for the fluid as a heat source. The simulation uses a value of 1.9 W/m^3, but it is not clear how this value was determined. Operating data cited herein suggests 22.2 MW/m^3 for an MSR.
- The study uses the Boussinesq approximation throughout, which is only accurate for "small" temperature
- The tube (metal) temperature profile ranges from 730-1050K, which is well outside the recommended range for FLiBe of 797-936K.

The study shows that each of the 3000 tubes could produce 50kW of energy, for a total of 150MW for the overall design.

2.3.3 Simulations with Experimental Verification

It is difficult to achieve test conditions that reflect actual MSR parameters, due to the high temperatures and heat generation rates involved. For this reason, most experiments conducted for CFD verification were done using substitute coolants.

A small, square-path test loop[42] was built at the Ulsan National Institute of Science and Technology (UNIST) in Korea. It was built to study a prototype DRACS system for the KALIMER-600 sodium-cooled fast reactor. It measures 0.80 m high x 1.54 m wide, and uses 0.023 m (1 inch) ID tubing. The heater and cooler are located on the vertical runs, but there is only a very small difference in elevation (0.5 m). Further, the heater is a coil type that is external to the tubing. Thus, a little bit of heat goes to the environment, rather than the working fluid, so the test rig may not accurately model systems where the working fluid generates heat internally. The design was based on integral effects test (IET), separate effects test (SET) and compact integral effects test (CIET) facilities at the University of California-Berkley, University of New Mexico and Ohio State University. However, these are used to study pebble-bed configuration MSR performance. The test rig used

[42] Y Shin, SB Seo, IG Kim, IC Bang, Natural Circulation with DOWTHERM RP and its MARS Code Implementation for Molten-Salt Cooled Reactors, International Journal of Energy Research 40:1122-1133 (2016)

DOWTHERM RP as the working fluid, which requires similarity scaling to match key parameters (i.e., Pr, Ra, Gr, Re) of molten salt. Experiments were conducted with heat input varying from 60–300 watts. Simulations were done using the MARS thermal-hydraulic system analysis code and ANSYS-CFX (2016). MARS is based on the Reactor Excursion & Leak Analysis Program (RELAP5) and COolant Boiling in Rod Arrays-Two Fluid (COBRA-TF[43]) codes. Physical parameters entered into the CFD codes included temperature-dependent relations for density and thermal expansion, but not viscosity. CFD results differ from experimental results by a considerable amount (30%), with the ANSYS-CFX results being closer to experimental data, see Figure 2–1 below.

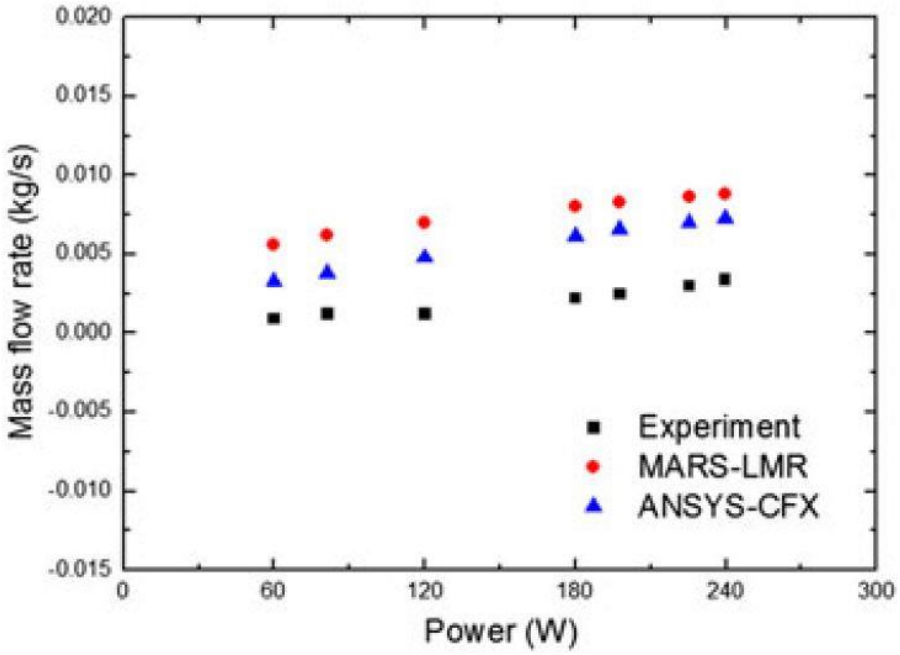

Figure 2–1 – MARS & ANSYS-CFX vs Experimental Data

DRACS systems are also studied at Genoa University's DIME-Tec Lab at Politecnico di Milano, as part of Italy's HORIZON 2020 program. The facility has two small natural circulation test loops. One (designated L2) is a 1 meter square-path loop, with 30 mm diameter tubing and a 2000-watt heater. The other (designated DYNASTY[44] – DYnamics of

[43] MJ Thurgood, et al, COBRA/TRAC – A Thermal-Hydraulics Code for Transient Analysis of Nuclear Reactor Vessels and Primary Coolant Systems, NUREG/CR-3046 – PNL-4385 (1983)
[44] A Cammi, et al, DYNASTY: An Experimental Loop for the Study of Natural Circulation with Internally Heated Fluids, 12th International Conference on Heat Transfer, Fluid Mechanics & Thermodynamics (2016)

NAtural circulation for molten SalT internallY heated), is a 38 mm diameter, 2.4 m wide x 3.2 m high rectangular-path loop with heaters that can be set from 0.5–10kW. Both use Hitec ® (a specially designed trinary sodium & potassium salt mixture) as the working fluid, and can model internal heat generation. Unfortunately, in both of these test rigs, the heat source and cooler are located on the horizontal runs of piping. Chapter 4 herein discusses why this results in unstable counter-flow in the vertical pipes, producing chaotic behavior[45]. Experimental results[46] confirm this. Simulations were done with a 1D "object-oriented" (O-O) code (based on the Modelica programming language), as well as the open-source CFD code, OpenFOAM. For the L2 rig, both the O-O and OpenFOAM CFD results match those from experiments, including capturing the unstable & chaotic behavior. However, for the DYNASTY rig, the O-O & OpenFOAM results are quite different, the O-O code not capturing the details of unstable (bi-directional) flow as well as OpenFOAM. While these results are indeed interesting from a certain viewpoint, it is not clear whether they have practical significance, since good engineering design practice should generally try to avoid unstable and chaotic phenomena.

Another small, square-path test loop[47] was built at the Bhabha Atomic Research Center (BARC) in Mumbai, India. It is 0.4 m high x 0.3 m wide, and uses 14 mm (1/2 inch Sch 40) ID tubing. Since the working fluid is LiF salt, the material used is Hastelloy-N, to avoid corrosion problems. It has six surface heaters, with a total power output of 500W. The heaters are located on a vertical run. The cooler is located on the upper horizontal run, which is sloped downward 5 degrees, to assist natural circulation. At the time of writing, experimental data were not available, but analytic values compared favorably with OpenFOAM CFD results. Simulations used the Boussinesq approximation for natural circulation, rather than curve fit values from experiments. Other fluid properties were considered constant (i.e., not varying with temperature). Simulations were done using an initial temperature of 600 °C (873.15K), but eventually the hot leg reached temperatures of

[45] Literature refers to this as the "Welander Problem," from P Welander, On the Oscillatory Instability of a Differentially Heated Fluid Loop, Journal of Fluid Mechanics 29:17-30 (1967)
[46] F Fanale, Development and Assessment of Computational Fluid Dynamics Models for the Study of Natural Circulation Dynamics, Thesis (2015)
[47] R Chouhan, et al, CFD Analysis of Molten Fluoride Salt Natural Circulation in Rectangular Loop, Thorium Energy Conference (2015)

about 960K, well above the recommended maximum value of 936K, so as to avoid material degradation. The steady state ΔT was 60°C and the maximum velocity achieved was only 0.024 m/sec, neither of which seem to take advantage of the full range of physical properties to make an efficient system. This is due to the very small relative difference in height between heater and cooler. A real, well-designed natural circulation system must have an adequate elevation difference. The study included transient simulations, which included heater startup and tripping, as well as a step increase from 50% power to 100% power.

Another small, square-path test rig was built at BARC (designated the Molten Salt Natural Circulation Loop – MSNCL)[48]. It is 2 m high x 1.5 m wide and uses 15 mm (1/2" Sch 80) ID tubing made from Inconel 625 (for corrosion reasons). One set of experiments used a 60:40 nitrate salt mixture of $NaNO_3$ and KNO_3 as the working fluid, which has a relatively low melting point. Heater output values of 1200-2000 W were used in the experiments, which consisted of both steady state and transient behavior, between 200–550 °C. The clever design allows the test rig to be configured with the heater & cooler in different configurations; i.e., on the horizontal or vertical tubing runs. This allows a variety of phenomena to be studied, although when located on the vertical sections, the elevation difference between heater and cooler is only 0.5 m. An in-house simulation code – Lead Bismuth Eutectic Natural Circulation Code (LeBENC) was previously developed and validated for the fluid contained in its name. It was readily adapted for use with the nitrate salt by changing the physical property variables within. Linear relations were used to express density, thermal conductivity and specific heat as a function of temperature, based on experimental data. A third order curve fit (rather than power law) was used for viscosity. Simulations for system startup, steady state, step power increase, heater trip, and loss of cooler events were conducted. With the exception of the heater trip, and to a lesser extent, the loss of heat sink (LOHS) CFD results compare very well with experimental data. See the last two plots in Figure 2–2 below. The deviation from experimental results in those cases was attributed to convective losses to ambient conditions.

[48] AK Srivastava, et al, Experimental and Theoretical Studies on the Natural Circulation Behavior of Molten Salt Loop, Applied Thermal Engineering 98:513-521 (2016)

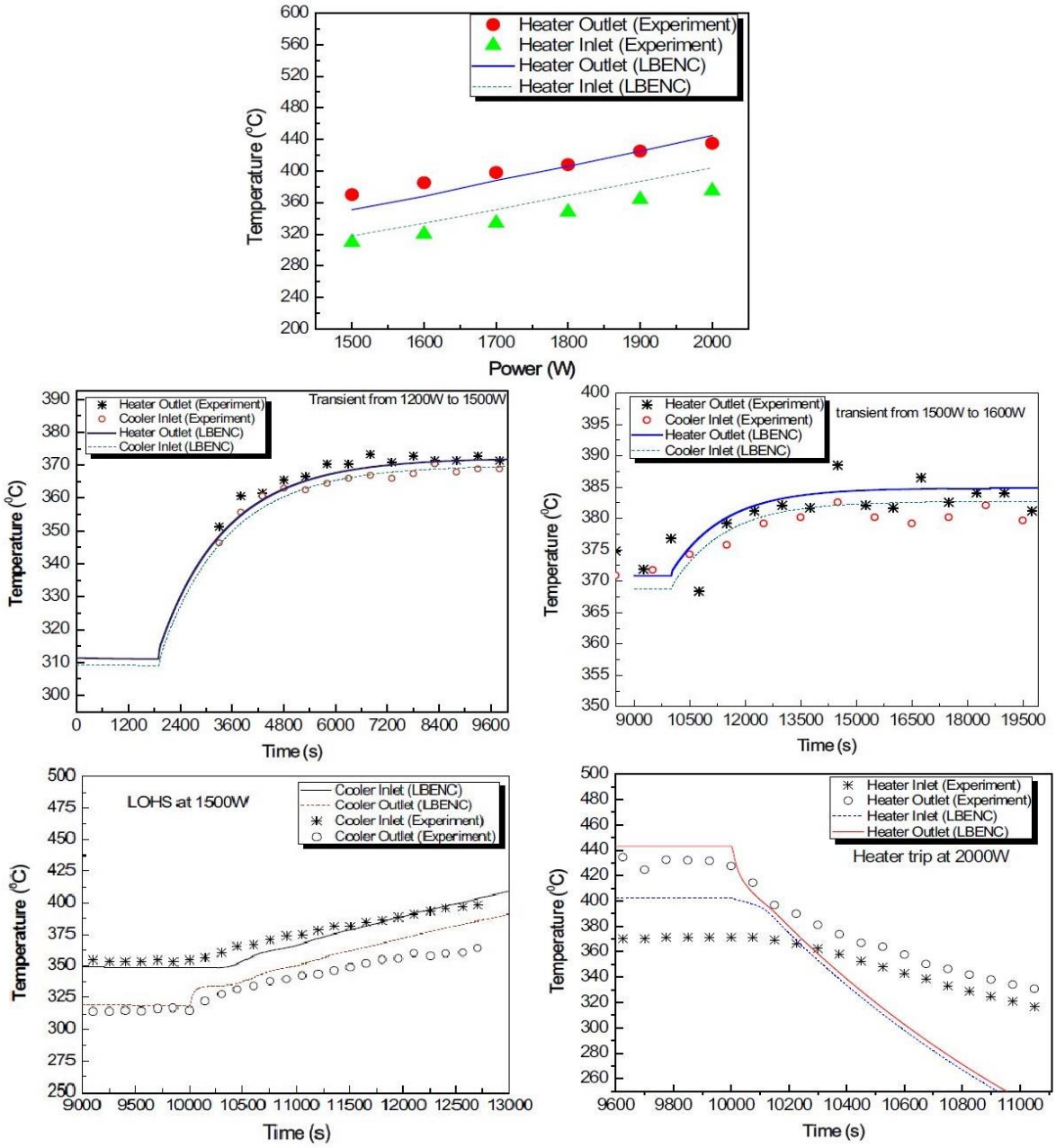

Figure 2–2 – LeBENC CFD vs Experimental Results

An interesting study was recently performed using the open-source OpenFOAM CFD code[49]. It models a small, rectangular-path natural convection loop, 2.2 m high x 1.42 m wide, with

[49] YS Jeong, SB Seo, IC Bang, Natural Convection Heat Transfer Characteristics of Molten Salt with Internal Heat Generation, International Journal of Thermal Sciences 129:191-192 (2018)

0.0269 m (1 inch) ID tubing. The experimental rig[50] was built at the BARC facility, where data were collected. The experimental rig can be operated with the heater and cooler on either the horizontal or vertical runs, thus several different configurations were studied. For the purpose of simulations related to the cited research, the heater & cooler were located on the vertical sections to avoid unstable flow conditions, with 0.83 m elevation difference between the two. Heat input of 1015 W was achieved using Nichrome wire wrapped around the tubing. For verification with experimental data, water was the working fluid. CFD results for the loop average temperature, system ΔT, and mass flow rate matched experimental values, within 20%. Simulations were then done with NaCl-KCl-(Pu, $^{238}U)Cl_3$ as the working fluid, with heat input from 51.3-460 kW. With a heater volume of 0.00415 m^3, this translates to power densities of 126.65-1108.77 MW/m^3, which seems unrealistically high. The interesting part of this study is the comparison of results for application of heat by external heat flux (EHF) vs internal heat generation (IHG). Figure 12 of the study (shown as Figure 2–3 below) shows the difference in temperature profiles and thermal & momentum boundary layer (BL) features, which are likely intuitively obvious for those with heat transfer experience. What may not be so obvious is how much this in turn affects the mass flow rate, velocity profile and Nusselt numbers of the system. These are shown in Figures 10, 13 and 11 of the study, respectively, which are shown in composite Figure 2–4 below. The most striking of these comparisons is the Nusselt number, which varies by almost two orders of magnitude.

Something worth noting from this study is from Figure 3 therein, which shows a cross-sectional view of the mesh for one of the simulations, repeated in Figure 2–5 below. Element density near the pipe wall would seem to be able to capture boundary layer effects. However, for some reason, there is an uneven distribution of nodes around the OD. Further, elements in the center part of the flow exhibit distortions, high aspect ratio and/or skewness. Some CFD utilities can evaluate and report element quality, to help users correct such conditions when they inevitably occur. The key takeaway from this research is the

[50] PK Vijayan, et al, Investigations on the Effect of Heater and Cooler Orientation on the Steady State, Transient and Stability Behavior of Single-Phase Natural Circulation in a Rectangular Loop, BARC/2001/E/034 (2001)

importance of modeling MSR heat sources as internal generation, rather than as an externally applied heat flux.

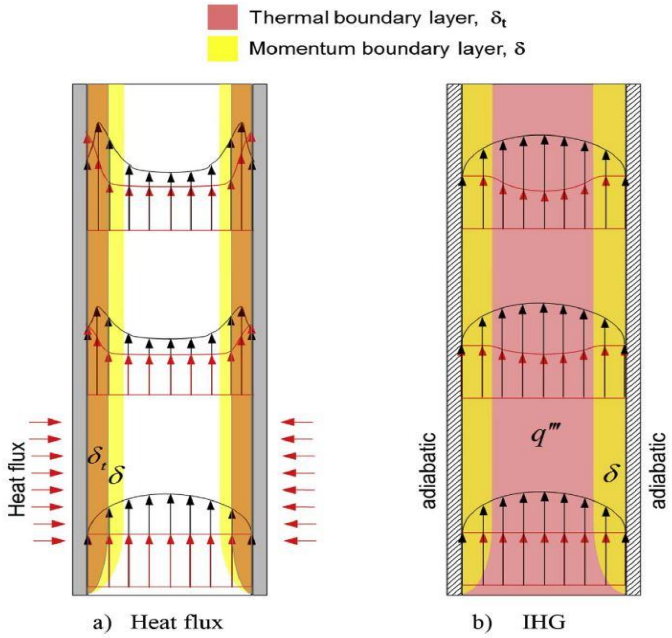

Figure 2–3 – EHF vs IHG – Temperature & BL Features

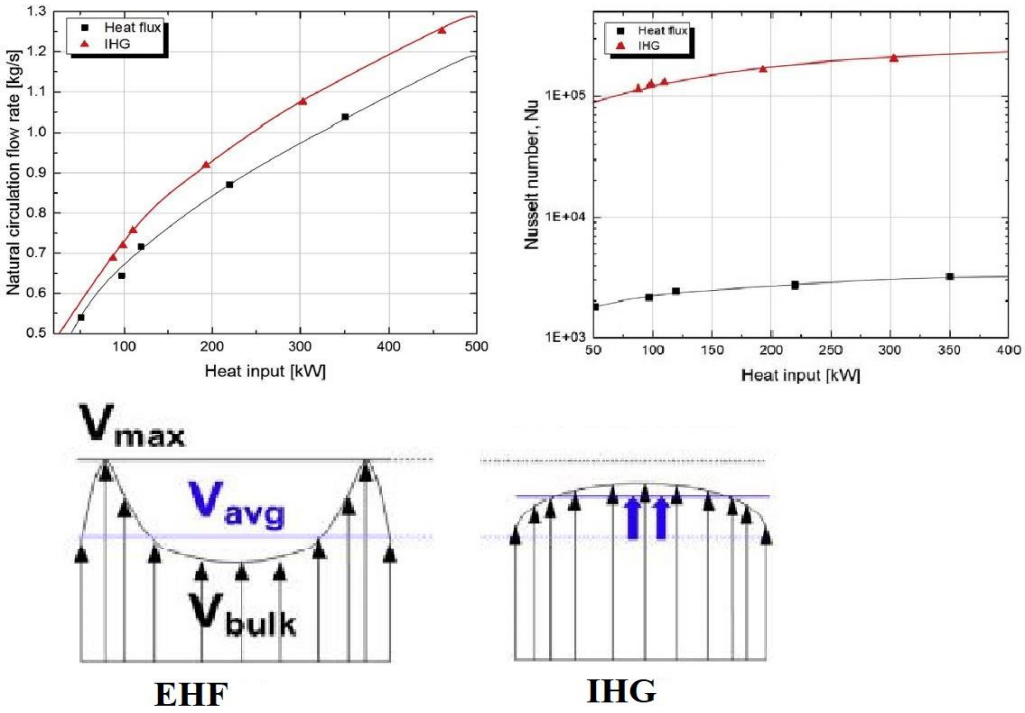

Figure 2–4 – EHF vs IHG – Flow Rate, Velocity & Nusselt Number

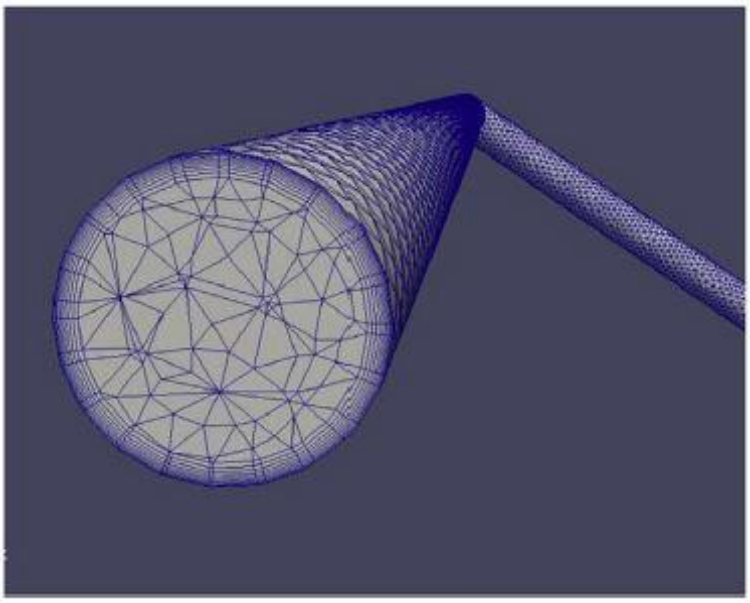

Figure 2–5 – BARC CFD Mesh

2.4 Comments

As previously mentioned, numerous design studies and experiments were conducted in the early years of MSR development. These produced lots of valuable results and lessons learned, some of which seems to have been overlooked in the design of recent experiments. These include nominal values for power density of fuel salt, recommended maximum and minimum temperatures, relative elevation difference, and pipe diameter studies for realistic natural circulation systems, which should be part of the design basis.

Very few of the previous studies used proprietary and/or specialized codes to conduct research. Many used open source codes (i.e., OpenFOAM) for CFD. It is worthwhile to note that some companies offer student versions of their commercial CFD software for academic purposes. While these versions come with fewer features and/or limitations on the number of elements/nodes, students and academic institutions can produce interesting and valuable results that contribute to the overall knowledge in this field with rather modest resources.

It is worthwhile to note that most of the recent papers include some kind of verification information; e.g., results are presented for several grid densities. However, some details seem to be left for the reader to discern, such as whether the selected variables show monotonic or cyclic convergence. Few quantify estimated uncertainties in the simulations or address uncertainties in the experimental data (i.e., instrument tolerance, etc.).

2.5 Unique Aspects of the Current Research

Tasks and goals of this dissertation start with fundamental results and lessons learned from initial concept and design studies conducted in the early years of MSR development, with respect to the relative elevation difference between the reactor vessel (heat source) & cooler (heat sink), pipe diameter, power density, etc., so as to provide information about realistic natural circulation systems (i.e., DRACS & power plants).

Previous design analyses are based on an assumed/desired temperature range (ΔT) (see sections 1.5 & 3.5 herein). Subsequent calculations for mass & volumetric flow rate, friction losses, etc. are based on being able to achieve that temperature range. However, it cannot be assumed that the chosen temperature range will be achievable under internal heat generation conditions in an MSR, due to residence times within the reactor and heat exchanger. The current research does not fix (or assume) the minimum & maximum temperatures. Rather, heating & cooling rates are determined by the power density within the reactor & heat exchanger. Residence times are determined by the resulting velocity caused by adding and removing heat.

This research starts with simple shapes, fluids, and schemes for entering physical property data. Simulations using fuel salt include temperature-density relations, rather than the Boussinesq approximation. All simulations herein use internal heat generation, rather than externally applied heat flux. Later simulations use more complex expressions for internal heat generation (variable power density), which account for negative temperature coefficient effects found in actual reactors with this inherent safety feature. No other research includes this feature.

The current research includes CFD results for the Test Rig in Idaho Falls. It has 2-1/2" diameter pipe, a 4 kW heater, and stands almost 18 feet (5.5 m) high. Further details are presented in Chapter 6 herein. The heater & cooler are both located on the vertical piping runs, so as to eliminate counter-flow and unstable/chaotic flow. The relative elevation difference is maximized, so as to study realistic systems. CFD results will be compared with analytic values. Experimental results (when available) can be compared to those from CFD.

The current research also attempts to provide CFD results for a reactor vessel that uses internal graphite bars as a moderator, and finally one that uses an external reflector (i.e., no internal structure). The latter case is from a proposed design, developed at Idaho Falls.

3 First Principles and Governing Equations

3.1 Abstract

This chapter provides:

- A review of the governing equations for conservation of mass, momentum and energy.
- A review of the equations for natural convection flow and the balance between the available head for flow and friction losses.
- Simplifications that can be applied, such as symmetry, and basic information for necessary approximations, such as turbulence models for CFD.

3.2 Conservation of Mass – Continuity

For a fluid passing through an infinitesimal, fixed-size control volume, the following (Eulerian) equation expresses conservation of mass (continuity)[51]

$$\frac{\partial \rho}{\partial t} + \boldsymbol{\nabla} \cdot (\rho \boldsymbol{v}) = 0 \qquad \textbf{(3.1)}$$

where

ρ is the fluid density = $\frac{m}{\forall}$

$\boldsymbol{v}$ is the fluid velocity vector

The first term in this equation is the rate of density increase within the control volume. The second term is the rate of mass flux passing out through the control surface (the boundary of the control volume) per unit volume. In a Cartesian coordinate system, this becomes[52]

$$\frac{\partial \rho}{\partial t} + \frac{\partial}{\partial x}(\rho u) + \frac{\partial}{\partial y}(\rho v) + \frac{\partial}{\partial z}(\rho w) = 0 \qquad \textbf{(3.2)}$$

[51] R. Pletcher et al, Computational Fluid Mechanics and Heat Transfer (3rd Ed), equation 5.1 (2013)
[52] IBID, equation 5.4

Using the product rule, equation 3.2 expands to

$$\frac{\partial \rho}{\partial t} + \rho \frac{\partial u}{\partial x} + u \frac{\partial \rho}{\partial x} + \rho \frac{\partial v}{\partial y} + v \frac{\partial \rho}{\partial y} + \rho \frac{\partial w}{\partial z} + w \frac{\partial \rho}{\partial z} = 0 \qquad \textbf{(3.3)}$$

Then, after regrouping,

$$\left[\frac{\partial \rho}{\partial t} + u \frac{\partial \rho}{\partial x} + v \frac{\partial \rho}{\partial y} w \frac{\partial \rho}{\partial z}\right] + \rho \left(\frac{\partial u}{\partial x} + \frac{\partial v}{\partial y} + \frac{\partial w}{\partial z}\right) = 0 \qquad \textbf{(3.4)}$$

The first group on the LHS is the time-material (substantial) derivative of a chosen physical quantity (*)[53]

$$\frac{D}{Dt}(*) = \frac{\partial}{\partial t}(*) + \boldsymbol{V} \cdot \boldsymbol{\nabla}(*)$$

This is often used to express continuity in the following form[54]

$$\frac{D\rho}{Dt} + \rho(\boldsymbol{\nabla} \cdot \boldsymbol{V}) = 0 \qquad \textbf{(3.5)}$$

A major simplification exists when the working fluid is at a constant temperature and is a liquid (i.e., incompressible). In that case,

$$\frac{D\rho}{Dt} = 0$$

Thus, equation 3.4 would simplify to

$$\frac{\partial u}{\partial x} + \frac{\partial v}{\partial y} + \frac{\partial w}{\partial z} = 0$$

The fluid in an MSR is a liquid. However, its temperature varies between parts of the system, and the resulting changes in density (along with differences in relative elevation of system components) provide the driving force for flow. The equations for buoyancy-driven flow (i.e., natural convection) are discussed later in this chapter.

[53] IBID, equation 5.2
[54] IBID, equation 5.3

Strictly speaking, density within a control volume in the reactor core is also not constant due to nuclear reactions. Details about fission, neutron interaction and energy conversion can be found in numerous other sources. Note that the modeled system is shown in schematic form in Figure 1-14, which includes in-line fuel/fluid processing. Overall, the effect of density changes due to nuclear reactions is very small. Further, the composition of fuel remains relatively constant throughout the system from one cycle to the next, due to in-line processing. For the purposes of this research, the effect of density changes due to nuclear reactions is considered to have little effect and is neglected.

Note that other physical properties of fluids vary with temperature (not necessarily linearly). Thus, empirical relations and/or stochastic methods will be used to simplify simulations, as described elsewhere herein.

3.3 Conservation of Momentum

3.3.1 The Navier-Stokes Equations

Newton's second law applied to a fluid passing through an infinitesimal, fixed control volume yields the momentum equation[55]:

$$\frac{\partial}{\partial t}(\rho \boldsymbol{V}) + \boldsymbol{\nabla} \cdot \rho \boldsymbol{V}\boldsymbol{V} = \rho \boldsymbol{f} + \boldsymbol{\nabla} \cdot \boldsymbol{P}_{ij} \qquad \textbf{(3.6)}$$

The first term is the rate of increase of momentum per unit control volume. The second term the rate of momentum loss due to convection (per unit volume) through the control surface surrounding the control volume. Note that $\rho\mathbf{VV}$ is a tensor, so $\boldsymbol{\nabla}\cdot\rho\mathbf{VV}$ is not a simple divergence. Using tensor identities, it can be converted to[56].

[55] R. Pletcher et al, Computational Fluid Mechanics and Heat Transfer (3rd Ed), equation 5.8 (2013)
[56] IBID, equation 5.9

$$\boldsymbol{\nabla}\cdot\rho\boldsymbol{VV}=\rho\boldsymbol{V}\cdot\boldsymbol{\nabla V}+\boldsymbol{V}(\boldsymbol{\nabla}\cdot\rho\boldsymbol{V})=\rho u_i\frac{\partial u_i}{\partial x_i}+u_i\left[\left(u_i\frac{\partial\rho}{\partial x_i}\right)+\left(\rho\frac{\partial u_i}{\partial x_i}\right)\right]$$

$$=2\rho u_i\frac{\partial u_i}{\partial x_i}+{u_i}^2\frac{\partial\rho}{\partial x_i} \qquad \textbf{(3.7)}$$

The first term on the RHS of equation 3.6 is the body force per unit volume. In the case of convection-driven MSRs/MSBRs, the body force is gravity. The force per unit mass (***f***) becomes the acceleration of gravity vector (***g***).

The second term on the RHS represents the surface forces per unit volume. These forces are due to normal and shear stresses. For a Newtonian fluid[57]

$$P_{ij}=-p\delta_{ij}+\mu\left(\frac{\partial u_i}{\partial x_j}+\frac{\partial u_j}{\partial x_i}\right)-\frac{2}{3}\delta_{ij}\frac{\partial u_k}{\partial x_k} \qquad \textbf{(3.8)}$$

If we make the substitutions of equations 3.7 & 3.8 into equation 3.6, we obtain something like the Navier-Stokes equation

$$\frac{\partial}{\partial t}(\rho\boldsymbol{V})+2\rho u_i\frac{\partial u_i}{\partial x_i}+{u_i}^2\frac{\partial\rho}{\partial x_i}=\rho\boldsymbol{g}+\boldsymbol{\nabla}\cdot\left[-p\delta_{ij}+\mu\left(\frac{\partial u_i}{\partial x_j}+\frac{\partial u_j}{\partial x_i}\right)-\frac{2}{3}\delta_{ij}\frac{\partial u_k}{\partial x_k}\right]$$

For a Cartesian coordinate system, we recall and introduce the following stress terms

$$\sigma_{xx}=\frac{2}{3}\mu\left(2\frac{\partial u}{\partial x}-\frac{\partial v}{\partial y}-\frac{\partial w}{\partial z}\right)\quad\sigma_{yy}=\frac{2}{3}\mu\left(-\frac{\partial u}{\partial x}+2\frac{\partial v}{\partial y}-\frac{\partial w}{\partial z}\right)\quad\sigma_{zz}$$
$$=\frac{2}{3}\mu\left(-\frac{\partial u}{\partial x}-\frac{\partial v}{\partial y}+2\frac{\partial w}{\partial z}\right)$$

$$\tau_{xy}=\tau_{yx}=\mu\left(\frac{\partial u}{\partial y}+\frac{\partial v}{\partial x}\right)\quad\tau_{xz}=\tau_{zx}=\mu\left(\frac{\partial w}{\partial x}+\frac{\partial u}{\partial z}\right)\quad\tau_{yz}=\tau_{zy}=\mu\left(\frac{\partial v}{\partial z}+\frac{\partial w}{\partial y}\right)$$

[57] IBID, equation 5.15, from Boundary Layer Theory, H Schlichting (1968)

Then, one can rewrite equation 3.10 in conservation-law form, for each vector direction[58]

$$\begin{aligned}
&\frac{\partial \rho u}{\partial t}+\frac{\partial}{\partial x}(\rho u^2+p-\sigma_{xx})+\frac{\partial}{\partial y}(\rho uv-\tau_{xy})+\frac{\partial}{\partial z}(\rho uw-\tau_{xz})=\rho f_x \\
&\frac{\partial \rho v}{\partial t}+\frac{\partial}{\partial x}(\rho uv-\tau_{xy})+\frac{\partial}{\partial y}(\rho v^2+p-\sigma_{yy})+\frac{\partial}{\partial z}(\rho vw-\tau_{yz})=\rho f_y \\
&\frac{\partial \rho w}{\partial t}+\frac{\partial}{\partial x}(\rho uw-\tau_{xz})+\frac{\partial}{\partial y}(\rho vw-\tau_{yz})+\frac{\partial}{\partial z}(\rho w^2+p-\sigma_{zz})=\rho f_x
\end{aligned} \qquad \textbf{(3.9)}$$

When the gravity vector is along the –z axis

$$f_x = f_y = 0$$

Incorporating this result, with the relation of equation 3.6, and applying the product rule to the first terms on the LHS, the result is the conservation of momentum equations

$$\begin{aligned}
&\rho\frac{\partial u}{\partial t}-\frac{u}{c^2}\cdot\frac{\partial E}{\partial t}+\frac{\partial}{\partial x}(\rho u^2+p-\sigma_{xx})+\frac{\partial}{\partial y}(\rho uv-\tau_{xy})+\frac{\partial}{\partial z}(\rho uw-\tau_{xz})=0 \\
&\rho\frac{\partial v}{\partial t}-\frac{v}{c^2}\cdot\frac{\partial E}{\partial t}+\frac{\partial}{\partial x}(\rho uv-\tau_{xy})+\frac{\partial}{\partial y}(\rho v^2+p-\sigma_{yy})+\frac{\partial}{\partial z}(\rho vw-\tau_{yz})=0 \\
&\rho\frac{\partial w}{\partial t}-\frac{w}{c^2}\cdot\frac{\partial E}{\partial t}+\frac{\partial}{\partial x}(\rho uw-\tau_{xz})+\frac{\partial}{\partial y}(\rho vw-\tau_{yz})+\frac{\partial}{\partial z}(\rho w^2+p-\sigma_{zz})=-\rho g
\end{aligned} \qquad \textbf{(3.10)}$$

[58] IBID, equation 5.19

3.3.2 Turbulence Models

For slow-moving (laminar) flow, the Navier-Stokes equations may have a closed-form (analytical) solution. However, most flows of practical interest have turbulent flow, and thus can only be solved via numerical means.

> *"Turbulent fluid motion is an irregular condition of flow in which the various quantities show a random variation with time and space coordinates, so that statistically distinct average values can be discerned."*[59]

3.3.2.1 Aspects of Turbulence

A main feature of turbulent flow is a chaotic swirling motion, where vorticity can be quite intense. This occurs when a fast-moving flow passes over a solid surface, or when two neighboring flows pass by each other, moving in different directions.[60] One can observe the formation of large eddies, which then break down into smaller and smaller ones (i.e., an energy cascade), until finally the swirling motion is fully dissipated by friction (in the form of heat). Thus, turbulent fluid motion includes a wide range of temporal and spatial scales.[61]

3.3.2.2 The Impact of Turbulence on Simulations

Using numerical methods to solve fluid flow (i.e., CFD) requires the computational domain to be divided into discrete parts (discretization). For unsteady and transient flow, it also requires the specification of a time step. When the discretization and time steps are made infinitesimally small[62], this is known as Direct Numerical Simulation (DNS). This method requires vast computational resources; i.e., massively parallel processing, using ultra-fast processors, etc. Solutions require a great deal of time to achieve. Even so, DNS can only be used to solve for small domains, and very short duration time intervals. Thus, the DNS scheme is not practical for the current research.

---

[59] Turbulence, J Hinze (1975)
[60] Turbulence Modeling for CFD, D Wilcox (1998)
[61] Analysis of Turbulent Boundary Layers, T Cebici, A Smith (1974)
[62] For example, a length scale equal to the molecular mean free path.

The development and refinement of turbulence models has been going on for decades. It is a broad & expansive topic, with too many details to cover herein. Essentially, each term for a fluid flow property is broken down into two: one for its time-averaged value, and another term to represent fluctuations from the average. This leads to the Reynolds-averaged Navier-Stokes equation (RANS, in tensor form[63]).

$$\rho\frac{\partial u_i}{\partial t}+\rho u_j\frac{\partial u_i}{\partial x_j}=-\frac{\partial p}{\partial x_i}+\frac{\partial}{\partial x_j}\left(2\mu s_{ji}-\rho\overline{u'_j u'_i}\right)$$

Where

$s_{ij}=\frac{1}{2}\left(\frac{\partial u_i}{\partial x_j}+\frac{\partial u_j}{\partial x_i}\right)$ Strain-rate tensor, and

$-\overline{u'_i u'_j}=\tau_{ij}$ Time-averaged Reynolds stress tensor

The time-averaging process always results in more unknowns than there are equations to solve. This is the so-called closure problem.

There are several schemes that can be used to provide closure; 1-equation, 2-equation, large-eddy simulation (LES), detached eddy simulation (DES), etc. Each of these use assumed values for certain variables, then solving for the rest. In order to determine appropriate assumed values, CFD results are compared with experimental results.

Experimental results can also be evaluated using Fourier analysis, which provides frequency and wavelength information.[64] Information gathered over many experiments is applied to simulations.

Reasonable (i.e., achievable by practical means) values for minimum length, time and velocity can be determined using Kolmogorov's universal equilibrium theory[65]. It uses the turbulence kinetic energy per unit mass (*k*), which is transferred from larger eddies to smaller

[63] Turbulence Modeling for CFD, D Wilcox (1998)
[64] IBID
[65] Local Structure of Turbulence in Incompressible Viscous Fluid for Very Large Reynolds Number, AN Kolmogorov (1941)

ones, the rate at which larger eddies supply/generate that energy $\varepsilon = -\frac{dk}{dt}$, and the kinematic viscosity (ν). The relations for length, time and velocity (respectively) are as follows:

$$dx \equiv \left(\frac{\nu^3}{\varepsilon}\right)^{1/4}$$

$$dt \equiv \left(\frac{\nu}{\varepsilon}\right)^{1/2}$$

$$du \equiv (\nu\varepsilon)^{1/4}$$

It is worthwhile to note that the Kolmogorov length scale is orders of magnitude larger than the molecular mean free path, thus significantly reducing the computational resources required to obtain a solution.

When specifying the "final" (fine) grid/mesh size and time step, these values should be used to ensure the CFD results capture the most important aspects of the flow.

3.3.3 The k-ε Turbulence Model

Having defined the variables (k) and (ε) above, we now present one of the more popular and widely used turbulence models, the standard k-ε model[66]. This model describes how k (turbulence kinetic energy) and ε (energy dissipation rate) vary spatially and temporally, as follows[67]:

$$\frac{\partial k}{\partial t} + u_j \frac{\partial k}{\partial x_j} = \tau_{ij} \frac{\partial u_i}{\partial x_j} - \varepsilon + \frac{\partial}{\partial x_j}\left[\left(\nu + \frac{\nu_T}{\sigma_k}\right)\frac{\partial k}{\partial x_j}\right]$$

$$\frac{\partial \varepsilon}{\partial t} + u_j \frac{\partial \varepsilon}{\partial x_j} = C_{\varepsilon 1} \frac{\varepsilon}{k} \tau_{ij} \frac{\partial u_i}{\partial x_j} - C_{\varepsilon 2} \frac{\varepsilon^2}{k} + \frac{\partial}{\partial x_j}\left[\left(\nu + \frac{\nu_T}{\sigma_\varepsilon}\right)\frac{\partial \varepsilon}{\partial x_j}\right]$$

Where the kinematic eddy viscosity is defined as:

$$\nu_T \equiv \frac{C_\mu k^2}{\varepsilon}$$

[66] Application of the Energy Dissipation Model of Turbulence to the Calculation of Flow Near a Spinning Disc, BE Launder & BI Sharma (1974)
[67] Turbulence Modeling for CFD, D Wilcox (1998)

Values for the closure coefficients are as follows:

$$C_{\varepsilon 1} = 1.44 \quad C_{\varepsilon 2} = 1.92 \quad C_{\mu} = 0.09 \quad \sigma_k = 1.0 \quad \sigma_{\varepsilon} = 1.3$$

The mean eddy fluctuation frequency and turbulence length scale are (respectively):

$$\omega = \frac{\varepsilon}{C_{\mu} k}$$

$$l = \frac{C_{\mu} k^{3/2}}{\varepsilon}$$

Note that the reciprocal of the frequency is the turbulence time scale.

As previously mentioned, there are numerous turbulence models from which to choose. Some are better at simulating shear flow between two fluids, others are better at solving boundary layer flow around solid objects and still others do better at solving flows with compressible fluids. The k-ε turbulence model is chosen for this study, due to its general applicability.

3.4 Conservation of Energy

Similar to conservation of momentum, there is an equation for conservation of total energy of fluid passing through a control volume[68]

$$\frac{\partial E_t}{\partial t} + \boldsymbol{\nabla} \cdot E_t \boldsymbol{V} = \frac{\partial Q}{\partial t} - \boldsymbol{\nabla} \cdot \boldsymbol{q} + \rho \boldsymbol{f} \cdot \boldsymbol{V} + \boldsymbol{\nabla} \cdot (P_{ij} \cdot \boldsymbol{V}) \qquad \textbf{(3.11)}$$

where

(E_t) is the total energy per unit volume

$$E_t = \rho \left(e + \frac{V^2}{2} + g\Delta z + \cdots \right)$$

(e) is the internal energy per unit mass, the second term in parenthesis is kinetic energy, then potential energy, etc.

[68] IBID, equation 5.22

The first term on the LHS of equation 3.11 is the rate of increase in total energy in the control volume. The second term is the energy lost through convection through the control surface.

The first term on the RHS is the rate of heat production, either from internal or external sources. For an MSR, this refers to the internal heat generated by fission reactions & neutron thermalizing. There are no external sources of heat generation.

The second term on the RHS is the heat lost to the environment, through various means. The reactor vessel itself, and most of the other piping system components, will likely be buried and/or otherwise well-insulated. Thus, heat transfer via radiative means is considered negligible and will be ignored. However, there will be heat loss via conduction through the various components' surfaces.

Fourier's Law for conductive heat transfer applies, such that

$$\boldsymbol{q} = -k\boldsymbol{\nabla}T$$

where

k is the coefficient of thermal conductivity, and
T is the temperature

This is important for an MSR, because the values for thermal conductivity vary, based on the choice of materials used to build the reactor vessel and connecting systems. It is important to note that material strength (stress & stain) is not the only aspect to be considered. Resistance to corrosion must be considered, as well as resistance to damage caused by energetic particles (i.e., neutrons, fission fragments, etc.). These aspects will be discussed later herein.

Note that convective heat transfer was already identified on the LHS, via the second term. In an MSR, heat removed from the reactor vessel is transported to a heat exchanger. In a steady-state condition, the heat exchanger removes the same amount of energy as the reactor generates.

The third term on the RHS of equation 3.11 is the work done on the fluid in the control volume (per unit volume) by body forces. These include compression and gravity. Note that, unlike an engine, a natural circulation MSR has no moving parts (i.e., pistons, turbine blades, etc.). Thus, the only work done is by gravity via density changes, as previously discussed.

The fourth term is work done on the control volume by surface forces. These include shearing and friction losses at the interface with a solid boundary (wall). Thus, equation 3.11 is really the first law of thermodynamics; i.e., the increase of energy in the system is equal to the heat added plus the work done on the system[69].

Also, as before, equation 3.11 can be written in conservative form for Cartesian coordinates[70]

$$\begin{aligned}\frac{\partial E_t}{\partial t} - \frac{\partial Q}{\partial t} - \rho\left(f_x u + f_y v + f_z w\right) + \frac{\partial}{\partial x}\left(E_t u + pu - u\sigma_{xx} - v\tau_{xy} - w\tau_{xy} - w\tau_{xz} + q_x\right) \\ + \frac{\partial}{\partial y}\left(E_t v + pv - u\tau_{xy} - v\sigma_{yy} - w\tau_{yz} + q_y\right) \\ + \frac{\partial}{\partial z}\left(E_t w + pw - u\tau_{xz} - v\tau_{yz} - w\sigma_{zz} + q_z\right) = 0\end{aligned} \quad \textbf{(3.12)}$$

Note that $f_x = f_y = 0$ and $f_z = -g$ when gravity is oriented in the –z direction.

With no pressure sources (other than gravity)

$$\frac{\partial p}{\partial x} = \frac{\partial p}{\partial y} = 0$$

Thus,

$$\frac{\partial}{\partial x}(pu) = p\frac{\partial u}{\partial x} + u\frac{\partial p}{\partial x} = p\frac{\partial u}{\partial x} \quad and \quad \frac{\partial}{\partial y}(pv) = p\frac{\partial v}{\partial y} + v\frac{\partial p}{\partial y} = p\frac{\partial v}{\partial y}$$

Incorporating these and using Fourier's Law

[69] IBID, pg 252 summary
[70] IBID, equation 5.25

$$q_x = -k\frac{\partial T}{\partial x} \quad q_y = -k\frac{\partial T}{\partial y} \quad q_z = -k\frac{\partial T}{\partial z}$$

we obtain

$$\begin{aligned}\frac{\partial E_t}{\partial t} - \frac{\partial Q}{\partial t} - \rho g w + p\left(\frac{\partial u}{\partial x} + \frac{\partial v}{\partial y}\right) + \frac{\partial}{\partial x}\left(E_t u - u\sigma_{xx} - v\tau_{xy} - w\tau_{xy} - w\tau_{xz} - k\frac{\partial T}{\partial x}\right) \\ + \frac{\partial}{\partial y}\left(E_t v - u\tau_{xy} - v\sigma_{yy} - w\tau_{yz} - k\frac{\partial T}{\partial y}\right) \\ + \frac{\partial}{\partial z}\left(E_t w + pw - u\tau_{xz} - v\tau_{yz} - w\sigma_{zz} + -k\frac{\partial T}{\partial z}\right) = 0\end{aligned} \quad \textbf{(3.13)}$$

If we assume that all of the mass "lost" in the nuclear reactions eventually turns to heat (one way or another), then the expression for continuity (equation 3.7) can be solved for the change in (that part of the) energy over time and used for the change in heat energy, as follows

$$\frac{\partial E}{\partial t} = c^2\left(u_i\frac{\partial \rho}{\partial x_i} + \rho\frac{\partial u_i}{\partial x_i}\right) = \frac{\partial Q}{\partial t} \quad \textbf{(3.7a)}$$

Insert this result into equation 3.11 to obtain

$$\begin{aligned}\frac{\partial E_t}{\partial t} - c^2\left\{u\frac{\partial \rho}{\partial x} + v\frac{\partial \rho}{\partial y} + w\frac{\partial \rho}{\partial z} + \rho\left(\frac{\partial u}{\partial x} + \frac{\partial v}{\partial y} + \frac{\partial w}{\partial z}\right)\right\} - \rho g w + p\left(\frac{\partial u}{\partial x} + \frac{\partial v}{\partial y} + \frac{\partial w}{\partial z}\right) \\ + \frac{\partial}{\partial x}\left(E_t u - u\sigma_{xx} - v\tau_{xy} - w\tau_{xy} - w\tau_{xz} - k\frac{\partial T}{\partial x}\right) \\ + \frac{\partial}{\partial y}\left(E_t v - u\tau_{xy} - v\sigma_{yy} - w\tau_{yz} - k\frac{\partial T}{\partial y}\right) \\ + \frac{\partial}{\partial z}\left(E_t w + pw - u\tau_{xz} - v\tau_{yz} - w\sigma_{zz} + -k\frac{\partial T}{\partial z}\right) = 0\end{aligned} \quad \textbf{(3.14)}$$

The first term is the change in total energy per unit time. The second term ({} grouping) is the heat generated by nuclear reactions (the loss of mass converted to energy). Note that this grouping incorporates changes in density within the control volume. As previously stated,

density varies inversely with temperature. This is a very important aspect of reactor safety, known as a negative temperature coefficient. At low temperatures (higher density), more neutrons thermalize and interact with the fissile and fertile fuel, releasing energy. As the temperature increases, density is reduced. Thus, there is less chance for neutron interaction and thermalization, and more chances for neutrons to escape the reactor vessel. Overall, this reduces the amount of energy released, reducing the overall temperature. This will be discussed later herein.

The third term is potential energy due to gravity. The fourth term accounts for pressure changes as the fluid moves through the control volume.

The last three terms on the LHS are dissipative and include convective energy loss, normal & shear stress (friction losses) and conductive heat loss. However, it's important to note that there are spatial derivatives related to the total energy of a unit volume, specifically,

$$\frac{\partial}{\partial x}(E_t u), \quad \frac{\partial}{\partial y}(E_t v), \quad and \quad \frac{\partial}{\partial z}(E_t w)$$

Using the product rule, each of these become two terms; i.e.,

$$\frac{\partial}{\partial x}(E_t u) = \frac{\partial E_t}{\partial x} \cdot u + \frac{\partial u}{\partial x} \cdot E_t \qquad \textbf{(3.15)}$$

Obviously, there will be three such equations, to account for the three orthogonal direction vectors. The first term on the RHS of equation 3.15 accommodates changes in energy with respect to those vectors. This is important for an MSR, because the reactivity of the fuel also depends on its location within the reactor vessel. Neutrons that are emitted at the center of the vessel volume are more likely to be thermalized, which releases heat, and causes future fission reactions. Neutrons that are emitted near the vessel's walls can escape and be lost, without releasing heat or causing future fission reactions. Thus, in a real reactor, the energy released is not constant across the vessel (nor is the temperature).

Equation 3.14 includes aspects from continuity and conservation of momentum with energy (thermodynamics, heat transfer & nuclear reactions). It contains spatial and temporal derivatives. In the vast majority of cases of practical interest, the Navier-Stokes equations cannot be solved in closed form. Thus, simplifications and numerical models of section 2.3.2 are necessary.

3.5 Natural Convection Flow

Simply put, natural convection flow occurs in a system when buoyancy forces overcome friction forces.

Buoyancy forces (head pressure) originate from (are proportional to) changes in density (caused by the temperature difference in the working fluid) and a relative difference in elevation

$$p = \alpha_\rho \Delta T \Delta z \qquad \textbf{(3.16)}$$

Where α_ρ is the temperature coefficient of density [N/(m^3*K)].

In a typical design study, the choice of working fluid fixes the physical properties (i.e., temperature coefficient of density). Prudent (conservative) values for the minimum and maximum temperature are chosen, based on fluid properties and structural material limitations. Finally, an initial value for the relative difference in elevation can be chosen, and the result compared with the total friction forces.

The total friction loss in a typical MSR system consists of flow loss in the pipes, plus flow loss through fittings and entry/exit effects at transitions between different components, and the pressure drop through the heat exchanger

$$\begin{aligned} H_{Total\ Friction\ Loss} &= H_{Flow\ Loss} + H_{Fitting\ Loss} + H_{Heat\ Exchanger\ Loss} \\ &= f\frac{L}{d}\frac{v^2}{2g} + k\frac{v^2}{2g} + h_{HX} \end{aligned} \qquad \textbf{(3.17)}$$

The value for friction factor (*f*) can be estimated once the pipe material and fabrication method are known. The multiplier for fittings and components is normally determined by experiment, as is the value of head loss through a heat exchanger. Previous design studies (cited later herein) used a value for *k* of 1.6 in feasibility calculations.

The mass flow rate is determined by the required power, the temperature difference, and fluid properties

$$\dot{m} = \frac{P}{\Delta T \cdot c_P} \qquad \textbf{(3.18)}$$

The average velocity (*v*) is obtained by using density and a choice of pipe diameter (*d*).

As previously stated, natural convection flow occurs when the available head pressure exceeds the losses due to friction.

Such analytical methods are sufficient to arrive at meaningful conclusions for a design study. That is, they can determine the feasibility of a particular system to produce a desired power level. However, it's important to remember a few aspects about the equations used:

1) The equations use bulk/average values, whereas some properties (i.e., density, viscosity, heat capacity, etc.) vary with temperature and thus are not constant throughout the system.
2) One chooses the basis parameters for the analysis (specifically, the temperature change), which may not be achievable. At the required flow rate, is the residence time in the reactor vessel sufficient to achieve the desired ΔT? If the flow is too slow, the temperature increase of a fluid particle in the reactor vessel may exceed the chosen ΔT. If the flow is too fast, the temperature increase may be less than the required ΔT. The same questions can be asked regarding the heat exchanger's ability to extract the required thermal output.
3) The analytical method does not seem to account for recirculation within the reactor vessel itself, depending on its geometry. Such recirculation (if it exists)

would strongly affect the residence time in the reactor and thus the temperature of the resulting outflow. Several results herein do exhibit some recirculating flow.

4 First Simulation Results

4.1 Abstract

This chapter provides results for the first simulations of a simplified natural circulation system with internal heat generation. It uses simple/cylindrical shapes for the reactor vessel & heat exchanger, with water as the working fluid. Details & results include:

- Physical property data for water; i.e., density, viscosity, heat capacity, coefficient of thermal expansion.
- Size of the reactor vessel, heat exchanger, the relative elevation between the two, and the size of connecting pipes.
- General meshing techniques; i.e., edge sizing, number of nodes & elements.
- Operating conditions and initialization parameters for the simulation.
- Nominal velocity and temperature difference resulting from developing the desired power from the reactor system at different relative elevations.
- Comparison between CFD results and analytic solution for nominal velocity.

The purpose of these simplifications is to quickly determine the minimum required elevation difference needed to achieve realistic/useful temperatures & find the nominal pipe velocity. Such simple features and approximations will be improved upon to achieve the final result.

A total of 17 cases were run, starting at a relative height difference of zero feet, increasing by 12 inches (0.3048 m) in subsequent cases.

4.2 Reactor Vessel & Heat Exchanger Size, Elevation & Pipe Data

As previously stated, determination of the power density fixes the reactor vessel volume for a given desired output. A power density of 22.2 MW/m^3 requires a reactor vessel volume of 1.5 m^3 in order to obtain 10 MW_e, with 33.3% efficiency between thermal & electrical output.

The cylindrical reactor vessel & heat exchanger are identical in size & shape. The diameter and height is 48 inches (1.2192 meters), such that the aspect ratio is 1. These values were chosen so as to deal in round numbers. The resulting volume of each cylinder is 86,860 in^3 (1.4234 m^3), sufficiently close to the 1.5 m^3 target value so as to provide meaningful initial results. Identical (but opposite in sign) power density values will be used in both vessels.

A diameter of 12 inches (0.3048 m) was chosen for the connecting piping. This is a reasonable (standard) size, based on previously cited design studies. The horizontal distance between vessels is 50 inches (1.27 m), so as to minimize piping length and thus overall fluid system volume.

A 3D vertical half-section of the overall system was developed for each case, to take advantage of symmetry. Figure 4–1 shows the 3D model for Case #6.

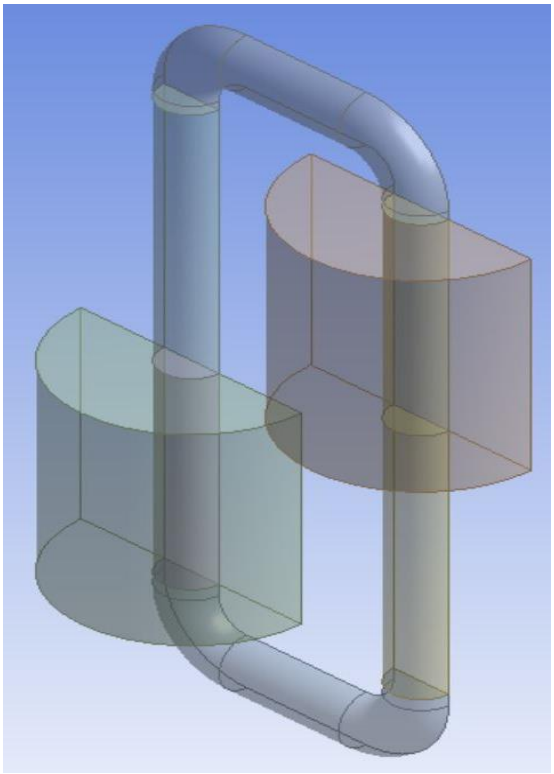

Figure 4–1 – 3D Model for Case #6

4.3 Why Elevation is Important

Recall that flow in a convection power plant is driven by difference in density, which is influenced by the difference in elevation of the components with different temperatures. That is, heat sources cause fluid to rise, while heat sinks cause it to fall.

In a trivial case, the reactor core (heat source and hottest part of the system) is located directly above the heat exchanger (heat sink and coldest part of the system), as shown in Figure 4–2 – Core Vessel (Hot) above HX (Cold). There is nowhere for hot fluid to rise, and nowhere for cold fluid to fall. Thus, no flow occurs, and no power/energy is extracted.

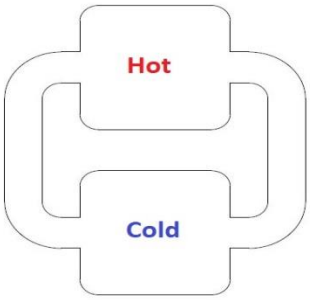

Figure 4–2 – Core Vessel (Hot) above HX (Cold)

Because flow is density/buoyancy-driven, the heat source cannot be located above the heat sink. One might think the opposite situation might produce the best results; i.e., when the reactor core is located directly below the heat exchanger (see Figure 4–3). However, this is not the case, because the hot fluid tries to move upward through both pipes and the cold fluid tries to move downward through both pipes. This means both pipes have two-fluid opposing shear flows, which is inefficient, due to dissipative (friction) forces.

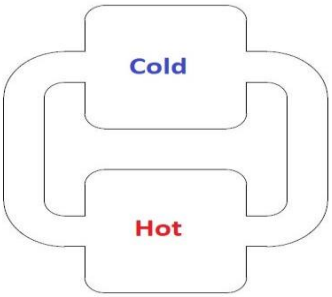

Figure 4–3 – HX (Cold) Directly Above Core Vessel (Hot)

This latter case was demonstrated experimentally[71], the experimental rig and schematic of which are shown in Figure 4–4.

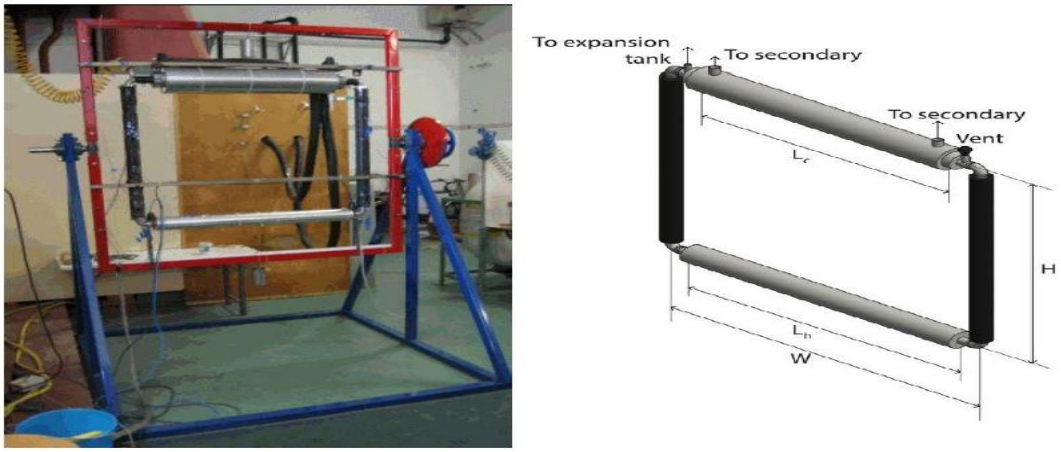

Figure 4–4 – Experimental Rig – Cold Above Hot

The cited document shows that this condition produces unstable flows; i.e., bi-directional oscillations in the vertically-oriented pipe sections. Figure 4–5[72] shows this effect, using non-dimensional parameters.

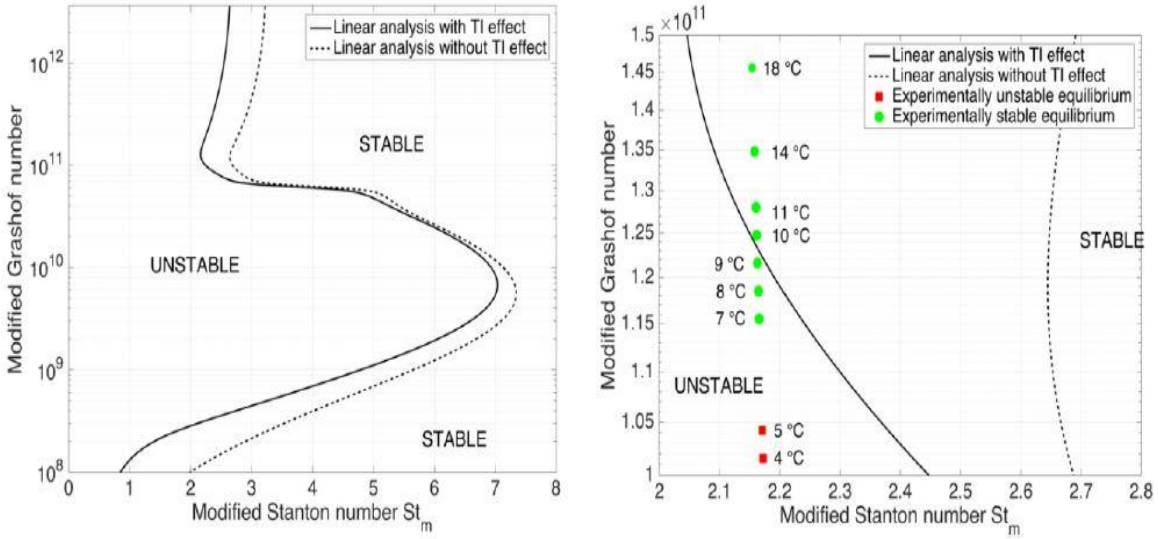

Figure 4–5 - Stable & Unstable Flow Regimes

[71] F Francesco, Development & Assessment of CFD Models for the study of Natural Circulation Dynamics, Master's Degree Thesis (2015)
[72] IBID

In the cited report, a 3D model was first created using ANSYS Workbench®[73]. It was converted for use in OpenFOAM®[74], a widely-used, open-source CFD code. Experimental results were compared to CFD and a simplified (1D) object-oriented (O-O) mathematical model[75]. Figure 4–6[76] shows these data, which bear the unmistakable mark of unstable (chaotic/random) flow. This is very undesirable for our MSR application. Those who have studied chaotic behavior may notice a resemblance to solutions of the Lorenz equation, but this was not mentioned in the cited report.

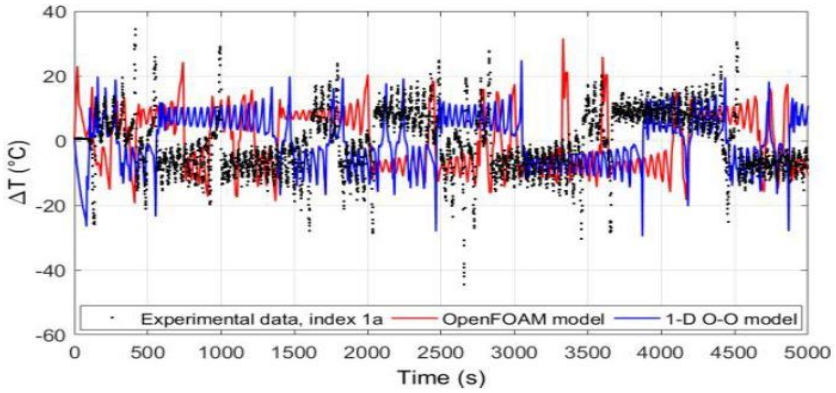

Figure 4–6 – CFD, 1D Model & Experimental Results

Clearly, the reactor core vessel (hot) and heat exchanger (cold) need to be located on separate vertical risers (piping runs). Figure 1-14 shows a block diagram of major MSBR components for the model simulated in the current research. The figure shows the reactor vessel & heat exchanger on separate vertical riser (pipe) runs, but, since it is a schematic, their relative height is not specified.

Previously cited designs wisely locate the reactor vessel (heat source) as low as possible, and the heat exchanger (heat sink) as high as practical, while minimizing overall fluid volume.

---

[73] ANSYS version 2016
[74] HG Weller, et al, A Tensorial Approach to Computational Continuum Mechanics Using Object-Oriented Techniques, COMPUTERS IN PHYSICS, VOL. 12, NO. 6 (1998)
[75] A Cammi, et al, The Influence of Wall Thermal Inertia Over a Single-Phase Natural Convection Loop with Internally Heated Fluids, Chemical Engineering Science (2016)
[76] F Francesco, Development & Assessment of CFD Models for the study of Natural Circulation Dynamics, Master's Degree Thesis (2015)

4.4 Overall Fluid Volume

Finding the initial volume (with zero elevation difference) is straightforward; it is 189,031 in^3 (3.097 m^3). This serves as a baseline value, from which subsequent cases can be compared. It is no surprise that volume increases linearly, in direct proportion to the elevation between vessels. This is an important consideration for MSR design, as increasing the volume of fuel salt adds to the operational expense and radiation hazard of the overall system.

4.5 Meshing Details

A structured mesh was imposed, to maintain sufficient control over this aspect during subsequent models, to ensure accuracy in the comparison of results. This consisted of using four sets of edge sizing controls, to help capture boundary layer effects. For the coarse mesh:

- The height of each vessel had 48 divisions, with a double-sided bias factor of 10.
- The OD and ID of both vessels had 36 divisions, with no bias factor.
- The pipe & vessel core diameters had 24 divisions, with a double-sided bias factor of 10.
- The reactor & heat exchanger (outside of the central area) had 24 divisions, with a one-sided bias factor of 10.

Figure 4–7 shows a portion of resulting coarse mesh for Case #10, with a total of 178,134 nodes and 158,526 elements.

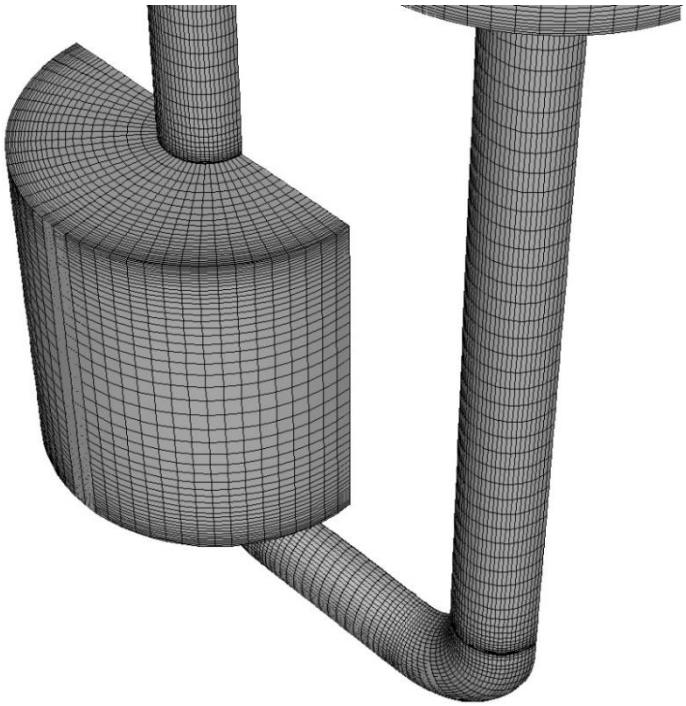

Figure 4–7 – Coarse Mesh – Case #10

4.6 Models & Materials Data

In the CFD program's Setup -> Models tab, the Energy option was turned on, and the Realizable k-ε turbulence model was selected. Gravity was turned on, and given the standard value of -9.81 m/sec^2 in the vertical direction (i.e., pointing downward). Based on a 400K nominal operating condition, the following values were entered into the CFD program via in the Setup -> Materials -> Fluid tab:

Table 4-1 – Physical Properties of Water @ 400K

Property & Units	**Relation Type**	**Value**
Density [kg/m^3]	Boussinesq	937.6
c_P (Specific Heat) [J/kg*K]	Constant	4182
Thermal Conductivity [W/m*K]	Constant	0.6
Dynamic Viscosity [kg/m*sec]	Constant	0.001003
Thermal Expansion Coefficient [1/K]	Constant	0.00086

4.7 Cell Zones & Boundary Conditions

As previously stated, energy sources were defined for the reactor vessel and heat exchanger, with a value of 22.2 MW/m^3. All interior elements were defined as fluid, with physical properties as noted above.

Boundary conditions were defined, selecting all the planar surfaces with symmetry, as well as selecting all the vessel and pipe outer surfaces as walls.

4.8 Operating Conditions, Solution Methods & Initialization

Under the Physics -> Operating Conditions tab, the options for steady-state and pressure-based were selected.

Under the Solution-> Methods tab, the following options were selected:

Table 4-2 – Solution Methods

Formulation	Implicit
Flux Type	Roe-FDS
Spatial Discretization	
Gradient	Least Squares Cell Based
Flow	Second Order Upwind
Turbulent Kinetic Energy	Second Order Upwind
Turbulent Dissipation Rate	Second Order Upwind

Controls were left in their default values, as were Equations and Limits. The target values for residuals were left in the default condition, with the exception of continuity, which was changed to 10^{-5}.

A Standard Initialization was chosen, with the following initial values:

Table 4-3 – Initialization Parameters

Parameter & Units	**Value**
Gauge Pressure [Pa]	0.0
X Velocity [m/sec]	0.1
Y Velocity [m/sec]	0.1
Z Velocity [m/sec]	0.1
Turbulent Kinetic Energy [m^2/sec^2]	0.1
Turbulent Dissipation Rate [m^2/sec^3]	0.1
Temperature [K]	323.15

Note that starting the solution process resembles that for an actual power plant; i.e., once a nominal temperature is achieved, one starts adding heat in the reactor and removing heat in the heat exchanger. Before starting the solution process, the mesh and case were checked for errors & suggestions. When found, these were implemented. The initial number of iterations was set to a few hundred, to ensure stability, and then later increased as needed.

It is also important to note that no assumptions were made as to the resulting overall steady-state behavior. That is, the hot fluid was not given an initial upward velocity, nor was the cold fluid given an initial downward velocity. Thus, the computational method determines the fluid behavior on its own, using natural/physical laws.

4.9 Delta T & Nominal Velocity Data Results

Once a stable solution was achieved, a plot of temperature contours at the symmetry plane was selected, and the temperature difference across the two vessels was obtained. Figure 4–8 shows example results for the coarse mesh of Case #10, with temperatures annotated.

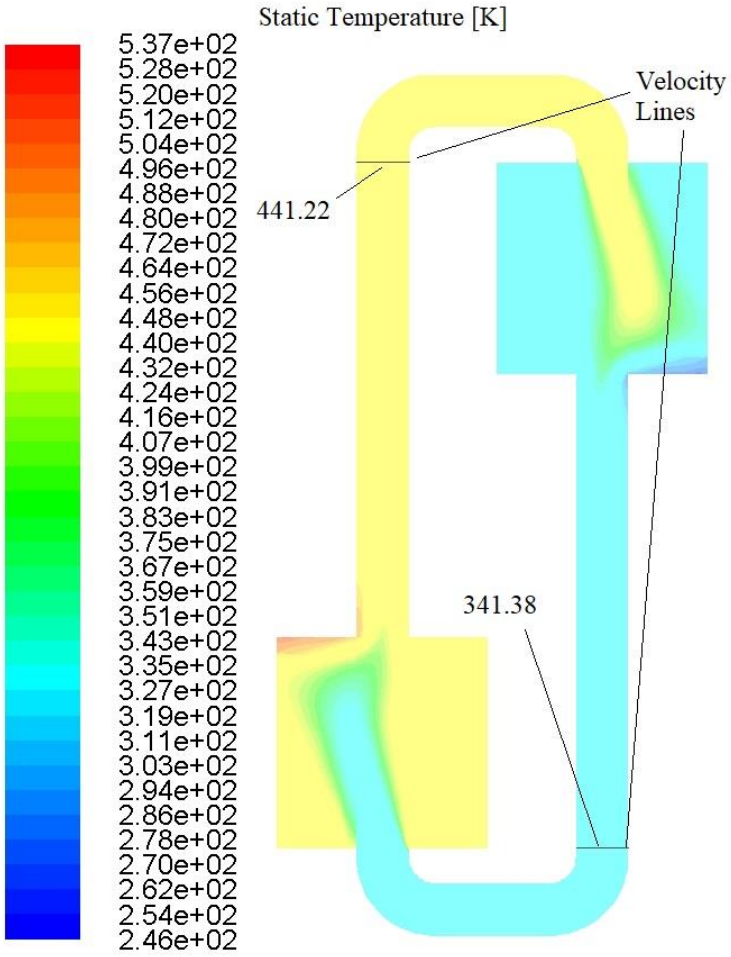

Figure 4–8 – Temperature Contours – Symmetry Plane – Case #10

Imaginary lines were drawn across the pipe (from wall to wall), so a velocity profile could be obtained. The locations are shown in Figure 4–8. Figure 4–9 shows the velocity profile obtained for Case #10, to demonstrate how the values were obtained. The weighted average velocity for Case #10 is 1.0853 m/sec. The shape of the velocity profile is not parabolic, as it would be for laminar flow. The range of Reynolds numbers for these simulations is 150,000 to 390,000, which tends to justify the use of a turbulence model.

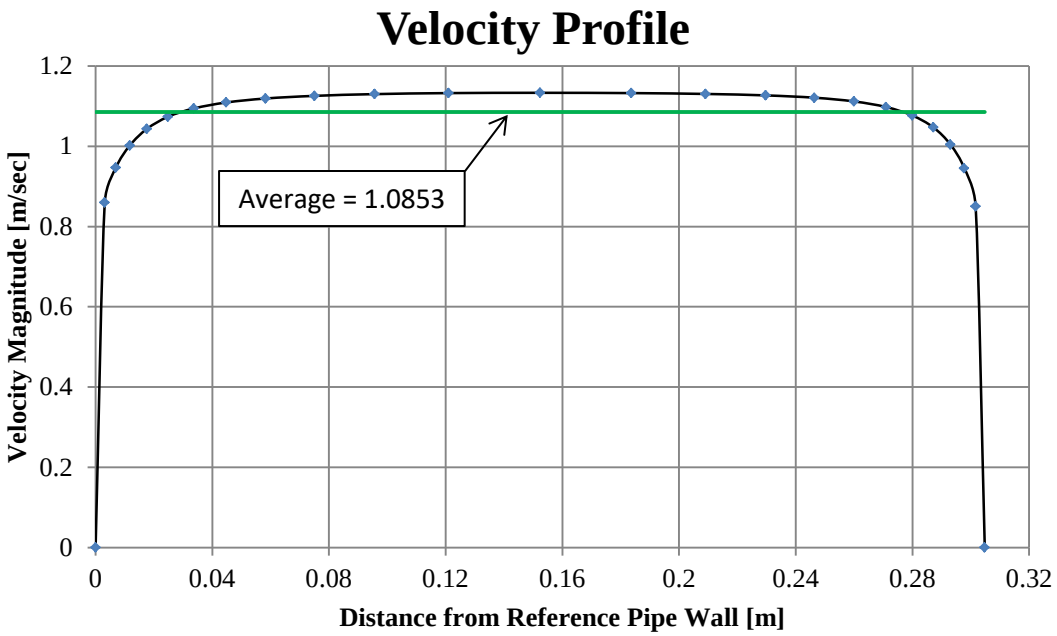

Figure 4–9 – Velocity Profile – Case #10

The same techniques, parameters, solution methods, etc., were used to obtain temperatures and average pipe velocity for each of the 17 cases, based on relative elevation difference, starting with zero as Case #1. However, equation 3.16 suggests that as the difference in elevation approaches zero, the difference in temperature must increase without bound in order to achieve any buoyancy forces. The simulation shows this, giving unstable solution behavior. Thus, Case #1 is omitted in the overall results.

The following table summarizes the hot & cold temperature data, the resulting ΔT, and the average pipe velocity for Cases 2 through 17.

Table 4-4 – Summary of CFD Results

Case	T_{hot} [K]	T_{cold} [K]	ΔT [K]	v_{avg} [m/sec]
2	470.76	316.23	154.522	0.5362
3	465.96	331.38	134.589	0.6514
4	463.16	335.26	127.907	0.7608
5	455.16	330.51	124.646	0.8353
6	452.23	337.49	114.745	0.8902

Case	T_{hot} [K]	T_{cold} [K]	ΔT [K]	v_{avg} [m/sec]
7	450.23	340.52	109.706	0.9556
8	452.23	344.14	108.083	1.0429
9	446.1	340.29	105.81	1.0768
10	441.22	341.38	99.839	1.0853
11	435.54	340.62	94.9201	1.1281
12	436.43	342.84	93.5905	1.2314
13	437.29	345.07	92.2235	1.2605
14	436.52	346.72	89.8038	1.2905
15	437.06	350.35	86.713	1.3188
16	436.5	349.05	87.4498	1.3374
17	430.66	345.06	85.6088	1.3512

Figure 4–10 presents these data in graphical form, to show how the values change/trend with increasing elevation. Note that the trend lines are not intended to be analytical – they just show the general trend of the data.

The results show that as the difference in elevation increases, the fluid velocity increases, as one would expect. As the fluid velocity increases, the temperature difference decreases, also as one would expect. However, note that in both cases there is a point of diminishing return; i.e., there is less & less change in ΔT & velocity with increasing elevation. This implies that the difference in elevation should only be as much as really needed.

Another important evaluation aspect is the target ΔT for the working fluid. In these simple simulations, one could establish a maximum practical ΔT for water of 95°C (an optimal range between freezing & boiling). The graph of Figure 4–10 shows (with a green line) that this is not achieved until the elevation exceeds 3.2 meters (10.5 feet). This is an important consideration for an MSR, due to restrictions on the low & high temperatures; to prevent salt freezing & structural material damage, respectively. Results below this height lead to an excessive temperature range, which is not achievable at atmospheric pressure.

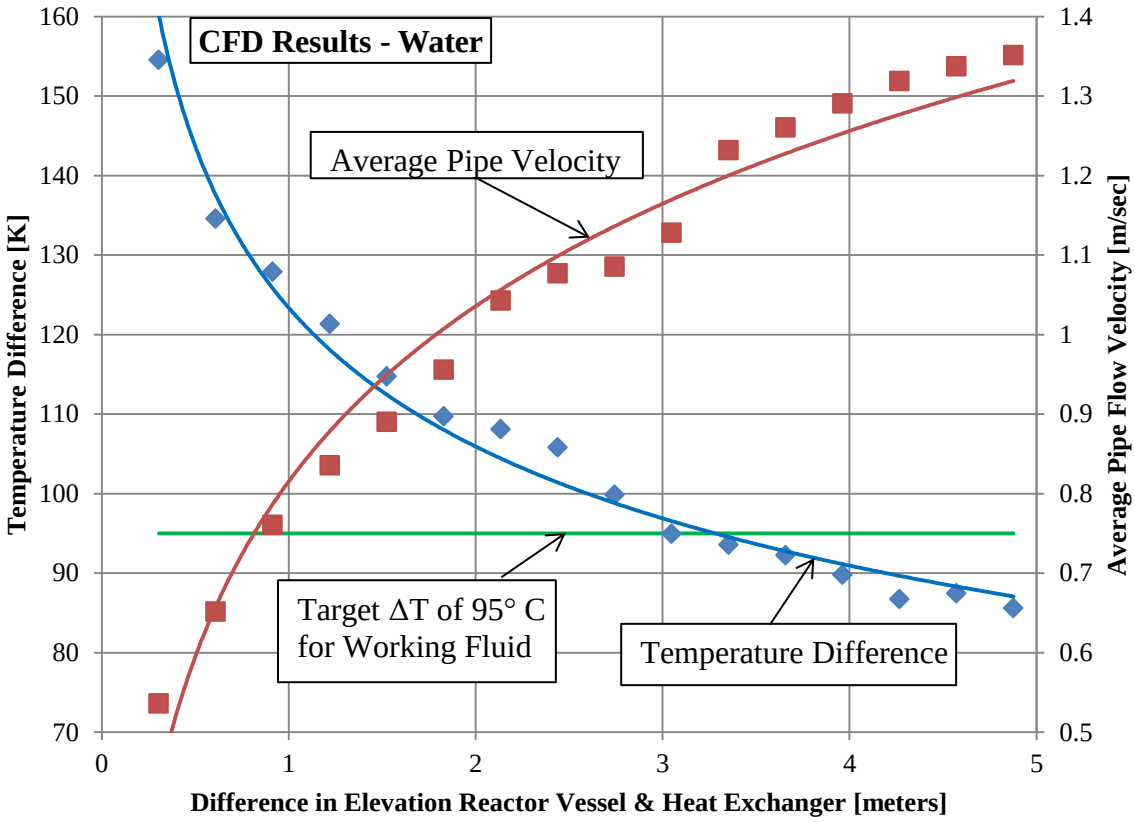

Figure 4–10 – Graphical Summary of CFD Data

Figure 4–11 shows the temperature profile at the symmetry plane for Case #17, which has the highest system velocity. Notice how a significant amount of the hot fluid entering the top of the heat exchanger simply passes right through without being cooled. The same condition exists at the reactor vessel; i.e., cold fluid entering at the bottom just passes through without being heated. Figure 4–12 shows a group of path lines originating at the elbow above the reactor vessel. They show that a significant number go right through the heat exchanger. This emphasizes a very important aspect of reactor system design & performance; i.e., residence time in the reactor vessel & heat exchanger. In these simple simulations, neither the reactor vessel nor heat exchanger has any internal structure. Thus, the fluid is free to flow through both vessels unimpeded. This feature will be addressed in the more complex simulations that follow.

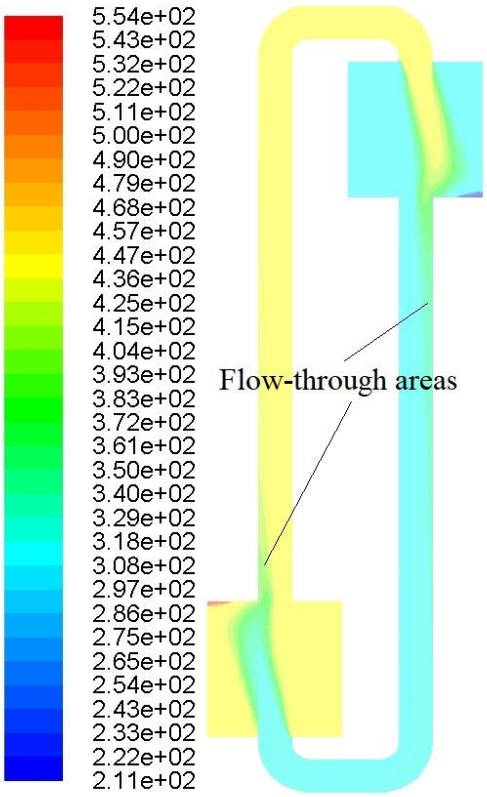

Figure 4–11 – Flow-Through Areas – Case #17

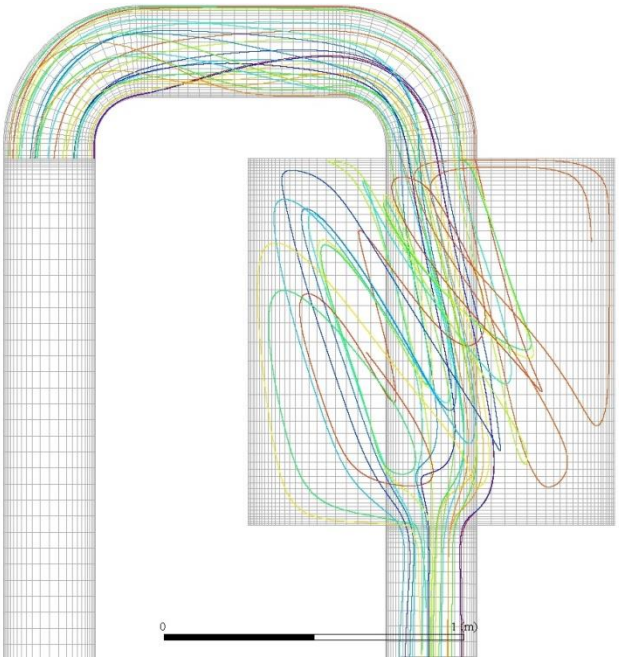

Figure 4–12 – Path Lines – Case #17

4.10 Comparison of CFD & Analytic Results

4.10.1 General Results

Equation **3.18** can be used to determine the required mass flow rate for a given fluid, given the desired power output and the temperature difference achieved by the system. Using the average fluid density, one can obtain an average pipe velocity, for comparison with the CFD values. Figure 4–13 shows the results for all cases. Recall that the Boussinesq approximation is valid for "small" temperature difference, which occurs at higher velocities. Thus, at low velocities, CFD results deviate more from the analytic values.

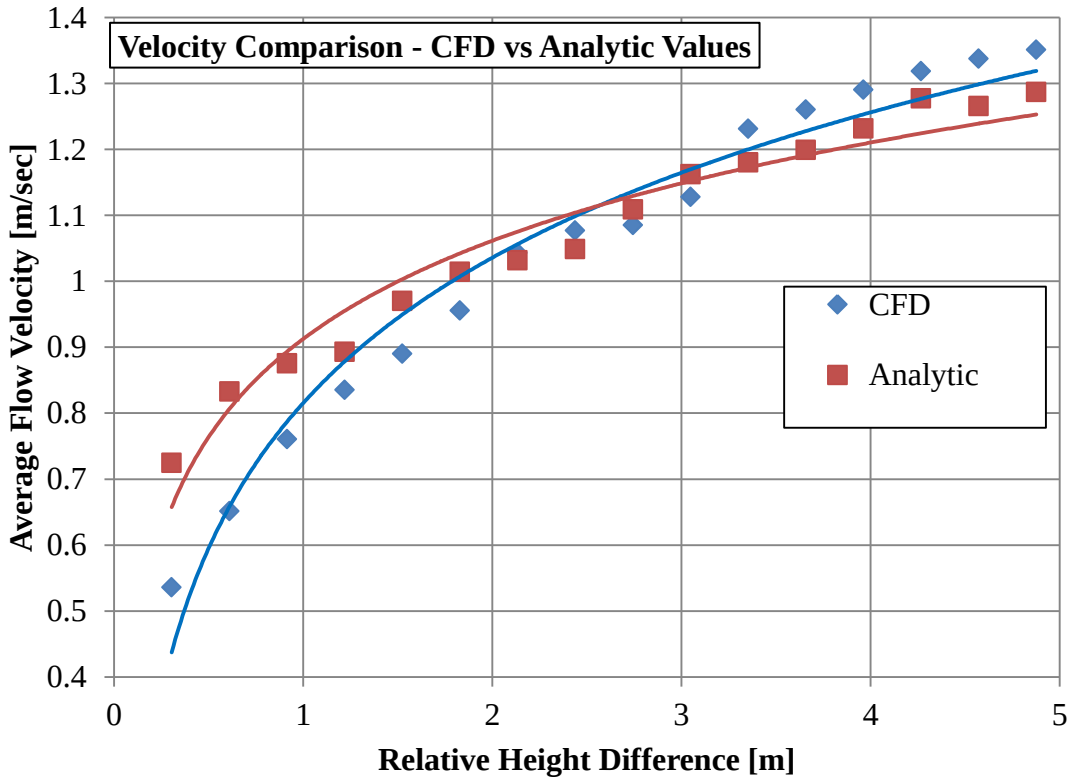

Figure 4–13 – Velocity Comparison – CFD vs Analytic Values

The mean absolute percentage error between CFD and analytic values for relative elevations 10 feet and above is 4.434%, which corresponds to 0.0547 m/sec.

4.10.2 Recirculation & Entrance Effects

In section 3.5 herein, with respect to equation **3.17**, it was noted that a value for *k* of 1.6 was used in feasibility calculations. This is to account for the pressure drop/loss as fluid moves from a (large) vessel into a (smaller) pipe and vice versa. It also accounts for pressure drop/loss as fluid moves through an elbow. CFD shows the resulting flow features that contribute to this phenomenon. Specifically, there are areas of recirculating flow, which dissipate flow energy. Figure 4–14 shows areas of recirculating flow at the pressure vessel outlet (left) and the heat exchanger vessel inlet (right).

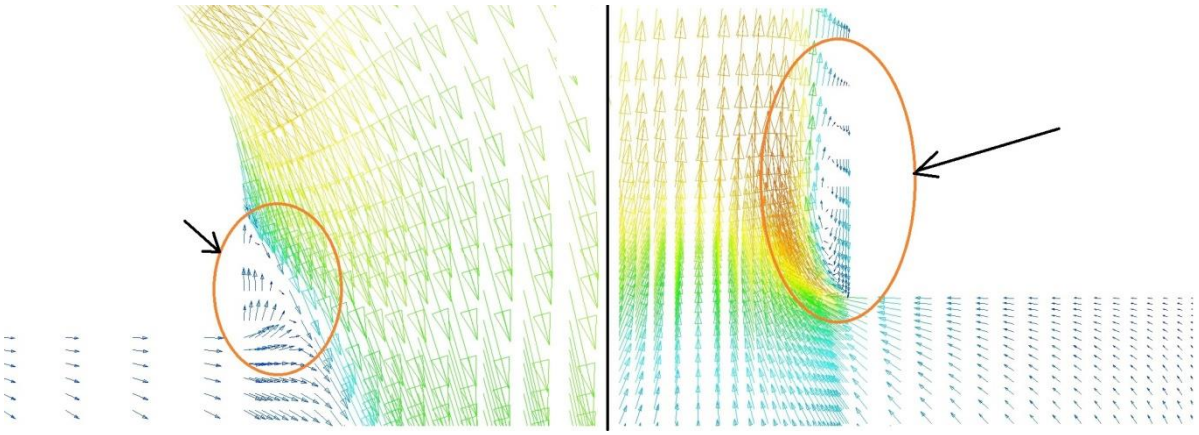

Figure 4–14 – Areas of Flow Recirculation

Due to the square corners of the reactor vessel and heat exchanger, values for *k* of between 1.8 (at low velocity) and 2.3 (at high velocity) provide good agreement.

4.11 CFD-Specific Information

4.11.1 Mesh Evaluation – Resolving Boundary Layer

A plot of y+ values for the hot & cold cylinder walls is shown in Figure 4–15. A total of 16,499 points exist for the fine mesh. Of these, 15,095 had y+ values ≤5 (91.5%). Thus, the mesh does a nominally adequate job of capturing boundary layer effects.

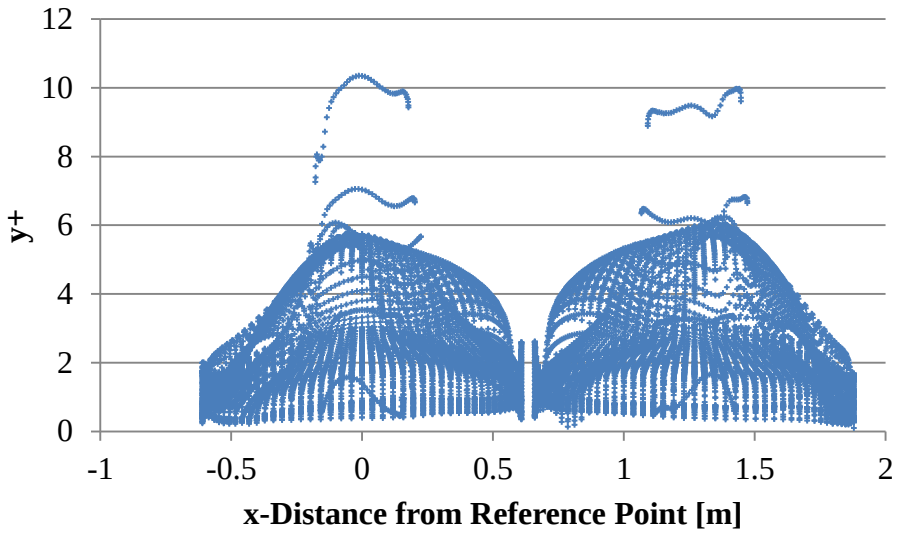

Figure 4–15 – Values for y+ Fine Mesh, Case #12

4.11.2 Turbulence Model Evaluation

All simulations herein use the k-ε turbulence model. It is available in most CFD applications and has broad applicability. Use of a turbulence model itself has pros & cons. Further, it isn't always clear which one is best for a particular model or application. The fine-mesh model for Case #12 was repeated using the k-ω SST turbulence model, for comparison. The results, tabulated below, show no appreciable difference between the two models. Thus, the CFD results using the k-ε turbulence model are considered valid.

Parameter	k-ε Model	k-ω Model	Percent Difference
T_{Hot}	436.43	436.16	N/A
T_{Cold}	342.84	342.46	
ΔT	93.5905	93.7038	0.121%
v_{Avg}	1.2314	1.2503	1.535%

4.11.3 Verification of CFD Results

In this section, a basic verification analysis is done for simulations using simple cylinders and water as the working fluid. It is important to remember that these first cases only serve to show that buoyancy-driven flow can be reliably simulated with CFD, noting that the results compare well with analytic methods. They illustrate the basic physics of the problem, but are only the first step along a path of increasing complexity, the overall goal of which is to show whether CFD can be used to model MSR operation.

While the results of this chapter are not trivial, they do not represent the overall focus or the most important conclusions. Thus, verification of one case (of the 16 total) will be done, to demonstrate the correctness of the results. Case #12 is chosen as the candidate, because it is the first one that meets the maximum ΔT requirements, without the excessive flow-through problems of subsequent cases (at higher velocity). CFD values of ΔT and v_{avg} will both be evaluated, using the Factor of Safety (FS) method[77].

4.11.3.1 Verification Basis Values

Mesh refinement was done using the number of elements as a metric. The number of elements was increased by a target factor of $\sqrt{2}$ from coarse to medium and from medium to fine. For cylindrical objects, edge sizing is done in the radial and axial directions. Increasing the number of elements reduces the spacing between nodes. Thus, the nominal mesh refinement ratio $r = \sqrt[4]{2} \approx 1.1892$. The following table shows how this was done for Case #12. The table includes the S_1, S_2 and S_3 CFD values for ΔT and v_{avg}.

[77] Xing, T., Stern, F., 2010, "Factors of Safety for Richardson Extrapolation," ASME Journal of Fluids Engineering, Vol. 132,No. 6, DOI: 061643

Table 4-5 – Verification Basis Values – Case #12

Mesh No.	**No. Elements**	**CFD Grid Designation**	**ΔT [K]**	**v_{avg} [m/sec]**
1 (Fine)	330,188	S_1	83.5580	1.1244
2 (Medium)	233,581	S_2	87.5909	1.1712
3 (Coarse)	165,006	S_3	93.5695	1.2318

4.11.3.2 Convergence Study

From the above data, one can obtain the FS method epsilon values (ε_{21} and ε_{32}) and solution ratio (R), as indicated in the following table.

Table 4-6 – Convergence Study Results – Case #12

Variable	**ΔT**	**v_{avg}**	**R (ΔT)**	**R(v_{avg})**
ε_{32}	5.9786	0.0606	0.6746	0.7723
ε_{21}	4.0329	0.0468		

Note that values for both ΔT and v_{avg} are $0 < R < 1$, indicating **monotonic convergence**.

4.11.3.3 Error Estimate

Next, the observed order of accuracy and error estimates are calculated, the results of which are given below. Recall that Table 4-2 shows second-order accurate solution methods, thus the theoretical accuracy (P_{th}) = 2.

Table 4-7 – Error Estimate – Case #12

δ_{RE}	**ΔT [K]**	**v_{avg} [m/sec]**
	8.3591	0.1587

4.11.3.4 Uncertainty Estimate

Finally, the estimated (grid) uncertainty values are calculated, as shown below. Note that use of the FS method implies a 95% confidence factor.

Table 4-8 – Uncertainty Estimate – Case #12

	ΔT [K]	**v_{avg} [m/sec]**
U_G	12.4084	0.2883
$U_G(\%S_1)$	14.85	25.64

4.12 Conclusions for this Set of Simulations

- The CFD results match calculated values from analytic methods within 4.4%. Thus, it seems that CFD software is able to model natural convection flow to the extent necessary to support MSR design basis studies, using simple (cylindrical) shapes and a common fluid (water).

- As expected, the Boussinesq approximation works well for "small" temperature changes. However, it may not be appropriate for engineering design studies of realistic/practical power plants. In those cases, the temperature difference would likely be maximized (given physical constraints) so as to maximize efficiency.

- For a $10MW_e$ natural convection MSR power plant, several criteria are used. The volume of the reactor is determined by the power density. The diameter of connecting piping is an engineering choice. Overall, the design criteria include achieving a certain maximum ΔT and minimizing the overall fuel salt volume. The single most important design parameter is the minimum relative elevation difference between the reactor and heat exchanger vessels. A conservative value for this parameter in a water system is 12 feet.

5 First Fuel Salt CFD Results

5.1 Abstract

This chapter provides information and results for CFD simulations of a simplified MSR system. It includes increased model complexity, based on lessons learned in the previous simulations. As before, it uses simple shapes for the reactor vessel & heat exchanger. However, a simple baffle is added to both, to reduce flow-through and increase residence time. Further, the working fluid is an actual, reactive fuel salt, with parameters that incorporate a negative temperature coefficient. Details & results include:

- Physical property data for the salt; i.e., composition, melting point, density, heat capacity, thermal conductivity, viscosity.
- Size and configuration of the reactor vessel & heat exchanger, relative elevation between the two, and the size of connecting pipes.
- General meshing techniques; i.e., edge sizing, number of nodes & elements.
- Operating conditions and initialization parameters for the simulation.
- Nominal velocity and temperature difference resulting from developing the desired power from the reactor system.
- Comparison between CFD results and analytic solutions for nominal velocity.

Results from the previous chapter were used to determine a starting point for these simulations, with regard to the relative elevation between the reactor vessel & heat exchanger. Further, previous results help determine initialization parameters for this series of simulations. A total of 10 cases were run, starting at a relative height of 8 feet (2.4384 m), and increasing by 6 inches (0.1524 m) in subsequent cases.

5.2 Reactor Vessel & Heat Exchanger Size, Elevation & Pipe Data

Some details in this chapter are the same as those from the previous chapter. The reactor & heat exchanger are identical in size & shape. The diameter & height are 50 inches (1.27 m), so the aspect ratio is 1. The volume of each vessel is 1.5004 m^3. The energy removal rate of

the heat exchanger remains at 22.2 MW/m^3, which provides 10 MW_e, given a thermal efficiency of 33.3%. The pipe diameter remains at 12 inches (0.3038 m), and the horizontal distance between vessel centerlines is 50 inches (1.27 m).

Changes include giving the vessel inlet & outlet surfaces a slight taper, to reduce abrupt velocity changes at sharp corners, without overcomplicating the model with radiused corners. In order to reduce flow-through observed in the first set of simulations, a very basic (24-inch wide by 1-7/8 inch thick) baffle plate was added to each vessel. This feature helped fine-tune the vessel volume. A 3D vertical half-section of the overall system was developed for each case, to take advantage of symmetry. Figure 5–1 shows the 3D model for Case #1.

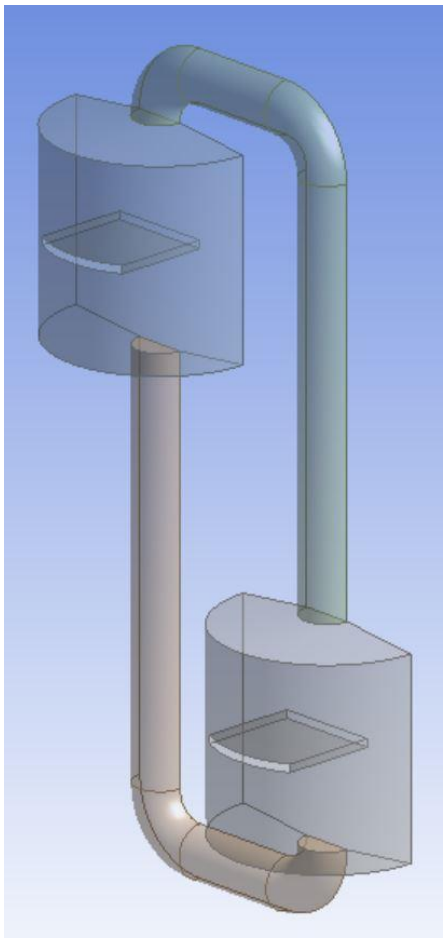

Figure 5–1 – 3D Model for Case #1

5.3 Meshing Details

As before, the overall intent was to impose a structured mesh using edge controls, like the previous simulations (see Section 4.5). Edge sizing details for the vessel height, OD and ID are the same. Edge sizing was added to the straight lengths of pipe, to keep the mesh straight in those sections. Due to the baffle plate, the software's meshing utility/module created an unstructured mesh for the reactor and heat exchanger vessels. Figure 5–2 shows part of the coarse mesh for Case 1, which has a total of 71,640 nodes and 188,484 elements.

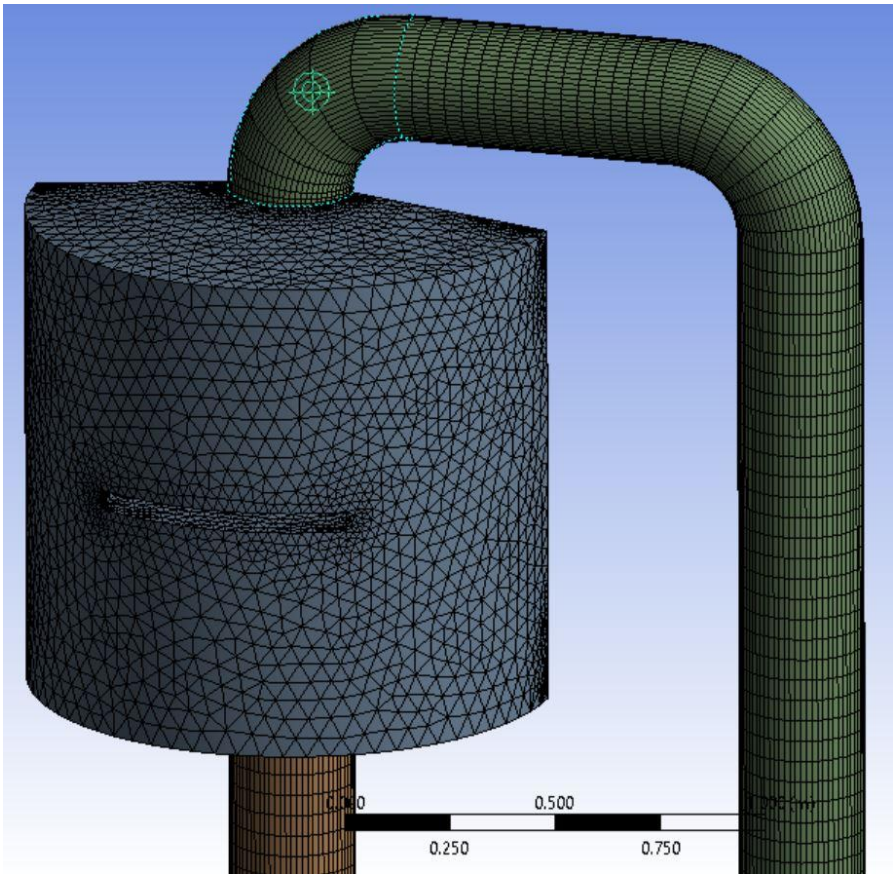

Figure 5–2 – Coarse Mesh for Case #1

5.4 Models & Materials Data (Fuel Salt Properties)

In the CFD Setup -> Models tab, Energy and gravity were left on, and the Realizable k-ε turbulence model was retained.

Detailed experiments show that fuel salt properties vary with temperature. Empirical results were developed into curve-fit expressions, which are incorporated to provide more realistic results. In addition, a scheme to account for changes in reactivity is included, so as to provide a negative temperature coefficient – a critical passive safety feature. The next sections describe how values were determined & entered into the CFD Setup -> Materials -> Fluid tab.

5.4.1 Salt Composition & Melting Points

Experimental evidence shows that the composition of the salt affects the fluid properties. Early design studies used a two-fluid heat exchange process; heat is generated by a "fuel salt," and transferred to a secondary system via a "cooling salt." Later studies showed that a two-fluid process is not necessary. Thus, these simulations use a single salt for fuel & coolant.

In general, FLiBe (cooling/flushing) salts are 66% LiF and 34% BeF_2 [78]. However, other compositions have very different melting points[79], as shown in the table below

Table 5-1 – Melting Point of Various FLiBe Mixtures

Composition LiF/BeF_2 [mol %]	Melting Point [°C]	Melting Point [K]
50/50	350	623
66/34	457	730
69/31	505	778

[78] S Cantor, et al, Physical Properties of Molten-Salt Reactor Fuel, Coolant and Flush Salts, ORNL-TM-2316 (1968)
[79] WR Grimes, et al, Chemical Aspects: Molten-Fluoride Salt Fuels, Chapter 12 (circa 1958)

For fuel salts, common compositions include[80]:

Table 5-2 – Composition & Properties of FLiBe Fuel Salts

Composition [mol %]	Melting Point [°C]	Melting Point [K]
67% LiF, 30.5% BeF_2, 2.5% UF_4	464	737
68% LiF, 20% BeF_2, 11.7% ThF_4, 0.3% UF_4 *	480	753

* Denoted as fuel salt "F3" in the cited report. Other fuel salts have a melting point of 495°C = 768K

Note that fuel salts with both UF_4 and ThF_4 are very similar with respect to physical properties[81]. For the purposes of subsequent simulations herein, the previously cited temperature range recommendation will be used; i.e., 797 – 936K.

5.4.2 Fluid Density

Experimental data provide two relations for density. The first is accurate from the melting point to the critical point[82].

$$\rho = 2415.6 - 0.49072 \cdot T[K] \left[\frac{kg}{m^3}\right]$$

The second is accurate for the range of temperature 788-1094K[83]

$$\rho = 2413.03 - 0.4884 * T[K] \left[\frac{kg}{m^3}\right]$$

In a practical sense, there is little difference between the two, thus, the first of these will be used in subsequent simulations.

---

[80] IBID
[81] S Cantor, et al, Physical Properties of Molten-Salt Reactor Fuel, Coolant and Flush Salts, ORNL-TM-2316 (1968)
[82] MS Sohal, et al, Engineering Database of Liquid Salt Thermo-physical and Thermochemical Properties, INL/EXT-10-18297 (2010)
[83] O Benes & RJM Konings, Comprehensive Nuclear Materials, Volume 3 – Molten Salt Reactor Fuel and Coolant (2012)

This relation was used in the Materials -> Fluid tab as a polynomial relation, rather than selecting the default Boussinesq relation, to achieve better accuracy. Recall that the Boussinesq relation is considered valid for "small" temperature changes.

5.4.3 Heat Capacity

The specific heat capacity at constant volume is relatively constant for the temperature range of interest. One source[84] cites an average value of 2365 J/kg*K. Another source[85] suggests a value of 2385 J/kg*K. For subsequent simulations herein, a constant value of 2370 [J/kg*K] will be used.

5.4.4 Thermal Conductivity

This physical property is reported to be difficult to measure, but it is an important aspect when quantifying heat transfer & thermal behavior. One source[86] suggests using a constant value of k = 1.10 W/m*K. However, this value is based on a small number of data points, taken at the low end of the temperature range of interest[87].

Several studies[88] [89] [90] have provided a theoretical relation for thermal conductivity of

$$k = 0.629697 + 0.0005 \cdot T[K] \left[\frac{W}{m \cdot K}\right]$$

[84] MS Sohal, et al, Engineering Database of Liquid Salt Thermo-physical and Thermochemical Properties, INL/EXT-10-18297 (2010)
[85] S Cantor, et al, Physical Properties of Molten Salt Reactor Fuel, Coolant ad Flush Salts, ORNL-TM-2316 (1968)
[86] O Benes & RJM Konings, Comprehensive Nuclear Materials, Volume 3 – Molten Salt Reactor Fuel and Coolant (2012)
[87] DF Williams, et al, The Influence of Lewis Acid/Base Chemistry on the Removal of Gallium by Volatility from Weapons Grade Plutonium Dissolved in Molten Chlorides, Nuclear Technology, 136, 367 (2001)
[88] VV Ignatiev, et al, Experimental Investigation of the Physical Properties of Salt Melts containing Sodium and Lithium Fluorides and Beryllium, Atomic Energy, 101(5), 822-829 (2006)
[89] DF Williams, Assessment of Candidate Molten Salt Coolants for the NGNP/NHI Heat-Transfer Loop, ORNL/TM-2006/69 (2006)
[90] T Allen, Molten Salt Database, http://allen.neep.wisc.edu/shell/index.php/salts, Nuclear Engineering and Engineering Physics Department, University of Wisconsin (2010)

It is worthwhile noting that this relation closely matches experimental data. Even though this physical property has a weak dependence on temperature, the linear relation above will be used for subsequent simulations.

5.4.5 Viscosity

Viscosity is an important fluid property, and is very dependent on temperature. For a 66/34 FLiBe composition, the following relation for dynamic viscosity is recommended[91]

$$\mu = 0.000116 \cdot \exp\left(\frac{3755}{T[K]}\right) \; [Pa \cdot sec]$$

The CFD software used for this research accepts numerous equations/relations for fluid properties; i.e., linear, polynomial, piecewise versions of these, power law, etc., but not the specific form above. However, the software does accept a power law relation for this property, the conversion of which is straightforward. Users have a choice of a two or three coefficient expression:

$$\mu = BT^n$$

or

$$\mu = \mu_0 \left(\frac{T}{T_0}\right)^n$$

For the 2-coefficient method, use of $B = 5 \times 10^{10}$ and $n = -4.336$ provides a good match. However, the use of such a large value for the constant *B* is concerning, as it can complicate the iterative/numerical processes that follow (i.e., equations can become "stiff").

For the 3-coefficient method, a reference value of 0.00845 for μ_0 is selected from the temperature range of interest, with corresponding values of 880 for T_0 and -4.5 for *n*. The mean absolute percentage error is 1.48%, which corresponds to 0.000134 Pa*sec. Figure 5–3 shows the equation values in (red) and the reference values (blue curve).

[91] S Cantor, et al, Physical Properties of Molten Salt Reactor Fuel, Coolant ad Flush Salts, ORNL-TM-2316 (1968)

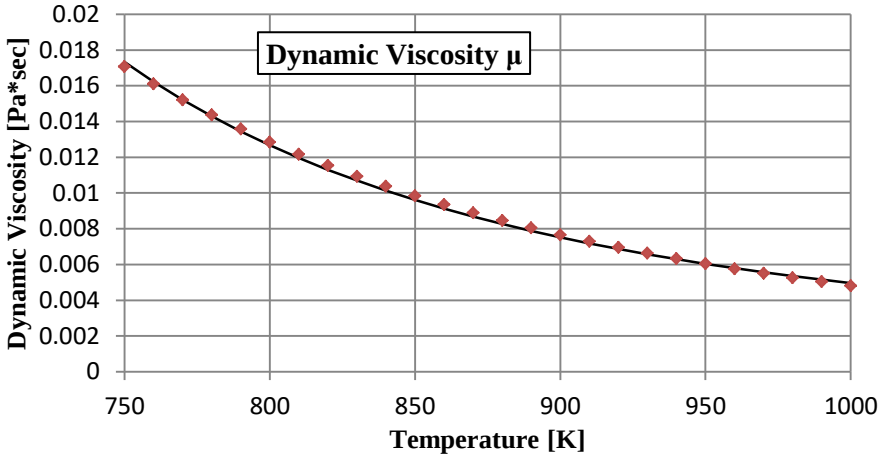

Figure 5–3 – Power Law Relation Results for Viscosity

5.4.6 Variable Reactivity (Energy Density)

In a real reactor, the primary (active) method of controlling reactivity is through the use of control rods. Once the rods are positioned to achieve a critical reactor, other factors can affect the reactivity of the fuel volume in the reactor. These include its location within the reactor, proximity to the moderator and temperature. Other operational factors include the fuel life, presence of generated poisons (i.e., xenon & samarium) and degradation of the moderator and structural materials. Further, the amount of fertile (vs. fissile) fuel significantly affects reactivity.

Figure 5–4[92] shows how the moderator, fuel salt & fertile salt factors affect the overall (natural/passive) reactivity, each of which varies with temperature. As temperature increases, both the moderator & fertile salt factors increase reactivity, while the fuel salt decreases reactivity (a negative factor). As temperature increases, density decreases. Decreased density increases the distance between fuel elements, reducing the likelihood of a fission-causing interaction. The overall effect (all factors combined) is a negative temperature coefficient, which as stated previously, is an important reactor safety feature.

[92] RC Robertson, et al, Two-Fluid Molten-Salt Breeder Reactor Design Study, ORNL-4528 (1968)

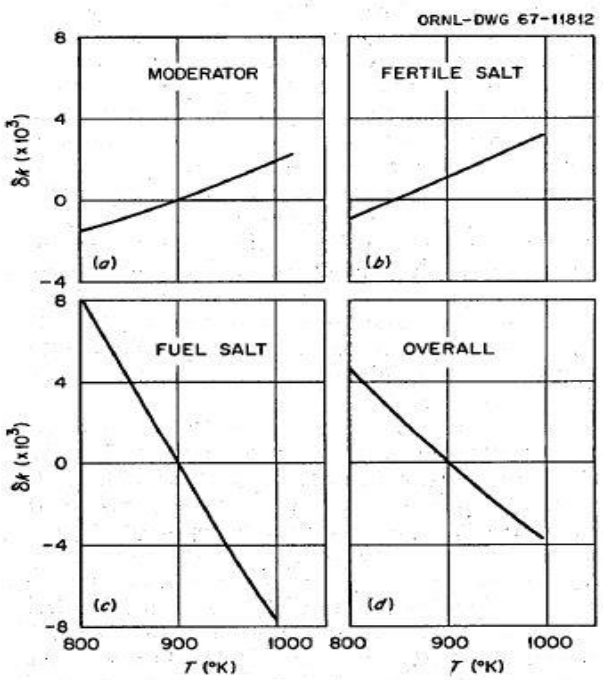

Fig. 6.10. MSBR Multiplication Factor vs Temperature.

Figure 5–4 – Temperature Effects on Reactivity

These effects are combined as follows[93]

$$\delta\rho_{fb} = \alpha_F \delta T_F + \alpha_G \delta T_G + \alpha_B \delta T_B$$

where "fb" refers to reactivity feedback,

"F" designates fuel

"G" designates graphite, and

"B" designates fertile material

Values for the temperature coefficients were given as

$$\alpha_F = -4.54 \times 10^{-5} \frac{\delta\rho}{°F}$$

$$\alpha_G = +1.12 \times 10^{-5} \frac{\delta\rho}{°F}$$

$$\alpha_B = +9.2 \times 10^{-6} \frac{\delta\rho}{°F}$$

[93] TW Kerlin, ORNL Correspondence MSR-67-102 (1967)

For a total temperature coefficient of

$$-2.5 \times 10^{-5} \frac{\delta\rho}{°F}$$

The MSRE had an overall negative temperature coefficient between -6.4 and -9.9 x 10^{-5}/°F[94] [95]. However, this doesn't include the effects of adding fertile fuel.

There are other sources of temperature coefficient data, but the one most relevant to this research is the design basis of the MSBR[96], which cites a total core average temperature coefficient of -0.87 x 10^{-5}/C. This value will be used for subsequent simulations.

The way reactivity will be included in this research is through the energy source feature for specified zones within the software. Previously, an average value of 22.2MW/m^3 was used as a constant energy source, regardless of the temperature of the reactor vessel fluid.

For the energy source in this section's simulations, a starting value "pivot point" temperature of 860K is used. As the temperature in the reactor vessel varies from this value, the temperature coefficient changes the amount of energy released. Temperatures below the pivot point will be slightly more reactive (generating more energy), and those above it will be less reactive (generating less energy). The system will eventually reach an equilibrium temperature value. The equation that expresses the reactor vessel energy density is

$$\left((T[K] - 860) \times -8.7 \times 10^{-5}\right) + 1) \times 22.2 \left[\frac{MW}{m^3}\right]$$

The expression entered into the software for the reactor vessel zone/volume energy source is

(((StaticTemperature-860 [K])*-8.7e-5 [K^-1]) + 1)*22200000 [W m^-3]

[94] RC Robertson, MSRE Design & Operations Report, Part I, Description of Reactor Design ORNL-TM-728 (1965)
[95] MW Rosenthal, et al, Molten-Salt Reactor Program Semiannual Progress Report, ORNL-4396 (1969)
[96] RC Robertson, Conceptual Design Study of a Single-Fluid Molten-Salt Breeder Reactor, ORNL-4541 (1971)

As the solution progresses/iterates, the user monitors the velocity & temperature for the hot & cold pipes, and adjusts the pivot point as needed to achieve an appropriate temperature range. This is exactly what a reactor operator would do; i.e., monitor the temperature and add/subtract reactivity to suit conditions, by withdrawing/inserting the control rods.

5.5 Cell Zones & Boundary Conditions

The heat exchanger was given an energy source value of -22.2 MW/m^3, as before. The reactor vessel was given a temperature-dependent energy source value, as previously cited.

Boundary conditions were defined, selecting all the planar surfaces with symmetry. All the vessel & pipe outer surfaces were defined as walls, as were the internal baffle surfaces.

5.6 Operating Conditions, Solution Methods & Initialization

Under the Physics -> Operating Conditions tab, options for steady-state and pressure-based solutions were selected. Using the Solution -> Methods tab, initial calculations were run using first order equations, in an effort to reduce overall solution time, switching to second order later.

The experienced CFD user will recognize that the use of variable fluid properties changes the nature of the partial differential equations, such that more terms become non-linear. Further, the added complexity of an energy density that is a function of temperature increases the possibility of an unstable solution. Finally, since the system has no inlet or outlet, one cannot specify certain boundary conditions (pressure & velocity) for which to solve. Thus, the system has many degrees of freedom, which means more iteration is required in order for the system to reach an equilibrium state, and there are oscillations about an average value. The initial use of first order equations, with an implicit solver helps minimize instability factors. Later, higher-order methods were employed.

Target values for residuals were left in the default condition, except for continuity, which was changed to 10^{-5}. This ensures that iterations will continue despite any momentary fluctuations that may occur. Simulations were initiated & "patched" as indicated in the table below. Initial conditions are based on actual (physical) conditions. Initial velocities are from the previous set of results (with water). Initial temperatures are the target high & low values for the fuel salt & structural materials, as cited previously.

Table 5-3 – Initialization Parameters

Region	**Pressure**	**u**	**v**	**w**	**k**	**ε**	**T**
Reactor Vessel & Hot Pipe	0	0.1	0.7	0	0.1	0.1	920
Heat Exchanger & Cold Pipe	0	-0.1	-0.7	0			800

5.7 Delta T & Nominal Velocity Data Results

As previously stated, due to the non-linear nature of the simulation and degrees of freedom, one cannot rely solely on residuals to determine when a solution is achieved. A series of cross-checks were used, to eliminate non-physical results. This was done using XY plots of temperature & velocity at selected locations in the hot & cold pipes. Values were calculated using a weighted average, to account for cross-sectional area in the pipe. From the average temperature & velocity, one can determine the density & mass flow rate. From the values of c_P and ΔT, one can verify the system power output, and cross-check results with the known value of energy extraction from the heat exchanger.

A plot of temperature contours at the symmetry plane was selected, and the temperature difference across the vessels was obtained. Figure 5–5 shows the results for Case #7, with temperatures annotated.

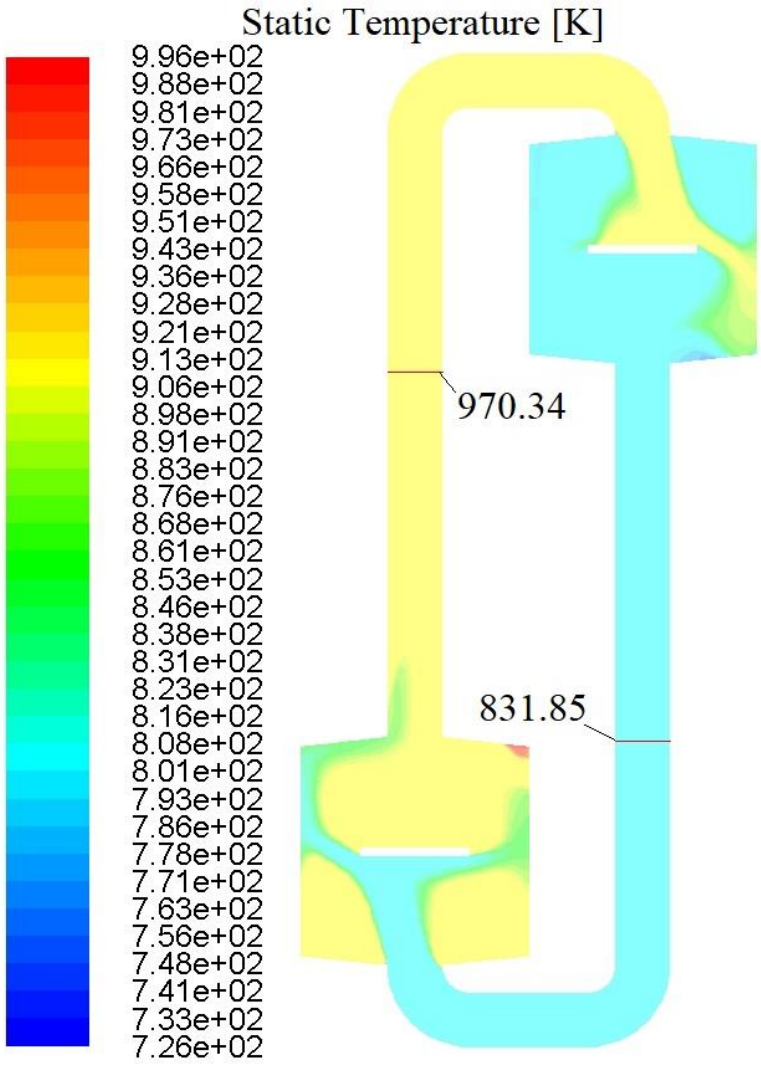

Figure 5–5 – Temperature Contours – Symmetry Plane – Case #7

An XY plot of the velocity profile was obtained, again by defining lines across the hot and cold pipes. Figure 5–6 shows the velocity profile for Case #7. As in the previous set of simulations, the velocity profile is not strictly parabolic, so the flow is not laminar. The resulting average flow for this case as calculated via CFD is 0.6959 m/sec (shown as a green line). As before, the average temperature and velocity were determined by using a weighted average based on cross-sectional area, to account for internal flow in the pipes. The range of Reynolds numbers for these cases is 38,000 to 56,000; i.e., turbulent flow.

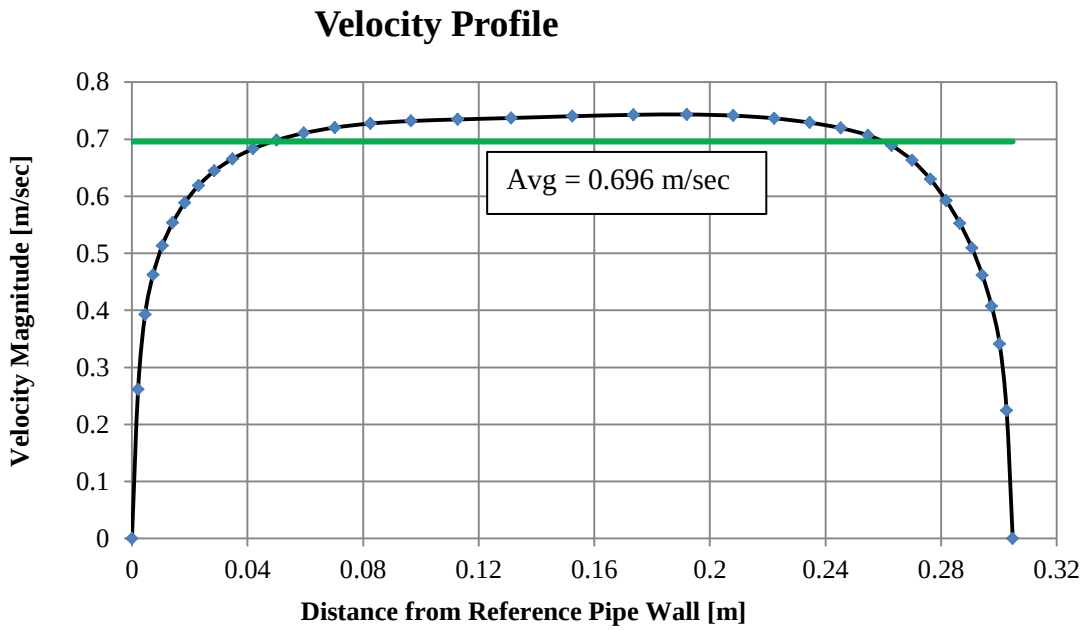

Figure 5–6 – Velocity Profile – Case #7

The same parameters, solution methods, etc., were used to obtain average temperatures and velocity for each of the 10 cases, based on the relative height difference (Δz) , starting at an initial value of 8 feet (96 inches, 2.4384 meters). The resulting values are shown in Table 5-4.

Table 5-4 – Summary of CFD Results

Case	Δz		ΔT [K]	v_{avg} [m/sec]
	Inches	Meters		
1	96	2.4384	157.0038	0.6231
2	102	2.5908	149.2662	0.6482
3	108	2.7432	146.2005	0.6601
4	114	2.8956	143.3009	0.6728
5	120	3.0480	139.8327	0.6837
6	126	3.2004	139.2011	0.6941
7	132	3.3528	136.7979	0.7059
8	138	3.5052	135.6517	0.7167

Case	Δz		ΔT [K]	v_{avg} [m/sec]
	Inches	Meters		
9	144	3.6576	135.4530	0.7248
10	150	3.8100	132.3394	0.7363

Figure 5–7 shows a plot of path lines originating at the reactor vessel outlet. The flow-through condition observed previously in the vessels was significantly reduced just by adding the simple baffle plate.

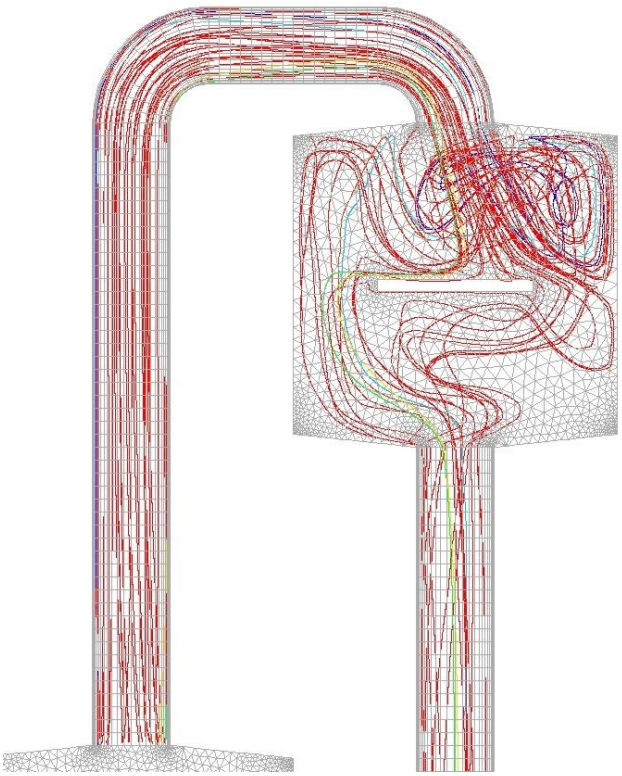

Figure 5–7 – Path Lines – Case #1

Figure 5–8 shows numerous path lines, colored by the value of static pressure, to illuminate any recirculating vortices.

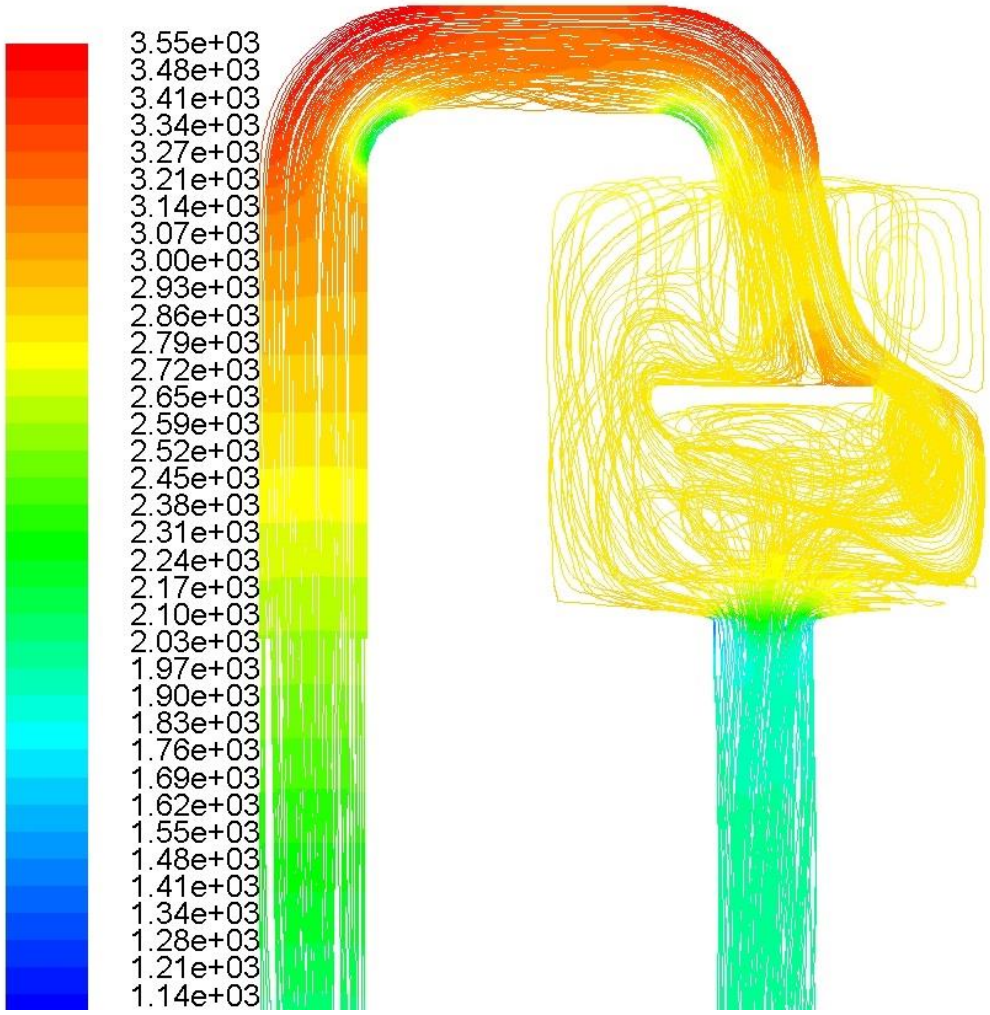

Figure 5–8 – Path Lines – Case #7 – Colored by Pressure

Figure 5–9 shows the average velocity and ΔT data in graphical form, to show how values change as a function of the difference in elevation between vessels. The solid lines are not intended to be analytical – they just show the general trend of the data.

The results show that Case #7 is the first one that achieves the target value for ΔT of 138 degrees. This corresponds to a height difference of 132 inches (11 feet, or 3.3528 meters), which is very similar to the simple cases using water. That elevation value was 3.2 meters, but recall that neither vessel had any internal structure (which would increase the pressure loss therein).

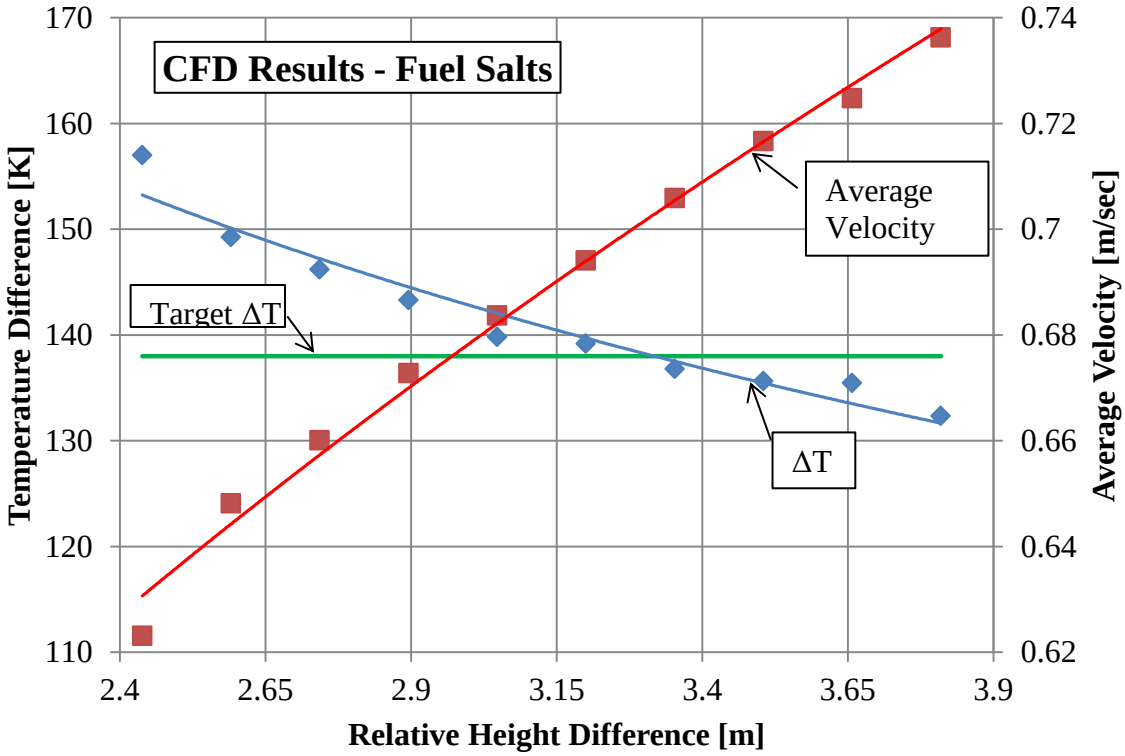

Figure 5–9 – Graphical Summary of CFD Data

5.8 Comparison of CFD & Analysis Results

As before, using the average fluid density, one can determine the average pipe velocity by analytic methods, for comparison with the CFD values. Figure 5–10 shows the result of this comparison. The mean absolute percentage error between CFD and analytic values is 0.5475%, which corresponds to 0.00374 m/sec.

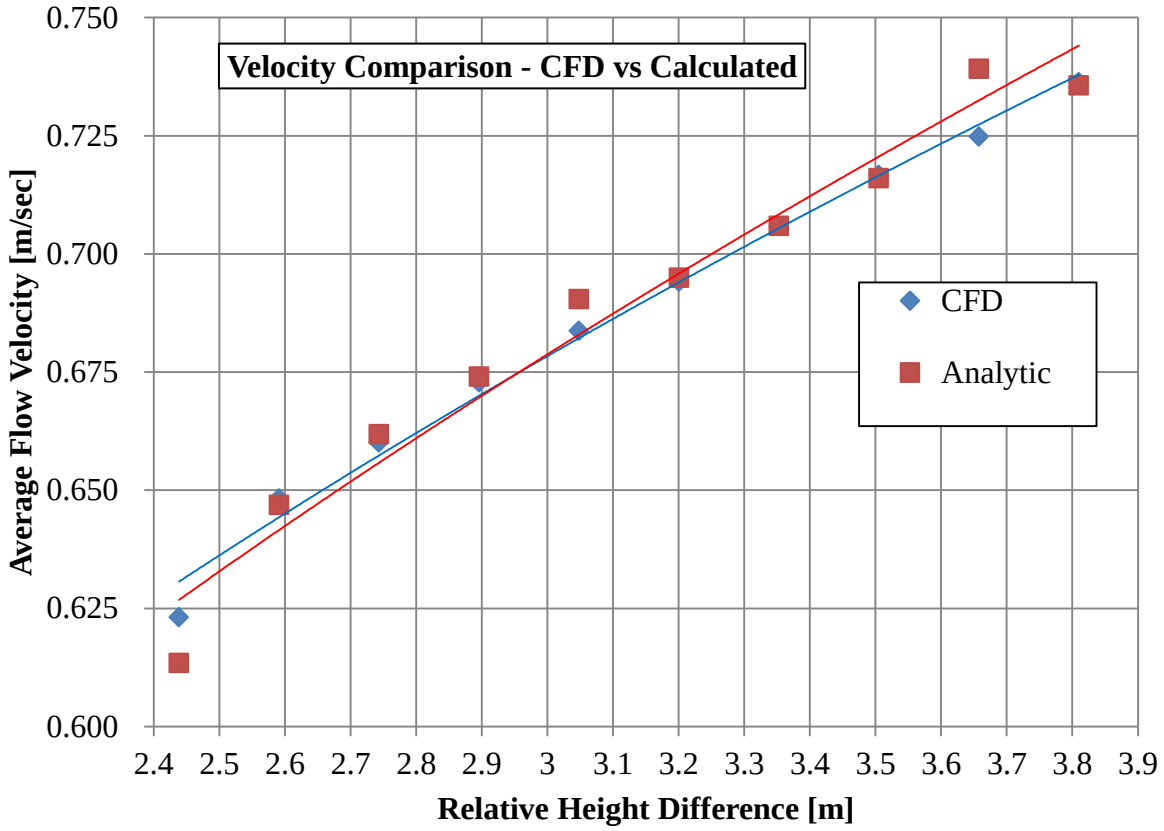

Figure 5–10 – Velocity Comparison – CFD vs Calculation

5.9 CFD-Specific Information

5.9.1 Mesh Evaluation – Resolving Boundary Layer

A plot of y+ values for the piping is shown in Figure 5–11. A total of 23,086 points exist for the fine mesh. Of these, 20,860 had y+ values ≤5 (90.36%). Thus, the mesh does a nominally adequate job of capturing boundary layer effects.

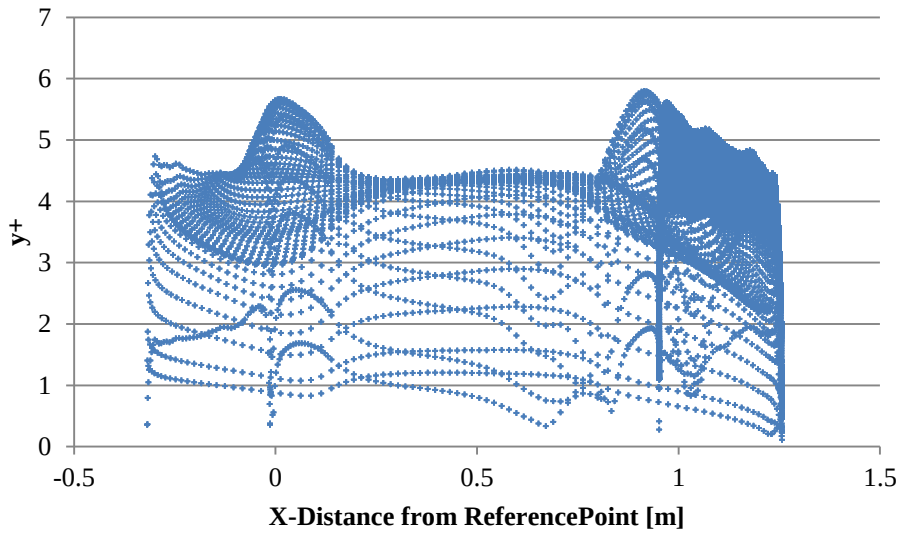

Figure 5–11 – Values for y+ Fine Mesh, Case #7

5.9.2 Turbulence Model Evaluation

As in the previous chapter, results obtained by using the k-ε turbulence model were compared with those using the k-ω model. The results, tabulated below, show no appreciable difference between the two. Thus, use of the k-ε model is valid. It is worthwhile to note, however, that use of the k-ω model takes somewhat more time per iteration, and seems more sensitive to changes made during the iteration process.

Parameter	k-ε Value	k-ω Value	% Difference
ΔT [K]	138.49	137.03	1.06
v_{avg} [m/sec]	0.6959	0.6958	0.01

5.9.3 Verification of CFD Results

As before, a basic verification analysis is presented to demonstrate the quality of results. Case #7 is chosen as the candidate, because it is the first one that met the maximum ΔT

requirement. CFD values for ΔT and v_{avg} are both evaluated using the Factor of Safety (FS) method.

5.9.3.1 Verification Basis Values

As before, mesh refinement was done using the number of elements as a metric, such that the nominal mesh refinement ratio $r = \sqrt[4]{2} \approx 1.1892$. The following table shows how this was done for Case #7. The table includes the S_1, S_2 and S_3 CFD values for ΔT and v_{avg}.

Table 5-5 – Verification Basis Values – Case #7

Mesh No.	**No. Elements**	**CFD Grid Designation**	**ΔT [K]**	**v_{avg} [m/sec]**
1 (Fine)	435,816	S_1	138.49	0.6959
2 (Medium)	308,168	S_2	137.93	0.6981
3 (Coarse)	217,906	S_3	136.80	0.7059

5.9.3.2 Convergence Study

From the above data, one can obtain the FS method epsilon values (ε_{21} and ε_{32}) and solution ratio (R), as indicated in the following table.

Table 5-6 – Convergence Study Results – Case #7

Variable	**ΔT**	**v_{avg}**	**R (ΔT)**	**R(v_{avg})**
ε_{32}	0.5552	0.0022	0.4883	0.2821
ε_{21}	1.1369	0.0078		

Note that values for both ΔT and v_{avg} are $0 < R < 1$, indicating **monotonic convergence**.

5.9.3.3 Error Estimate

Next, the observed order of accuracy and error estimates are calculated, the results of which are given below. Recall that second-order accurate solution methods were used for the final solution (after numerous iterations). Thus, the theoretical accuracy (P_{th}) = 2.

Table 5-7 – Error Estimate – Case #7

δ_{RE}	**ΔT [K]**	**v_{avg} [m/sec]**
	0.5299	0.00086

5.9.3.4 Uncertainty Estimate

Finally, the estimated (grid) uncertainty values are calculated, as shown below. Note that use of the FS method implies a 95% confidence factor.

Table 5-8 – Uncertainty Estimate – Case #7

	ΔT [K]	**v_{avg} [m/sec]**
U_G	10.1297	0.0389
U_G (%S_1)	7.3144	5.6003

5.10 Conclusions for this Set of Simulations

- The CFD results match calculated values from analytic methods within 0.55%. Thus, it seems that CFD software is able to model natural convection flow to the extent necessary to support MSR design basis studies, using simple cylinders with minimal internal structure, and an actual fuel salt fluid.

- Use of the Boussinesq approximation is not required to achieve CFD results. To increase accuracy and reflect realistic conditions for an actual power plant, users can

enter complex relations for fuel salt properties. The software's solvers and numerical methods are able to handle these. Further, variable energy density can be added by the user, to reflect the complex interaction between temperature and reactivity.

- As before, the single most important design parameter is the difference in relative elevation between the reactor and heat exchanger vessels. A conservative value for this parameter in an actual fuel salt system is 12 feet.

6 Benchmark Simulations for Future Comparison

6.1 Abstract

This chapter provides:

- A detailed description of a natural-circulation Test Rig, constructed at the University of Idaho in Idaho Falls, ID.
- Estimated performance of the test rig, based on analytic methods.
- Modeling & meshing information for the parts & system.
- Pressure drop information for the heater & cooler, based on CFD.
- CFD results for the test rig at its full-rated power.

6.2 Experimental Rig Design, Configuration & Operating Parameters

An experimental Test Rig was designed and built at the University of Idaho campus in Idaho Falls, for investigating natural circulation flow as it relates to MSR design parameters. Figure 6–1[97] shows the as-built dimensions of the rig, and the location & type of instrumentation provided.

Pipe & fittings are 2-1/2" schedule 80, made from alloy 304 stainless steel with an inside diameter of 2.323 inches (.0590042 meters). The nominal pipe length around the whole loop is 472 inches (39.33 feet = 11.989 meters). There are a total of 17 fittings (tees & elbows). The relative difference in elevation between the cooler and heater is 165 inches (13.75 feet = 4.191 meters).

[97] J Richards, University of Idaho, via private e-mail.

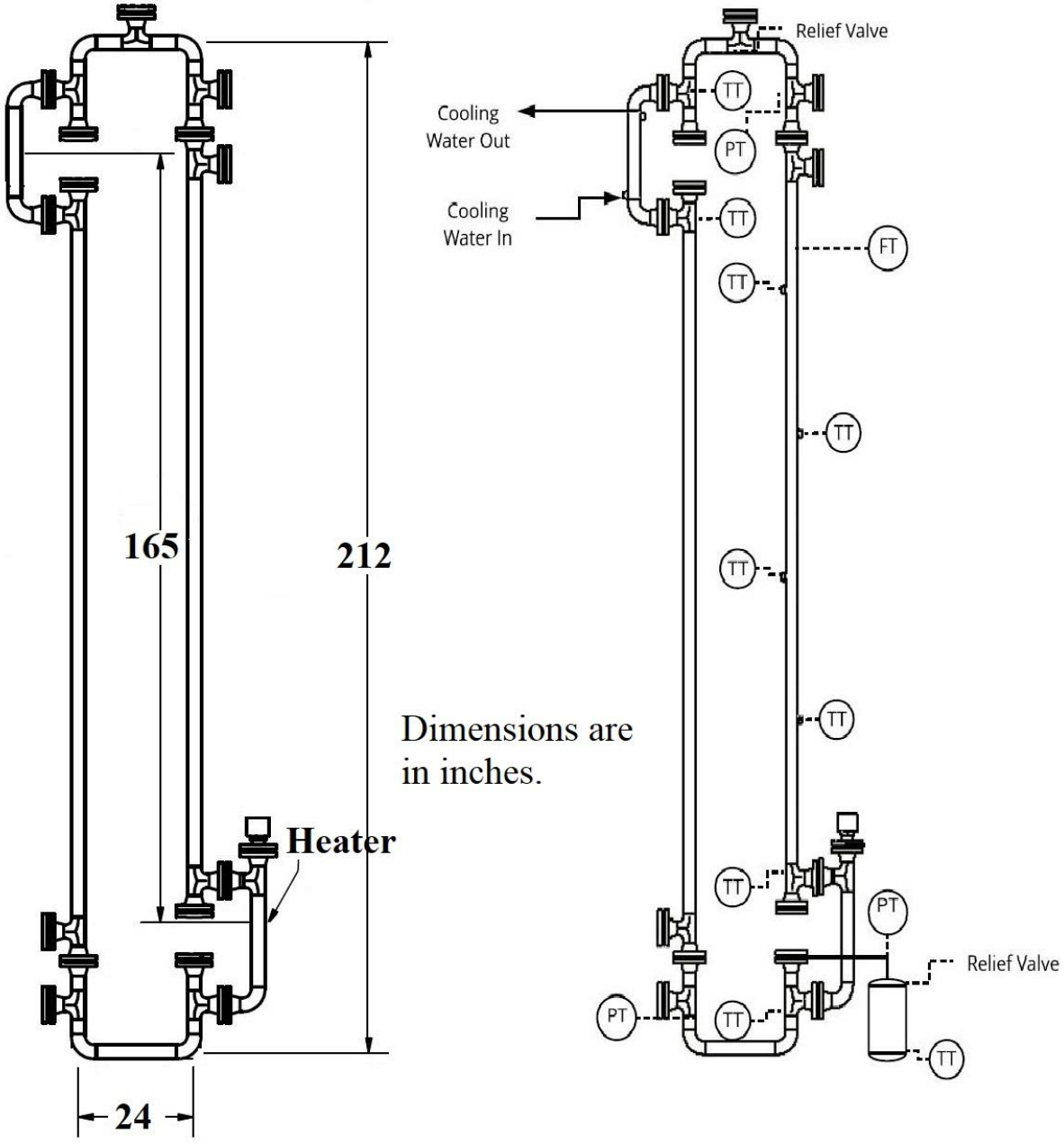

Figure 6–1 – Experimental Rig Dimensions & Features

The rated energy output of the heater is 4000W. It is a dual-element immersion type, as shown in Figure 6–2.

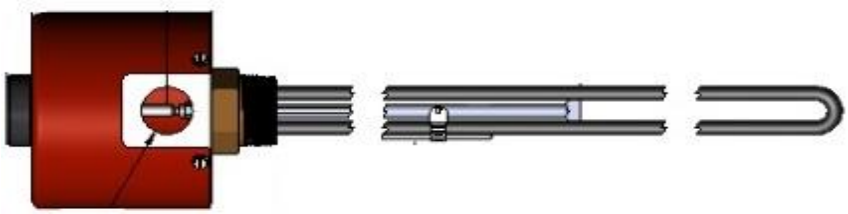

Figure 6–2 – 4000W Dual Element Immersion Heater

The volume of the assembly (i.e., pipe & tee) enclosing the heater is 72.43 in^3 = 0.001187 m^3 (not including the element itself). Thus, the nominal value for the heater component as an energy source is 3,370,000 W/m^3. Note that an immersion type heater more closely resembles internal heat generation, as opposed to a wire wrapped around the exterior of the tubing. Information in Chapter 2 herein discusses this important aspect of heaters used to model fluids with internal heat generation, such as an MSR reactor vessel.

The cooler is a shell & tube heat exchanger, with a total of eight 3/8-inch diameter tubes arranged in a support plate as shown in Figure 6–3[98].

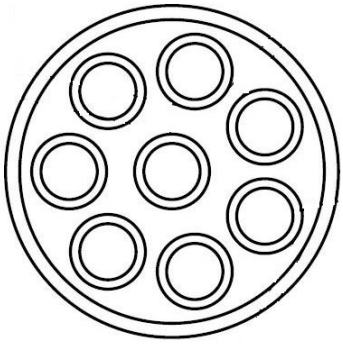

Figure 6–3 – Cooler's Tube Bundle Arrangement

The total cooling tube internal volume is 16.556 in^3 = 0.0002713 m^3. Thus, assuming the cooler dissipates the same amount of energy the heater adds (for equilibrium conditions), the nominal value for the cooler as a heat sink is -14,741,815 W/m^3.

[98] IBID

6.3 Adiabatic Performance Analysis

6.3.1 Flow Rate

Water is the working fluid (heat transfer medium) for the test rig. It has a relatively constant heat capacity of 4180 J/kg*K. Thus, for a given temperature range (ΔT), the required mass flow rate to achieve a certain power level (P) can be determined by

$$\dot{m} = \frac{P}{\Delta T \cdot c_P}$$

The following graph shows the required mass flow rate for selected temperature ranges, in order to achieve various power levels, up to the maximum value of 4000W. The larger the fluid's temperature difference, the less mass flow is required.

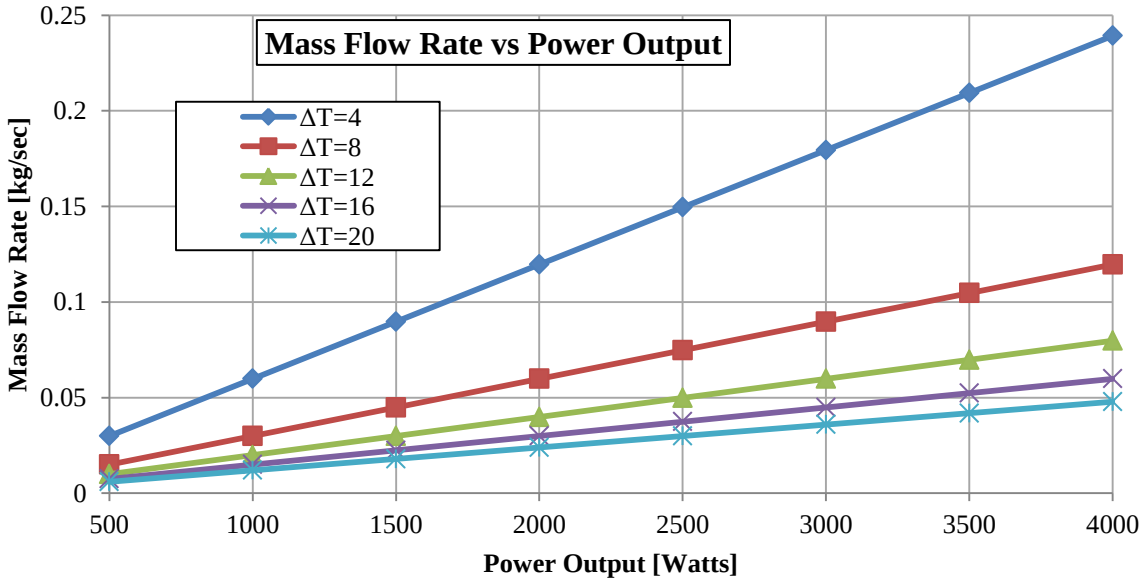

Figure 6–4 – Mass Flow Rate vs Power Output

Using an average fluid density for the temperature range, one can find the corresponding volumetric flow rate. Using the cross-sectional area of the pipe, one can determine an average velocity in the pipe.

The following table lists temperature ranges, mass & volumetric flow rates, and average pipe velocity required to achieve a 4000W power level. The larger the ΔT, the lower the average velocity required to achieve the required power level.

Table 6-1 – Mass & Volume Flow with Average Velocity Data

Temperature Range ΔT [°K]	Mass Flow Rate $\dot{m}$ [kg/sec]	Volumetric Flow Rate $\dot{V}$ [10^{-4} m^3/sec]	Average Pipe Velocity [m/sec]
2	0.4785	4.8025	0.1756
4	0.2392	2.4020	0.0878
6	0.1595	1.6018	0.0586
8	0.1196	1.2018	0.0439
10	0.0957	0.9618	0.0351
12	0.0797	0.8018	0.0293
14	0.0684	0.6875	0.0251
16	0.0598	0.6018	0.0220
18	0.0532	0.5351	0.0196
20	0.0478	0.4818	0.0176

6.3.2 Available Head Pressure for Flow

The available head (pressure) to generate flow can be determined from the relative difference in elevation (Δz) and temperature range (ΔT), as

$$p = \alpha_\rho \Delta T \Delta z$$

Where α_ρ is the temperature coefficient of density [N/(m^3 * K)]. This is the equation cited in previous reactor design studies. However, since density is a function of temperature, a difference in density for a given fluid can be determined from the high & low temperatures. Thus, one can also find the available pressure head from

$$p = \Delta\rho \cdot \Delta z \cdot g$$

The difference in elevation (Δz) for the Test Rig is 4.191 m. Using a value of 300K for the baseline (low) temperature, the following table and graph shows the available head pressure resulting from temperature (density) differences at that elevation.

Table 6-2 – Available Head for Flow at Various Temperature Ranges

Temperature Range ΔT [K]	Available Head Pressure for Flow [Pa]
2	23.0237
4	24.6682
6	50.5699
8	77.7049
10	106.4845
12	136.9087
14	168.1551
16	200.6349
18	234.7593
20	269.7059

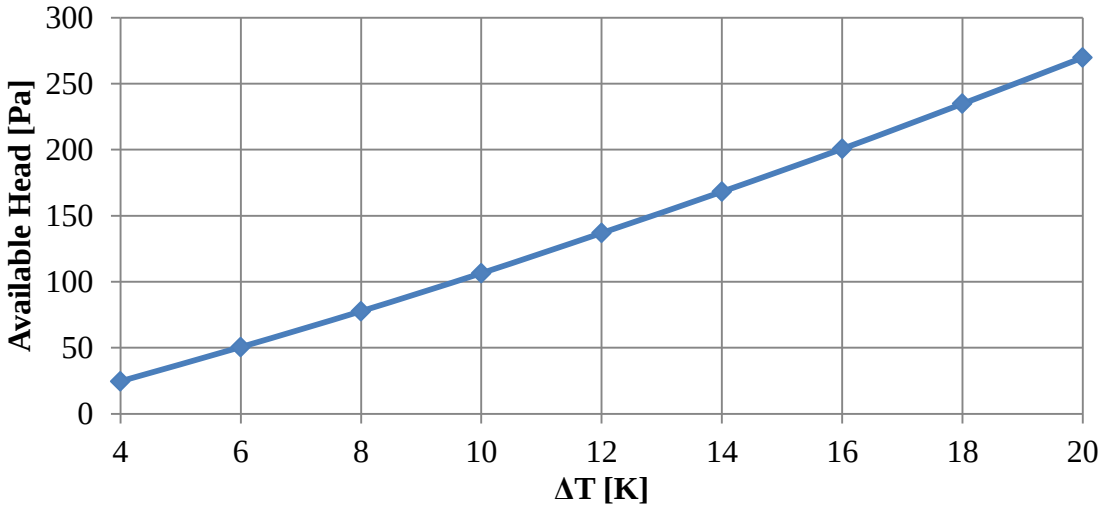

Figure 6–5 – Available Head vs ΔT

6.3.3 Head Losses

As previously stated, the total loss is the sum of flow losses in the pipe & fittings, entry & exit effects at the vessels, and losses through the heater & cooler. The following equations express this in terms of "head" (i.e., a distance, or difference in elevation).

$$H_{Total\ Friction\ Loss} = H_{Pipe\ Flow\ Loss} + H_{Fitting\ Loss} + H_{Heater\ Loss} + H_{Cooler\ Loss} = f\frac{L}{d}\frac{v^2}{2g} + k\frac{v^2}{2g} + h_{HL} + h_{CL} \quad \textbf{(6-1)}$$

The first term on the right hand side is the Darcy-Weisbach relation, which is valid for both laminar & turbulent flow. A good value for the friction factor (*f*), based on drawn stainless steel pipe is 0.02, which is consistent with previous design studies (e.g., Figure 1-12).

Equation 6-1 can be converted to pressure by using an average value of fluid density; i.e.,

$$\Delta P_{Total} = \Delta P_{Pipe\ Flow} + \Delta P_{Fittings} + \Delta P_{Heater} + \Delta P_{Cooler} = f\frac{L}{d}\frac{v^2}{2}\cdot\rho + k\frac{v^2}{2}\cdot\rho + \Delta P_{Heater} + \Delta P_{Cooler}$$

Values for *k* can be obtained from various sources, based on experiments for elbows, tees used as elbows, with straight or branching flow, etc. As noted in section 3.5 herein, previous design studies (with large diameter pipes, smooth transitions and no recirculating flow) used a value of $k = 1.6$. Thus, a 12" nominal diameter standard elbow has a k-value of 0.40. Since there were four elbows, $k = 1.6$.

In contrast, the Test Rig has:

- 7 long radius elbows, each with a k factor of 0.54
- 5 tees used in a flow-through configuration, each with a k factor of 0.36
- 5 tees used in a branch-flow configuration, each with a k factor of 1.08

This gives an overall value for $k = 10.98$. Note that the test rig has 8 temperature probes, 2 pressure probes, and a flow meter, which also affect the flow, albeit by a small amount. For the purpose of this analysis, a value of $k = 12.3$ will be used.

Normally, a heater/cooler manufacturer will provide pressure drop information for a range of expected flows. However, since this equipment is custom-made, such information is not

available. Thus, simulations were conducted to determine the pressure drop for the individual heater & cooler, based on the expected range of average pipe velocities.

6.3.3.1 Simulating Individual Heater & Cooler Performance

The meshes for individual heater & cooler assemblies are much finer than for the whole system, since the full number of nodes & elements can be used in a much smaller volume. Figure 6–6 shows the mesh for the cooler, for example. This subassembly had 424,364 nodes and 506,090 elements; very close to the maximum number allowed.

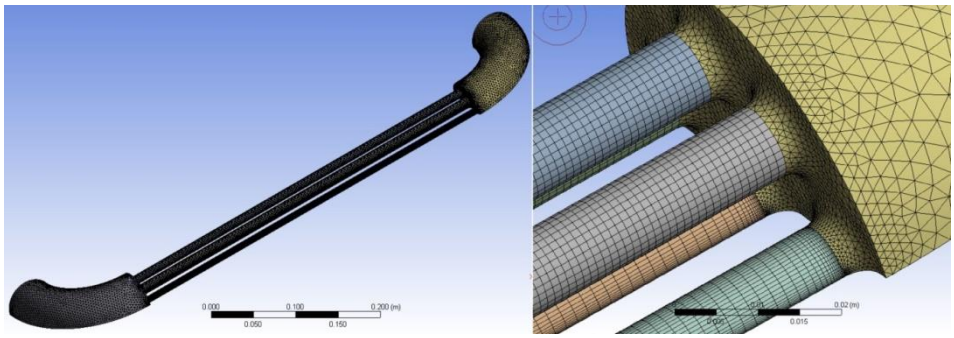

Figure 6–6 – Mesh Details for Cooler-Only Model

Figure 6–7 shows the mesh for the heater. This subassembly had 98,616 nodes and 481,390 elements; also very close to the maximum number allowed.

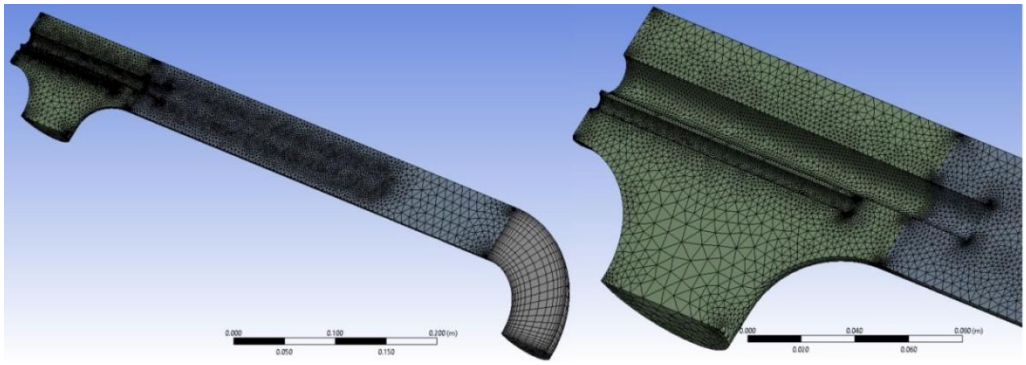

Figure 6–7 – Mesh Details for Heater Only Model

In each case, a constant/uniform velocity was imposed at the inlet, while atmospheric pressure was imposed at the outlet. The values of inlet velocity were the same as those presented in Table 6-1. The results of calibration simulations are presented in the table & graph below.

Table 6-1 – Individual Component Losses vs Inlet Velocity

Inlet Velocity [m/sec]	Heater Loss [Pa]	Cooler Loss [Pa]
0.0878	14.7046	231.5075
0.0586	7.6661	126.3357
0.0439	4.8626	87.7023
0.0352	3.4827	66.7479
0.0293	2.6652	52.9653
0.0251	2.1306	43.9856
0.0220	1.7582	37.1920
0.0196	1.4863	32.2196
0.0176	1.2804	28.7521

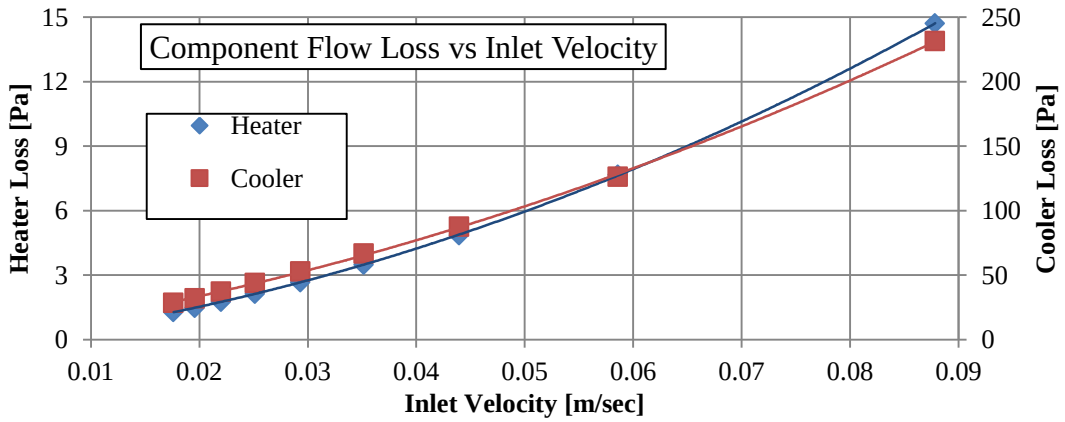

Figure 6–8 – Component Flow Loss vs Inlet Velocity

For reference, the following second-order polynomial expressions are good curve-fit for the above data; i.e., pressure drop (y) vs inlet velocity (x).

Heater: $y = 1{,}232.8717\,x^2 + 61.3424\,x - 0.1904$

Cooler: $y = 15{,}492.5619\,x^2 + 1{,}238.1867\,x + 2.6934$

The following table summarizes flow & fitting losses (calculated by using analytic values) and pressure drop through the heater & cooler (from CFD) for flow velocities corresponding to the listed ΔT values from Table 6-1.

Table 6-2 – Summary of Head Losses for Temperature Range

Temperature Range ΔT [K]	Pipe Flow Loss [Pa]	Fitting Loss [Pa]	Heater Loss [Pa]	Cooler Loss [Pa]	Total Loss [Pa]
2	62.4450	189.0047	46.9901	744.4088	1042.8486
4	15.6159	47.2654	14.7046	231.5075	309.0935
6	6.9426	21.0135	7.6661	126.3357	161.9579
8	3.9065	11.8240	4.8626	87.7023	108.2954
10	3.0417	9.2066	3.4827	66.7479	92.1661
12	2.5011	7.5700	2.6652	52.9653	80.3017
14	1.7375	5.2589	2.1306	43.9856	62.6269
16	1.2770	3.8652	1.7582	37.1920	51.2584
18	0.9781	2.9604	1.4863	32.2196	42.8887
20	0.7731	2.3401	1.2804	28.7521	36.8191

Note that the cooler is the largest contributor to friction/flow losses. One way to improve this condition would be to increase the tube ID from 3/8 to 1/2 inch.

6.3.4 Conditions for Natural Convection Flow in the Test Rig

In order to achieve natural convection flow, the available head must be larger than the total friction losses. The following table makes this comparison, based on data presented in the previous tables. The row highlighted in green is the point at which the available head for flow exceeds the total friction losses.

Table 6-3 – Comparison of Flow Head vs Losses

Temperature Range [K]	Available Head for Flow [Pa]	Total Friction Loss [Pa]
2	23.0237	1042.8486
4	24.6682	309.0935
6	50.5699	161.9579
8	77.7049	108.2954
10	92.9170	92.1661

Temperature Range [K]	Available Head for Flow [Pa]	Total Friction Loss [Pa]
12	106.4845	80.3017
14	136.9087	62.6269
16	168.1551	51.2584
18	200.6349	42.8887
20	234.7593	36.8191

Figure 6–9 shows these data with a smoothed curve added, to suggest the point above which natural convection flow occurs. It appears that when the ΔT is ≈ 9 °C, natural convection flow should occur. Using curve-fit equations, a value of 9.067 °C was obtained. The table below the graph shows the nominal ΔT for steady-state flow by natural circulation.

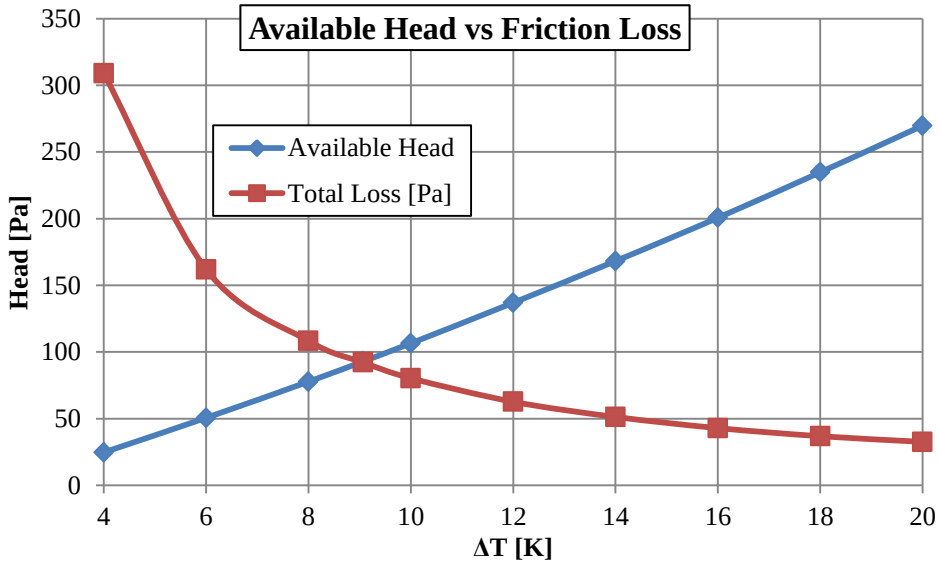

Figure 6–9 – Flow Head & Friction Losses for ΔT

Temperature Range [K]	Available Head for Flow [Pa]	Pipe Flow Loss [Pa]	Fitting Loss [Pa]	Heater Loss [Pa]	Cooler Loss [Pa]	Total Loss [Pa]
9.067	92.9170	3.0417	9.2066	4.0572	75.8606	92.1661

It is worthwhile to review the factors that are in balance under steady-state conditions:

- Adding heat to the fluid increases its temperature and reduces its density. Removing heat from the fluid decreases its temperature and increases its density.

- The longer the fluid is in contact with the heat source/sink, the greater the temperature and density changes will be.
- The difference in density and relative elevation results in a difference in pressure, which drives fluid velocity.
- So, heating & cooling the fluid changes its temperature & density, thus increasing its velocity.
- However, as fluid velocity increases, so does the friction caused by the flow through the pipe and fittings. Friction forces act to oppose the fluid velocity.
- As fluid velocity increases, the residence time within the heater/cooler decreases. As residence time decreases, the amount of energy exchanged with the fluid decreases.
- Thus, for a constant energy density (W/m^3), the potential for temperature change within the fluid decreases with increasing velocity. Refer to the first bullet point in this series.

This balance of forces emphasizes the benefit of using energy sources/sinks in the analysis, rather than choosing a ΔT for the system, as previous design studies did. Residence time is a key factor in determining whether the chosen ΔT is actually achievable.

6.3.5 Adiabatic Simulation of Test Rig Operation

As before, 3D models of each component part were created, using the Autodesk Inventor application. An assembly was created, which places the parts in their respective location. In this respect, the "parts" are really models of the fluid within the pipes, fittings, heater & cooler. The models and assembly are half-sections, to take advantage of symmetry. The result is shown in Figure 6–10. The entire system (to scale) is on the left, with enlarged sections to right showing the cooler (top) and heater (bottom).

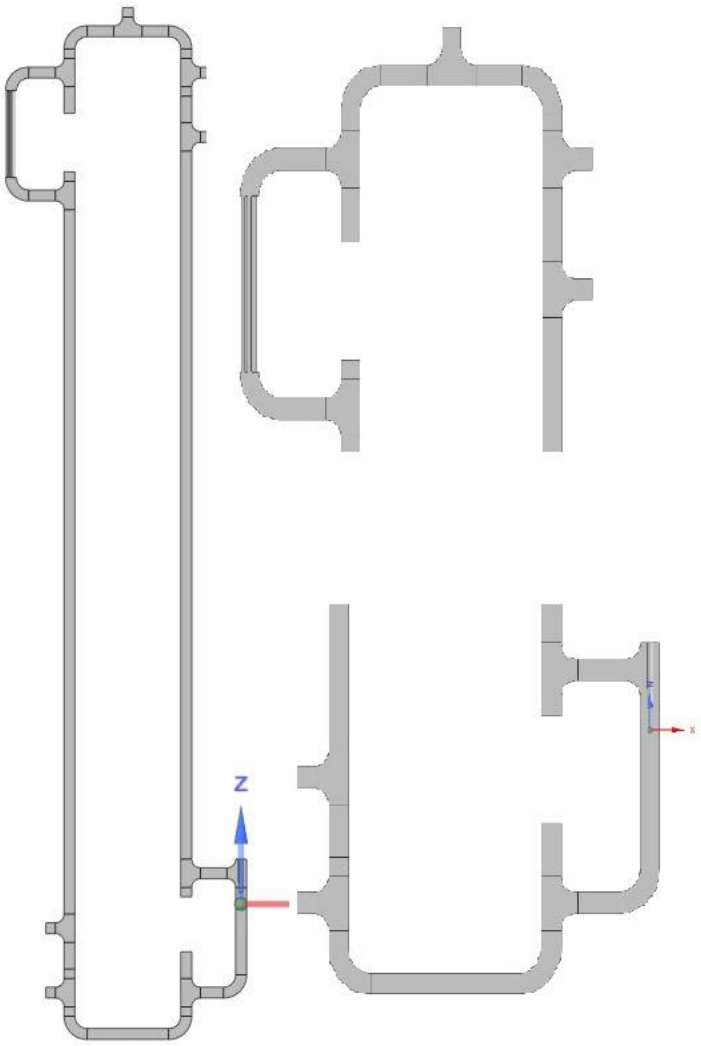

Figure 6–10 – System Model & Enlarged Features

A structured mesh was imposed for most of the system, as before. Details for the heater and cooler mesh are shown in Figure 6–11. Experienced CFD users will immediately notice that the mesh density is not sufficient to capture boundary layer effects in some locations. This is the result of restrictions on the number of nodes and elements. This model has 247,380 nodes and 481,267 elements; very close to the limit.

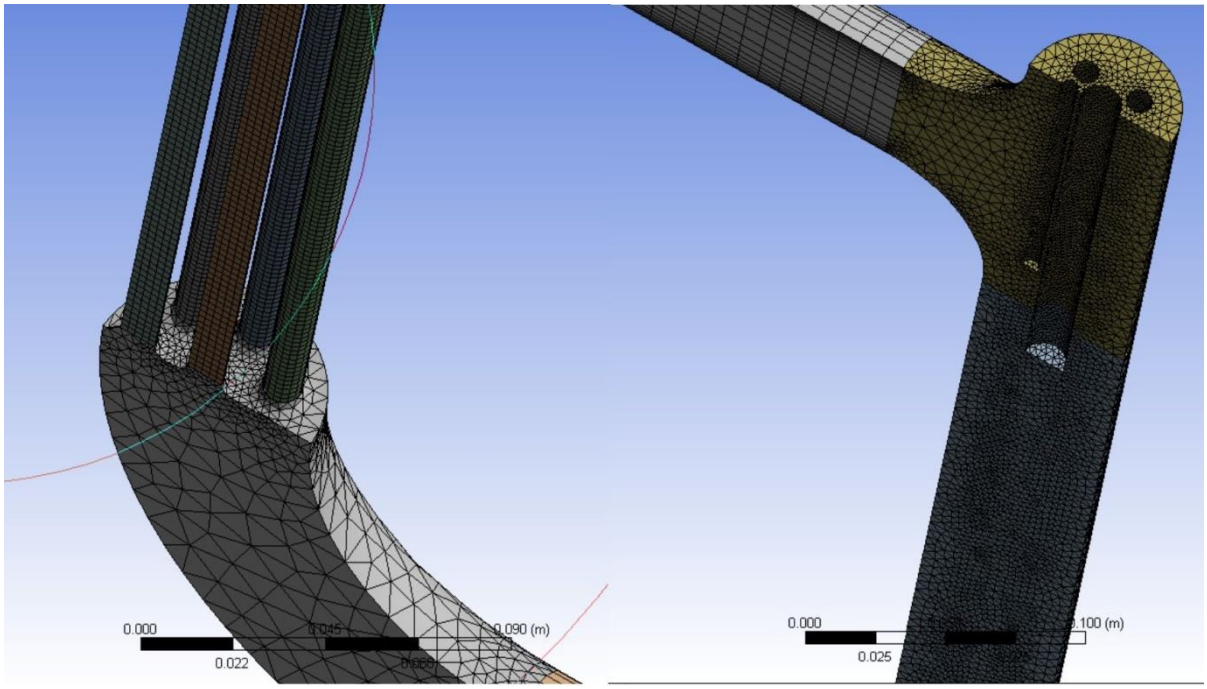

Figure 6–11 – System-Wide Mesh for Cooler (Left) & Heater (Right)

Other features of the simulation model included defining the symmetry plane and walls. The working fluid is liquid water, with an initial temperature of 300K, to fix physical properties. The simple Boussinesq density/temperature relation was chosen, with constant (default) values for specific heat, thermal conductivity and expansion coefficients.

Instead of arbitrarily choosing a temperature range, rate of energy exchange at the heater & cooler was specified instead, using the energy density values previously stated. The "Energy" feature was enabled within the ANSYS Fluent CFD program, and gravity was turned on in the z-direction. The mesh was checked & passed. However, a few elements had a large value for skewness.

The simulation was initialized with zero velocity in all directions. Second-order solvers were used at the start, switching to third-order later. It was allowed to run for 53.7k+ iterations; residuals for the last 10,000 of which are shown in Figure 6–12. The results indicate nominal convergence and it seems clear that the values have stabilized.

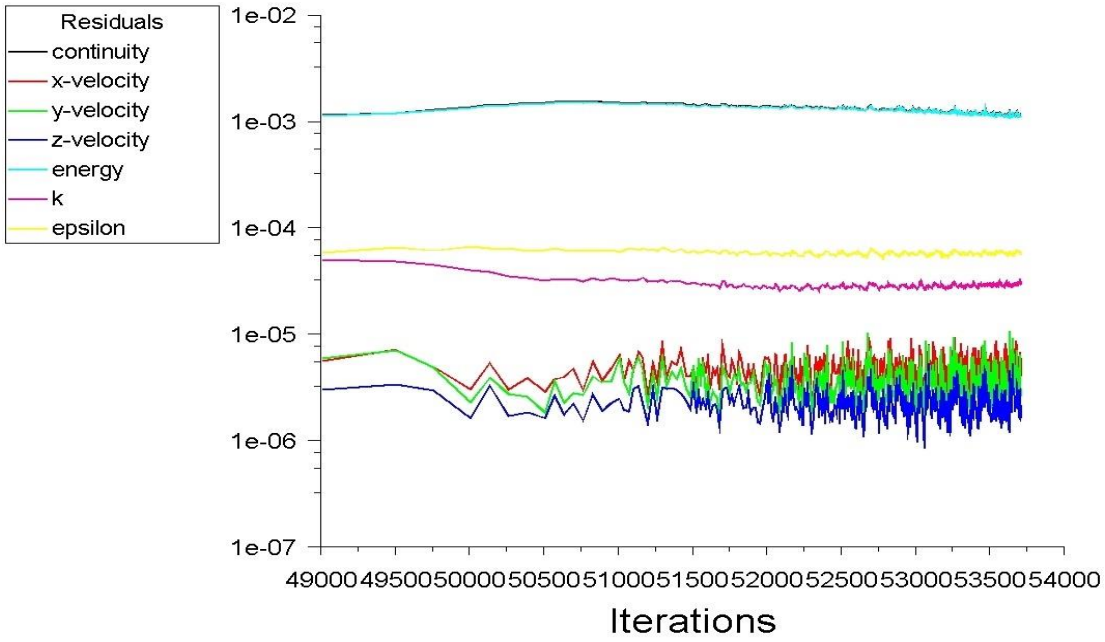

Figure 6–12 – Full System Model Residuals

6.3.5.1 Adiabatic Simulation Temperature Results

Figure 6–13 shows the resulting temperature profile at the symmetry plane, with annotated values at the approximate location of sensors in the actual test rig. The ΔT from CFD is 9.121 °C, which is within 0.6% of the analytical value of 9.067 °C.

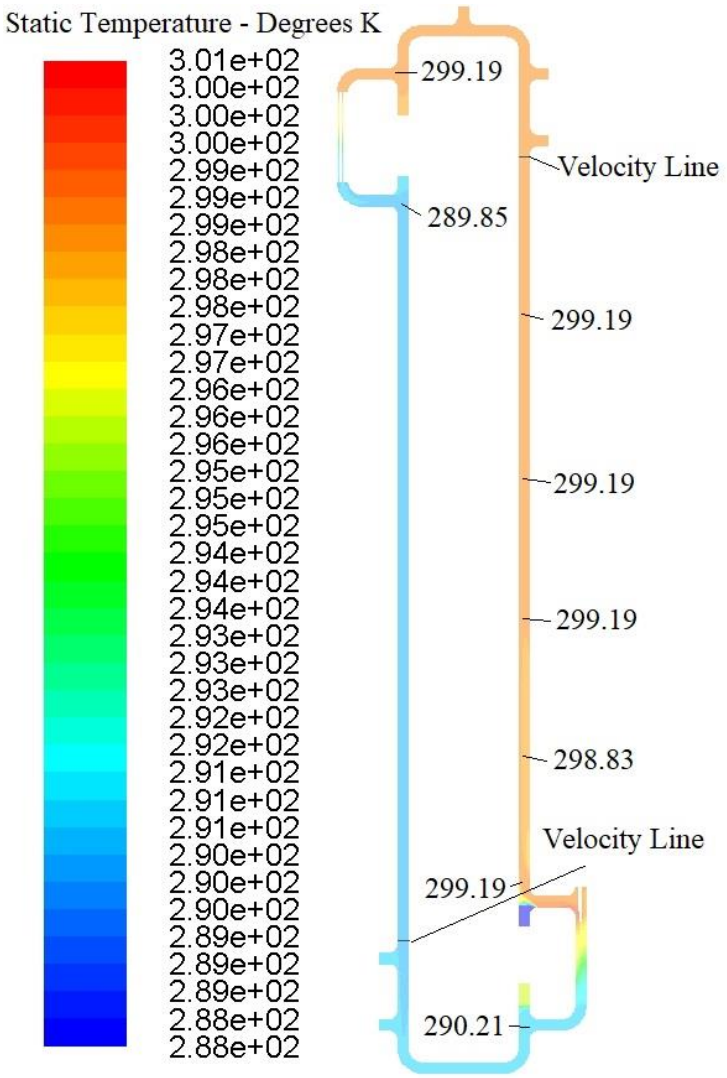

Figure 6–13 – Full System Temperature Profile & Data Points

6.3.5.2 Adiabatic Simulation Pressure Results

Figure 6–14 shows the pressure values at several points of interest. These include the location of pressure sensors in the test rig, as well as across the heater and cooler, for cross-check of individual CFD values for these components. The cooler is the focus of values on the top; the heater for values on the bottom. Note that the pressure drop across the cooler & heater is 69.52 Pa and 5.563 Pa, respectively. This is within 30% of the 76.44 Pa and 4.06 Pa (respectively) obtained from the previous/detailed CFD values for individual components.

The main reason for the discrepancy is that the inlet velocity profile for the simulation was constant across the inlet face, rather than parabolic (for laminar flow). Another reason is the use of constant values for density & dynamic viscosity of water at 20 °C, rather than at the actual temperature.

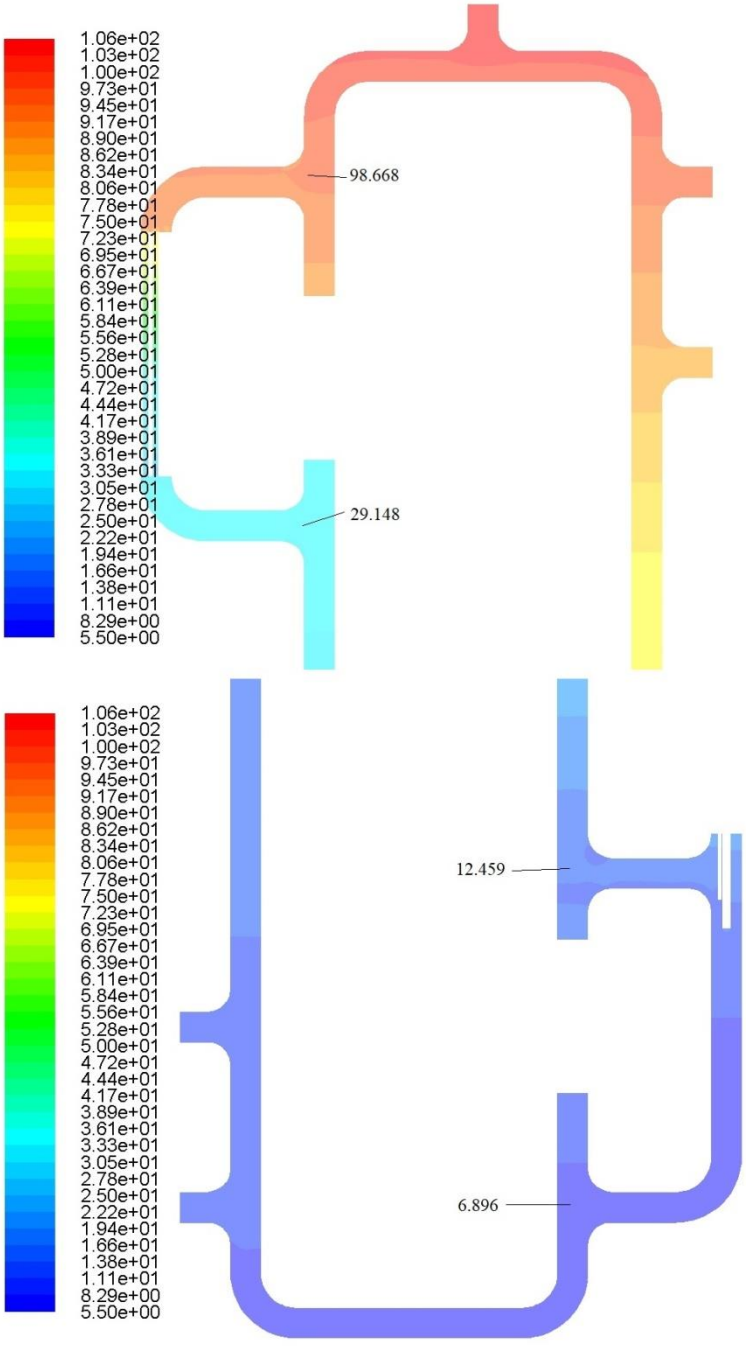

Figure 6–14 – Full System Pressure Profile & Data Points [Pa]

6.3.5.3 Adiabatic Simulation Velocity Results

Figure 6–15 shows velocity vectors at the cooler (left) and heater (right).

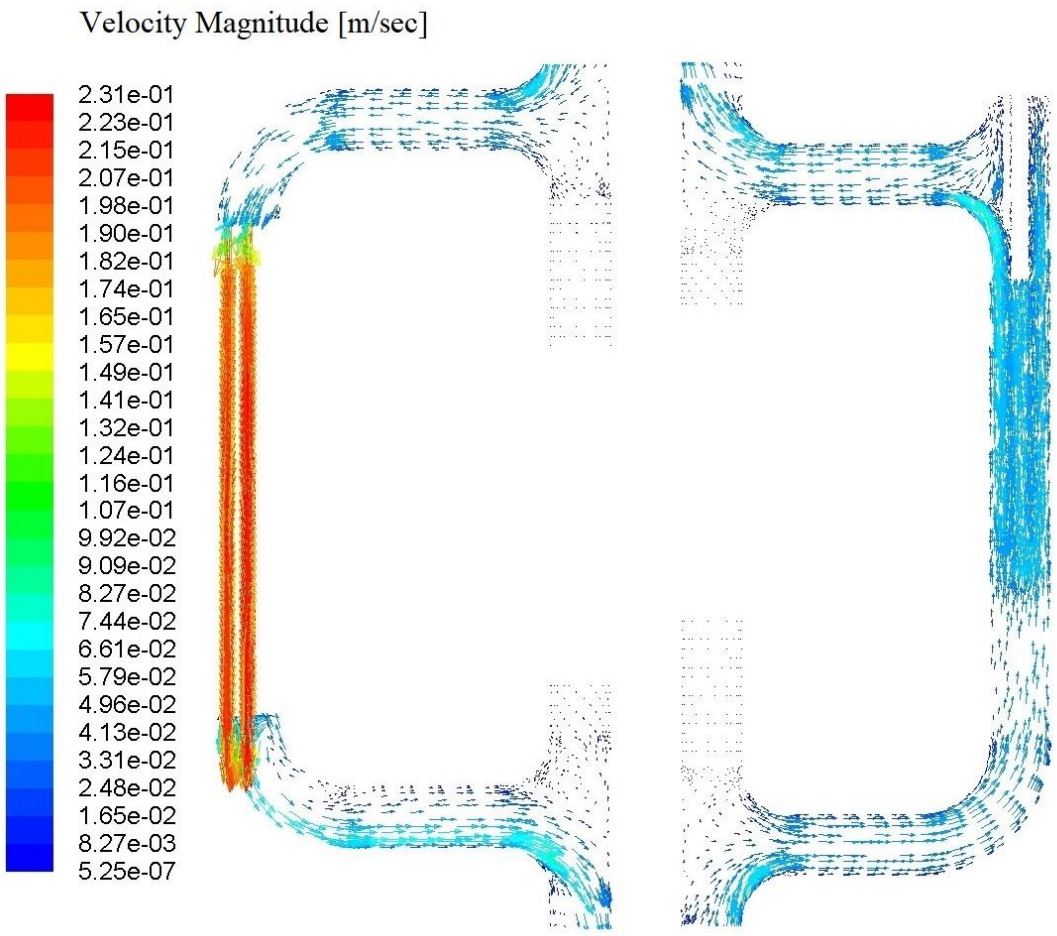

Figure 6–15 – Full Model Velocity Vectors [m/sec]

Figure 6–16 shows a close-up view of the recirculating flow at the exit of the cooler (left) and heater (right). It is important to remember that the analysis estimated a value of 0.02 for surface roughness, and an overall value of 12.3 for K in the friction loss equation **(6-1)**.

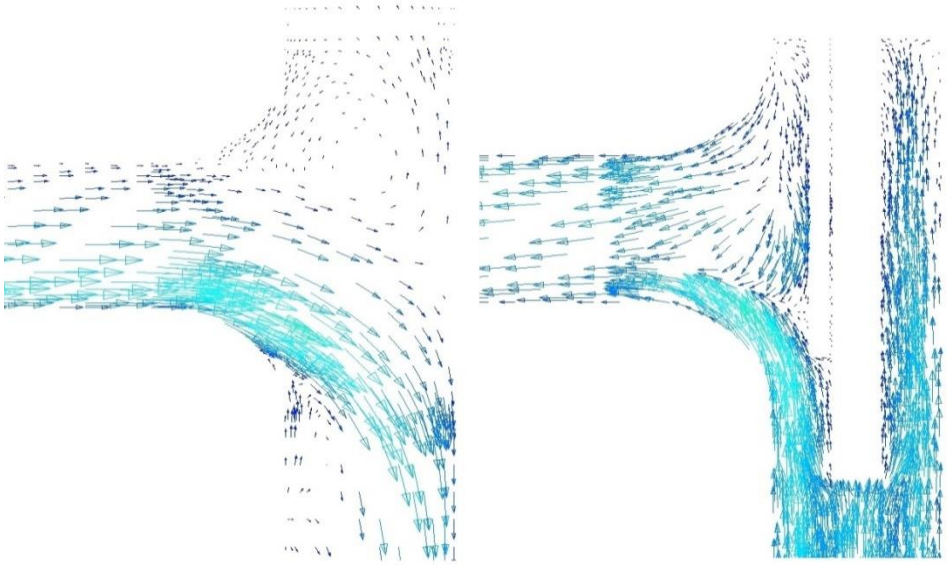

Figure 6–16 – Recirculating Flow at Cooler (Left) & Heater Exit (Right)

As before, reference lines were drawn across the pipe, to determine the average velocity. The lines are shown in Figure 6-13. Figure 6–17 shows the resulting velocity profile (black line with blue markers). The maximum value is 0.0526 m/sec, with a weighted average value of 0.0386 m/sec (green line). This is within 0.485% of the average velocity of 0.0388 m/sec from the analytic method. Note that the Reynolds number for the steady-state condition is 1980, which indicates laminar flow. This agrees with the parabolic shape of the velocity curve, as seen in the figure.

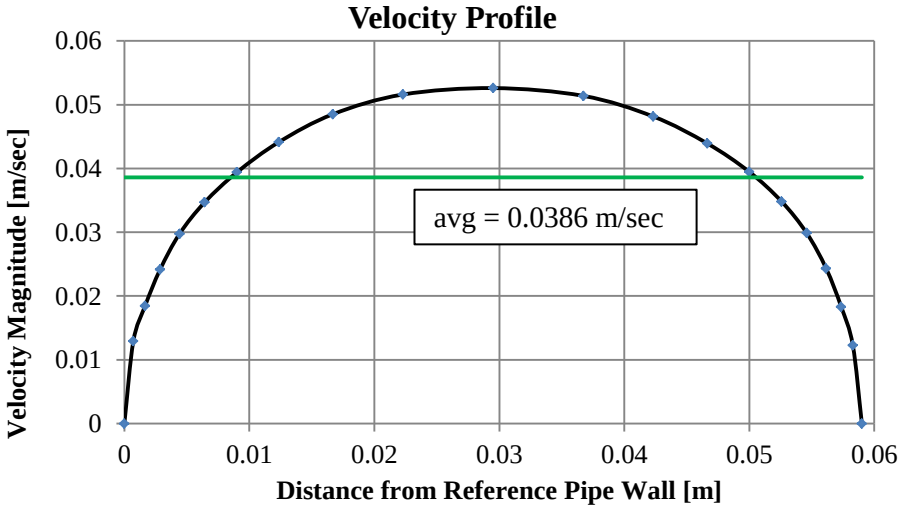

Figure 6–17 – Fully-Developed Velocity Profile

Figure 6-18 shows some path lines, colored by pressure, to indicate whether vortices are present. The results show that some flow moves through the blanked tees, but none seem to continuously circulate like a vortex.

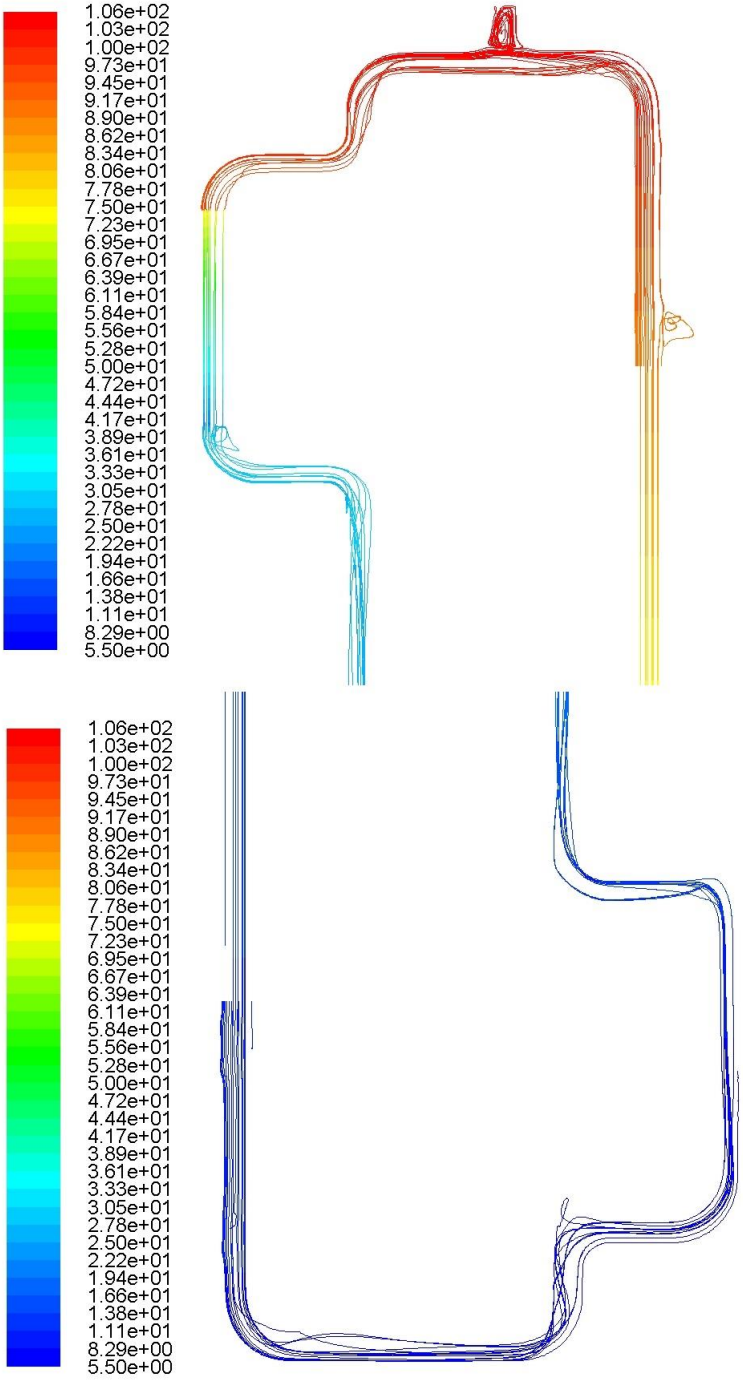

Figure 6–18 - Test Rig Path Lines [Pa]

6.4 Refined Performance Analysis

With this first set of results, one can revisit the simplifications and assumptions used therein, so as to refine subsequent simulations for better agreement with experiments and achieve more realistic results.

For example, the analyses used a constant value for heat capacity. The simulations also used constant values for thermal conductivity, thermal expansion and viscosity. Further, the simulations used the Boussinesq approximation for fluid density, based on a nominal value of 998 kg/m^3, which is the value for water at 20 °C. Given that the overall system ΔT is 9 °C, these still seem reasonable. However, given the overall size of the experimental rig, it seems reasonable to evaluate the assumed fully adiabatic condition for the system.

6.4.1 Heat Loss Analysis

As previously stated, pipe & fittings used in the rig are 2-1/2" Sch 80; ID = 2.323" (0.0590 m), OD = 2.875" (0.0730 m), wall thickness of 0.276" (0.0070 m). The material is 304 stainless steel, which has a thermal conductivity k = 16.3 W/m*K.

Paper-backed, rigid fiberglass insulation was applied to the outside of the pipe & fittings, with a wall thickness of 1/2" (0.0127 m). The insulation has an R value of 2.2, a heat flow rate of 0.23 BTU @ 75 °F, and thermal conductivity k = 0.039 W/m*K.

Ambient temperature of the lab is nominally 68 °F (293.15 K), with no special air circulating equipment at the experimental rig. A reasonable estimate for the convective heat transfer coefficient h = 20 W/m^2*K.

Figure 6-19 shows the as-built test rig before installing insulating material.

Figure 6–19 – As-Built Test Rig

The test rig and CFD model both have identical hot & cold piping legs; i.e., the same length, volume & surface area. A 1D heat transfer analysis can be done, based on the general cross-section (looking axially) in the following figure.

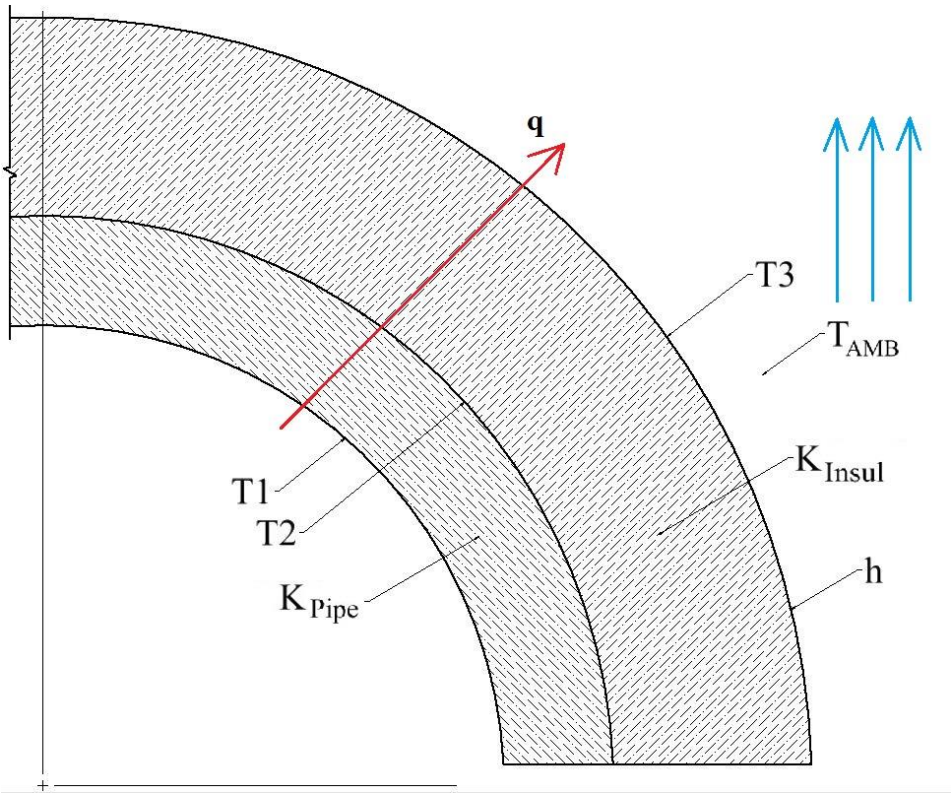

Figure 6–20 – 1D Heat Transfer Analysis

The equation for the heat rate per unit length is

$$\frac{q}{L} = \frac{T_1 - T_{AMB}}{\frac{ln\left(\frac{Pipe\ OD}{Pipe\ ID}\right)}{2\pi \cdot K_{Pipe}} + \frac{ln\left(\frac{Insul\ OD}{Insul\ ID}\right)}{2\pi \cdot K_{Insul}} + \frac{1}{h \cdot \pi \cdot Insul\ OD}}$$

The heat loss for the hot leg is 10.18 W/m, while the heat gain for the cold leg is 5.48 W/m. As previously stated, the hot and cold leg lengths are the same, at about 12 m. Thus, the hot leg loses 122 W, while the cold leg gains 66 W. The net energy added to the entire test rig system from the environment is about 56.4 W; only 1.4% of the heater capacity. Thus, it isn't necessary to include any additional refinements to the simulation for a water system.

However, if a different working fluid (such as a low melting point salt) were used in the experiment, this would be a factor to consider.

6.5 CFD-Specific Information

6.5.1 Mesh Evaluation – Resolving Boundary Layer

A plot of y+ values for the system components is shown in Figure 6-21. A total of 32,753 points exist. Of these, 29,497 had y+ values ≤5 (90.06%). Thus, the mesh does a nominally adequate job of capturing boundary layer effects.

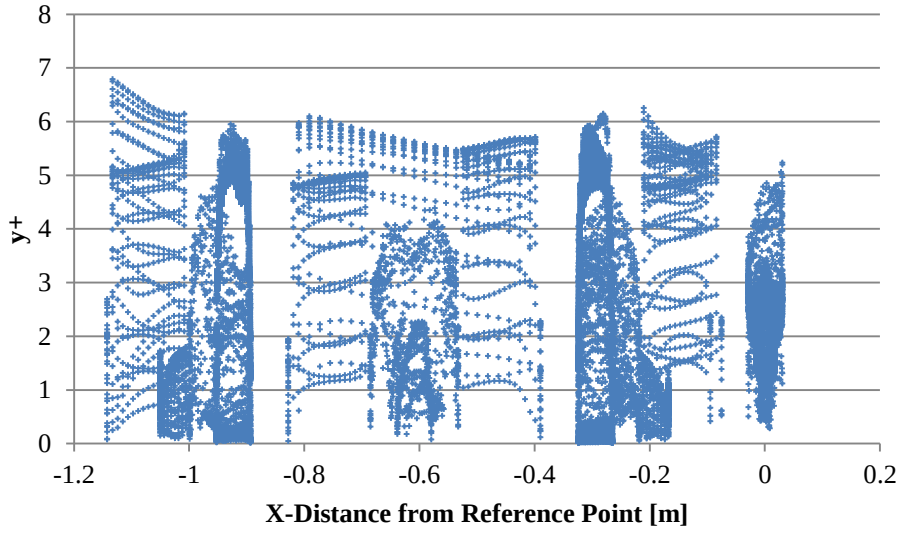

Figure 6–21 – Values for y+, Component Walls

6.5.2 Turbulence Model Evaluation

As before, results obtained using the k-ε turbulence model were compared with those using the k-ω SST model. The results (tabulated below) indicate that values from the k-ε model more closely matched those from analytic means. Thus, use of the k-ε model is valid. It is worthwhile to note that use of the k-ω model takes significantly more time per iteration. Further, it prolongs oscillations during the solution process; i.e., significantly more iteration is needed to achieve a steady state.

Parameter	Analysis Value	k-ε Value	k-ω Value
ΔT [K]	9.067	9.121	9.599
v_{avg} [m/sec]	0.038785	0.038600	0.037951

6.6 Verification of CFD Results

A basic verification analysis was not performed for the CFD results of this system. When actual experimental results become available, a comparison between the CFD and experimental values will be much more meaningful.

6.7 Conclusions for this Set of Simulations

- The CFD results match calculated values from analytic methods within 0.49%. Thus, it seems that CFD software is able to model natural convection flow to the extent necessary to conduct experiments and perform meaningful comparisons to complete benchmarking of the overall process presented herein.

7 Simulating an MSR System – Reactor Vessel with Internal Moderator

7.1 Abstract

This chapter uses previous results herein, adding another level of complexity to the model. Specifically, it provides:

- CFD results for an MSR with idealized reactor core design. It has internal structure, based on the "slab" moderator bar concept previously described.
- A description of required simplifications and a revised design.
- A description of the setup, initialization and running of the simulation.
- CFD results; temperature profile & velocity vectors for steady-state conditions.

7.2 Idealized Reactor Vessel Core Design

Using the slab moderator-element concept described in section 1.4.7.2 herein, an idealized reactor vessel core was designed. The moderator bars are 19.372 inches wide by 2.124 inches thick, with 0.320 inches between bars (fluid passage width). The cylindrical reactor vessel is 85" in diameter x 89 inches tall (i.e., height nearly equal to diameter for aspect ratio ≈ 1). The design is shown in Figure 7–1 below. As before, this model takes advantage of half-section symmetry.

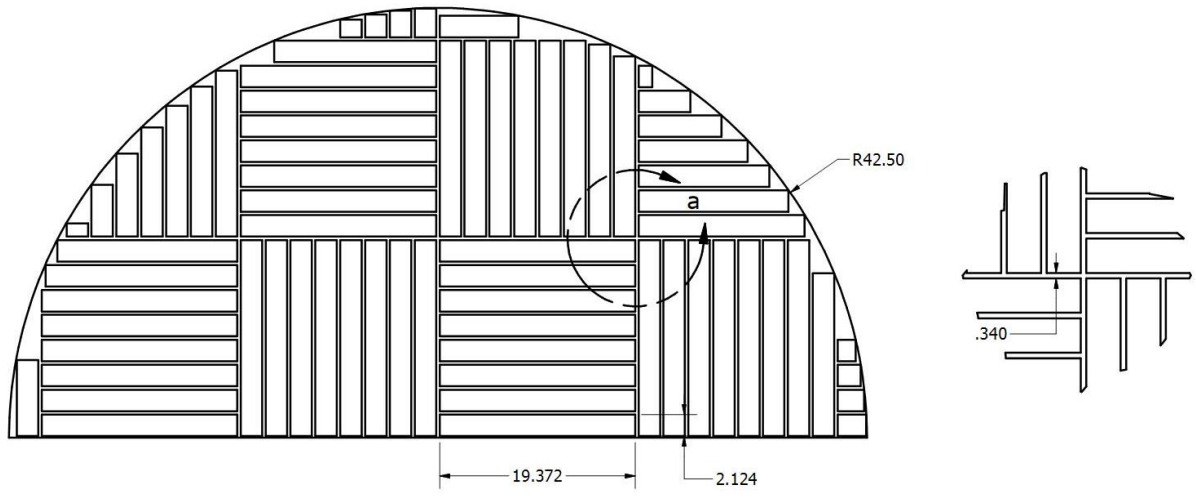

Figure 7–1 – Initial Reactor Vessel Core Design – Top View & Detail

The overall system model uses the same size heat exchanger as before (i.e., 48” diameter by 50.4” high). It uses 16” diameter connecting piping with short-radius elbows. There is a nominal 12-foot difference in elevation between the heat exchanger & reactor vessel.

While attempting to transfer the model (with heat exchanger & connecting piping) from the 3D modeling program to the CFD application, a software limitation was encountered. Specifically, the SpaceClaim utility in ANSYS Workbench has a restriction of 300 faces and 500 edges. The idealized design greatly exceeded this value – the reactor vessel alone had 438 faces. Thus, simplifications were required.

7.3 Simplified Reactor Vessel Core Design

Simplification of the reactor vessel core, with the goal of reducing the number of faces was achieved by reducing the number of moderator bars. An acceptable design is shown in Figure 7–2. It has moderator bars that are 19.5 inches wide by 2 inches thick. The spacing between bars (fluid channels) is 0.5 inches.

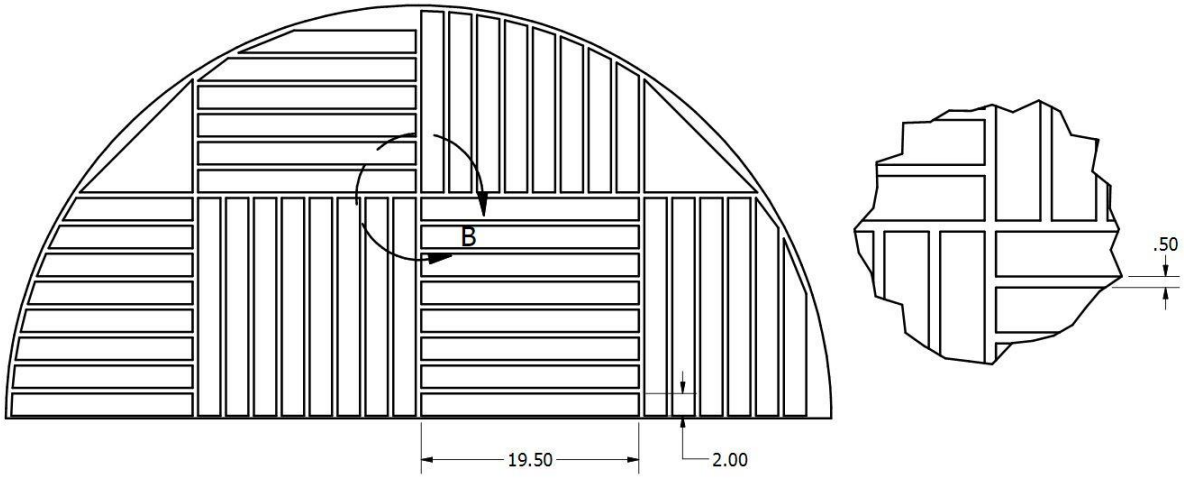

Figure 7–2 – Simplified Reactor Vessel Core Design

The revised reactor vessel has a 74 inch diameter x 80 inch height. The heat exchanger is 44.5 inches in diameter x 60 inches high. The complete assembly, shown in Figure 7–3, has *exactly* 300 faces. It includes the reactor vessel interior structure as shown above.

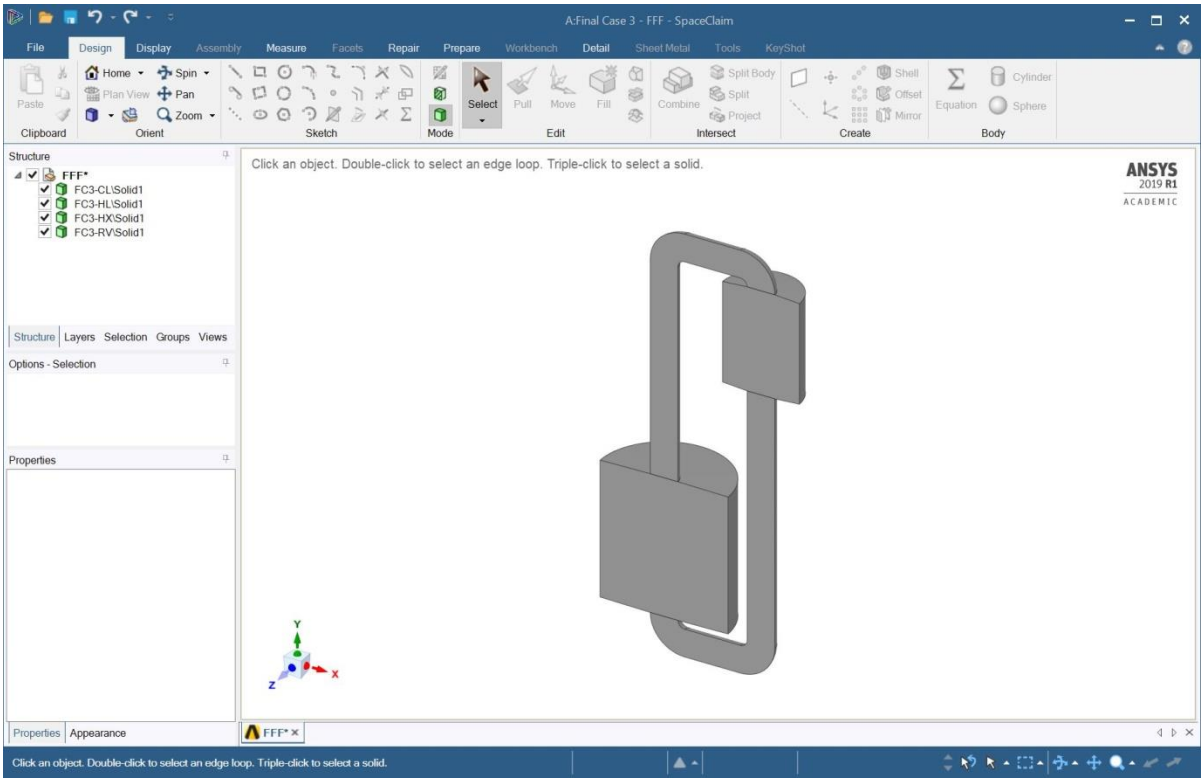

Figure 7–3 – Full Model in SpaceClaim Application

The fluid passage volume is 12.3% of the reactor vessel core (vs the graphite moderator volume), which falls within the desired range for an MS(B)R.

Once saved, the Design Modeler application was opened, where objects were named, symmetry surface of symmetry was designated, as well as fluid boundaries (walls).

The Meshing application allows inspection of contact regions (mesh interfaces within the fluid boundary). Edge controls were added, to achieve a largely structured mesh. This includes appropriate biasing, to concentrate elements in areas of interest; i.e., walls & transition features.

Note that most pressure vessels (i.e., reactor & heat exchanger) normally have rounded corners. Further, transitions from vessels to pipe would have a radius. These features are not included in the model, due to face restrictions – this will undoubtedly affect fluid flow. The coarse mesh, shown in Figure 7–4, has 255,471 elements. Thus, it is possible to improve on

the results as well as perform a verification analysis. A minimum of three solutions are required to perform these evaluations[99]. The fine mesh has 510,897 elements.

Figure 7–4 – Coarse Mesh

7.4 Simulation Setup

Once transferred from ANSYS Meshing to Fluent, the fluid properties for FLiBe, as listed in Chapter 5 herein were entered.

As before, under the "Domain" tab in Fluent, the "energy" module was turned on, and the Realizable k-ε turbulence model was selected. A mesh check was conducted, which passed. There are four "cell zones" in this model (i.e., reactor vessel, heat exchanger, hot & cold connecting pipes). All were assigned FLiBe as the working fluid.

The heat exchanger was given an energy source term with a constant value of -22.2 MW/m^3. Since it has a volume of 91750.214 in^3 = 1.504 m^3, this means 33.3 MW_t is being drawn off

[99] T Xing, Computational Fluid Dynamics, Lecture Notes for Session17 (2017)

using this component. When coupled to a power generating system with 33% efficiency, this creates 10 MW_e, which is the design goal. This value was constant throughout the simulation.

The reactor vessel zone was given an energy source expression as stated in section 5.4.6 herein. Its volume is 91642.53 in^3 = 1.502 m^3. Thus, at steady state, the amount of energy added should equal the amount removed.

Under the "Physics" tab in Fluent, a density-based, steady-state solution was selected. Gravity was turned on, with 9.81 m/sec^2 as the standard value. Operating conditions were changed to reflect a nominal operating temperature = 830 K and density = 2008.3024 kg/m^3 (corresponding to that temperature).

Under the "Solution" tab in Fluent, Limits were imposed, specifically with regard to temperature. A static minimum of 300K and maximum of 2000K were entered, only to aid in convergence. Simulations results outside this range would not meet the design criteria anyway. Default solvers were used for the first simulations.

7.5 Initializing and Running the Simulation

Due to the complexity of the system, a "standard" initialization was done, with the gauge pressure and all initial velocities set to zero. Turbulent kinetic energy was set to a nominal value of 0.5 m^2/sec^2, with a dissipation rate of 0.3 m^2/sec^3. Initial temperature is 830K.

A small value was initially given for the number of iterations, to ensure the solution tends to convergence. Afterwards, the simulation was allowed to run for many thousands of iterations, to ensure a steady-state was achieved.

Note the similarity between the simulation initialization and an actual reactor startup. In an actual system, one would heat up the salt mixture to ensure it is fully melted. Then, one would start withdrawing control rods and removing energy at the heat exchanger. Once criticality is achieved, the system will seek equilibrium between the energy released in the

reactor vessel and that removed from the heat exchanger. This is analogous to the monitoring and adjustments done to reach a steady-state solution in the simulation.

7.6 Results

A sample plot of residuals is shown in Figure 7–5, which suggests nominal convergence. Beyond a certain point, residual values do not change with increased iteration. That is, the pattern between 10–12k iterations is the same as between 50–52k, 70–72k, etc. As explained in section 5.6 herein, the use of variable energy density (as a function of temperature) makes the equations non-linear. Thus, one cannot rely solely on residuals to determine whether a steady-state condition has been reached. Variables of interest must be tracked as a function of the number of iterations until they do not appreciably change[100]. These include weighted average hot & cold leg temperatures, the resulting ΔT, and weighted average hot & cold leg velocities.

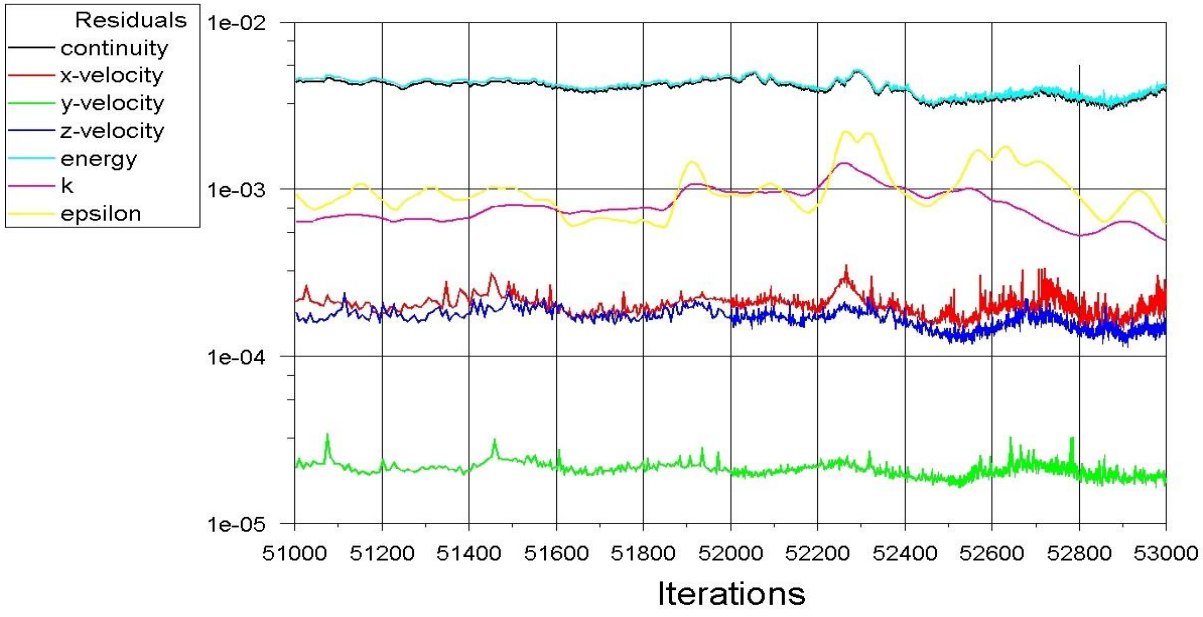

Figure 7–5 – Residuals

[100] M Kuron, 3 Criteria for Assessing CFD Convergence, The Engineer (2015)

Temperature contours are shown in Figure 7–6. The fluid temperature at the reactor outlet is 939.84K and 813.39K at the inlet for a ΔT of 126.45K. Thus, the model nominally meets the design parameters.

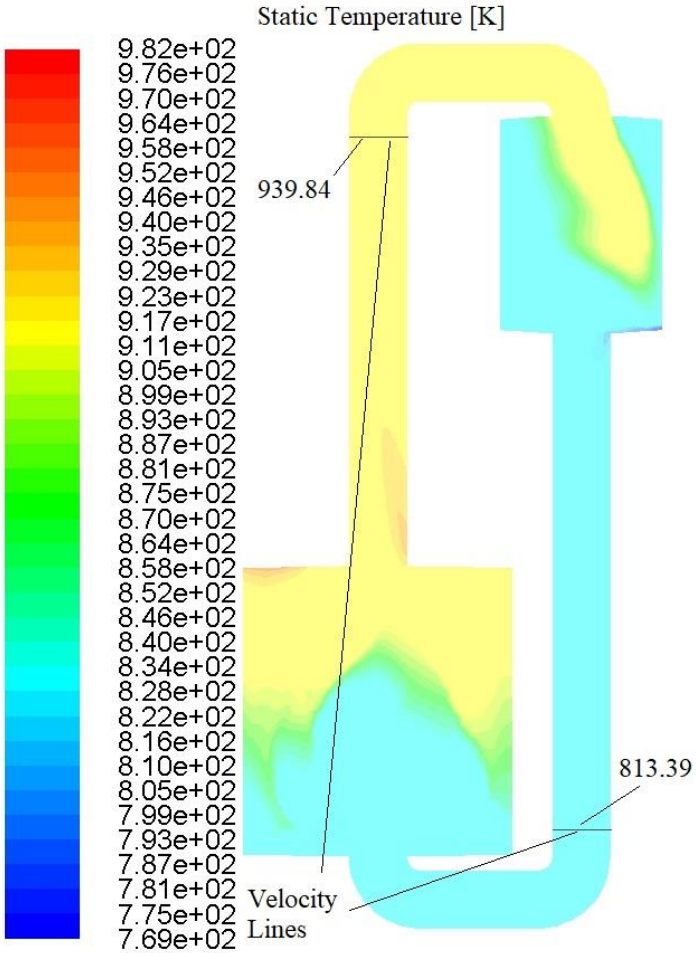

Figure 7–6 – Temperature Contours

Velocity vectors are shown in Figure 7–7. It is clear that the sharp corners where the pipes join the vessels do have an effect on the results. Also, the reactor outlet riser shows a little bit of backflow just above the connection point.

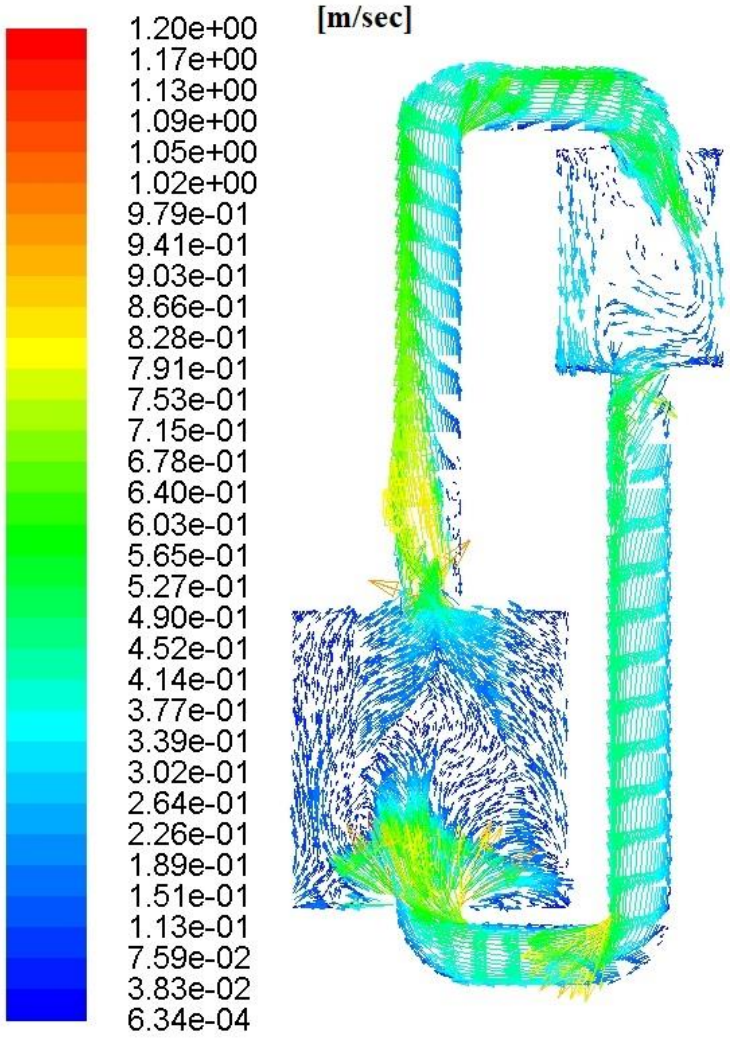

Figure 7–7 – Velocity Vectors

As before, reference lines were drawn across the pipe, to determine the average velocity. The lines are shown in Figure 7-6. Figure 7-8 shows the resulting velocity profile (black line with blue markers). The maximum value is 0.4458 m/sec, with a weighted average value of 0.4227 m/sec (green line). The Reynolds number for the steady-state condition is 42,350, which indicates turbulent flow.

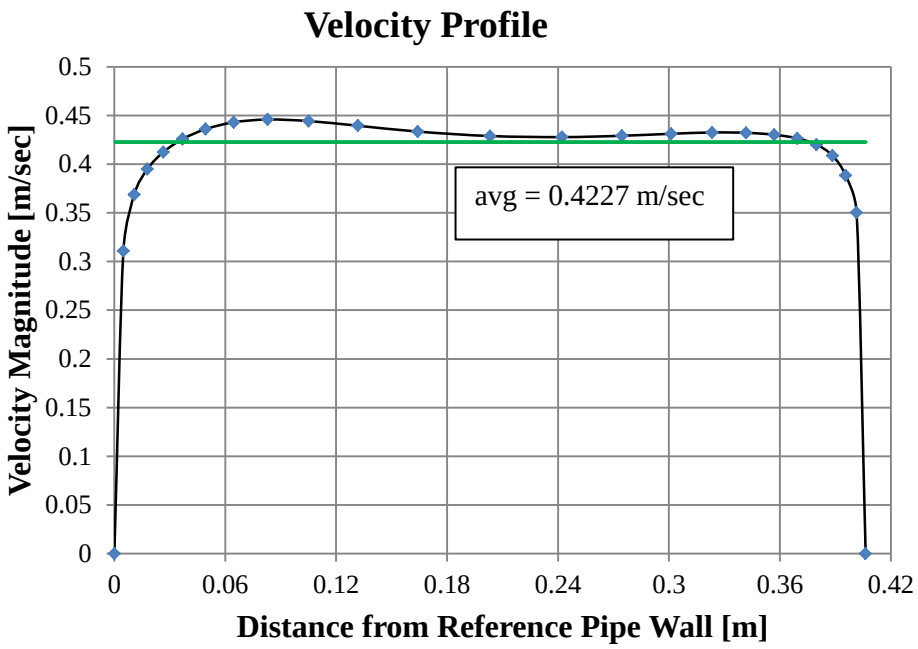

Figure 7–8 - Velocity Profile

The figure below shows path lines originating from nodes in the velocity lines. The lines are colored by pressure [Pa], to indicate where vortices might exist. The results suggest that, while there are regions of flow circulation in the vessels, none seem to form vortices.

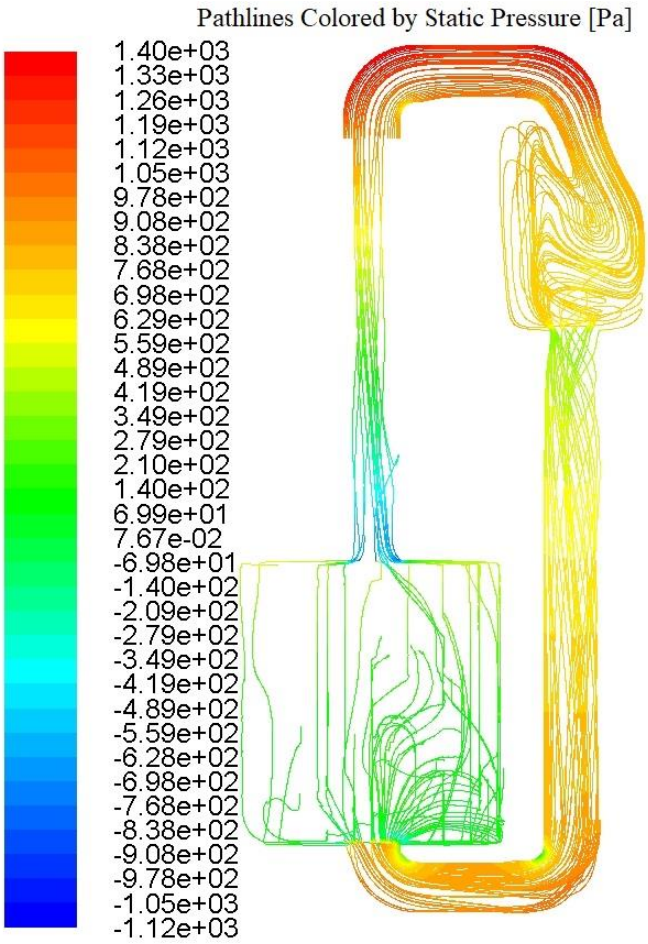

Figure 7–9 – Path Lines Colored by Pressure [Pa]

7.7 Comparison with Analysis

Results from Chapters 4, 5 and 6 herein were accompanied by comparisons with analytic methods. This was possible due to well-established values for pressure/flow losses through the pipes and fittings comprising the system. However, for this case, pressure/flow losses through the reactor vessel can only be vaguely guessed, due to the complex internal structure. Thus, comparison with analysis has very little meaning and is omitted for this simulation for that reason.

7.8 Comparison with Chapter 5 Results

There are several key differences between the model of this chapter and Chapter 5:

- The reactor vessel has a complex interior structure, due to the array of graphite moderator bars.
- The heat exchanger does not have a baffle to prevent/reduce the flow-through condition.
- The connecting pipe size is increased from 12" to 16" diameter.

Overall, the model of this chapter has a lower ΔT and average velocity than that of Chapter 5. The biggest factor in this is the larger pipe diameter. The temperature contour and path line plots suggest that a baffle isn't necessary to reduce flow-through in the heat exchanger. The moderator bars prevent flow-through in the reactor vessel.

This basic comparison shows the tradeoff in overall fuel salt volume; i.e., a larger pipe diameter can reduce the required difference in elevation (Δz).

7.9 CFD-Specific Information

7.9.1 Mesh Evaluation – Resolving Boundary Layer

A plot of y+ values for the system components is shown in Figure 7-10. A total of 13,670 points exist for the reactor vessel wall. Of these, 11,316 had y+ values $\leq$5 (82.78%). Thus, the mesh does not adequately capture boundary layer effects. Thus, the actual average velocity in the pipe and overall ΔT could be slightly different than the CFD result. Of course, the way to remedy this is to use more nodes, which would require more computing time. For this research it also means that a different software program (or license) would be required (with some non-trivial difference in cost).

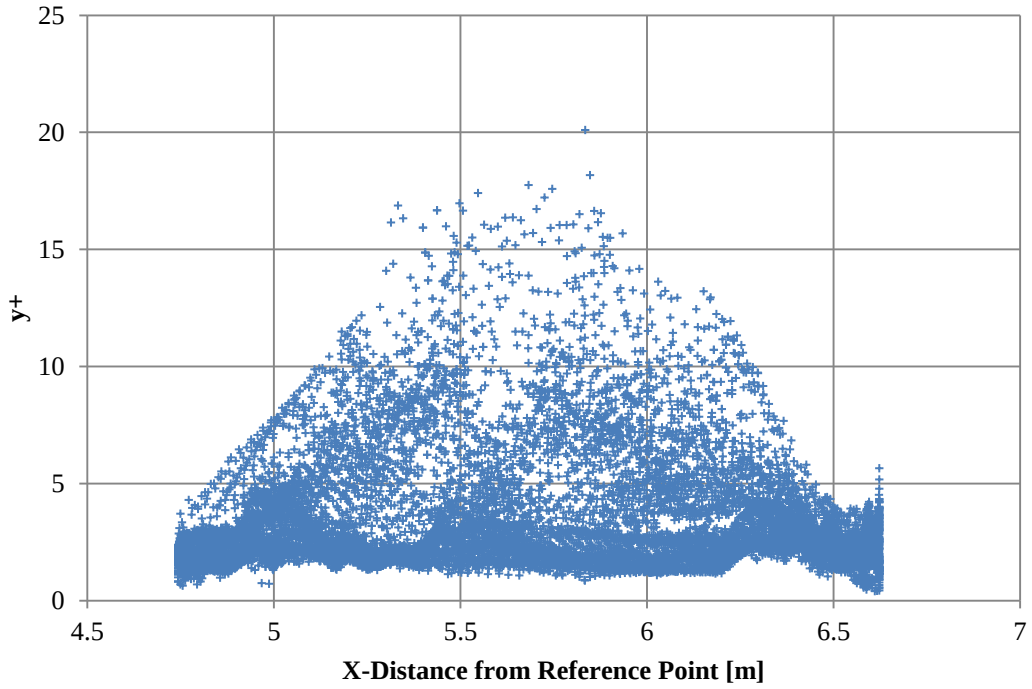

Figure 7–10 – y+ Values for Reactor Vessel

7.9.2 Turbulence Model Evaluation

As before, results obtained using the k-ε turbulence model were compared with those using the k-ω SST model. The results, tabulated below, show no appreciable difference between the two. Thus, use of the k-ε model is valid. It is worthwhile to note that use of the k-ω model takes significantly more time per iteration. Further, it prolongs oscillations during the solution process; i.e., significantly more iteration is needed to achieve a steady state.

Parameter	k-ε Value	k-ω Value	% Difference
ΔT [K]	126.454	126.566	0.0883
v_{avg} [m/sec]	0.409862	0.409609	0.0616

7.10 V&V Analysis

A basic verification analysis is presented to demonstrate the quality of results. Previous chapters selected one case as a representative, since several relative elevations were simulated. This chapter has one case, and thus it will be shown herein. CFD values for ΔT and v_{avg} will both be evaluated, using the Factor of Safety (FS) method.

7.10.1 Verification Basis Values

The same mesh refinement technique and refinement ratio was used as before. The following table shows how this was satisfied, using the number of elements in each model as the basis. The table also includes the S_1, S_2 and S_3 CFD values for ΔT and v_{avg}.

Table 7-1 – Verification Basis Values

Mesh No.	**No. Elements**	**CFD Grid Designation**	**ΔT [K]**	**v_{avg} [m/sec]**
1 (Fine)	510,897	S_1	126.454	0.4099
2 (Medium)	361,243	S_2	126.465	0.4103
3 (Coarse)	255,471	S_3	128.022	0.4227

7.10.2 Convergence Study

From the above data, one can obtain the FS method epsilon values (ε_{21} and ε_{32}) and solution ratio (R), as indicated in the following table.

Table 7-2 – Convergence Study Results – Case #7

Variable	**ΔT**	**v_{avg}**	**R (ΔT)**	**R(v_{avg})**
ε_{32}	0.01117	0.0004188	0.00718	0.03366
ε_{21}	1.55668	0.0124451		

Note that values for both ΔT and v_{avg} are $0 < R < 1$, indicating **monotonic convergence**.

7.10.3 Error Estimate

Next, the observed order of accuracy and error estimates are calculated, the results of which are given below. Recall that second-order accurate solution methods were used after numerous iterations, thus the theoretical accuracy (P_{th}) = 2.

Table 7-3 – Error Estimate – Case #7

δ_{RE}	**ΔT [K]**	**v_{avg} [m/sec]**
	0.000081	0.000015

7.10.4 Uncertainty Estimate

Finally, the estimated (grid) uncertainty values are calculated, as shown below. Note that use of the FS method implies a 95% confidence factor.

Table 7-4 – Uncertainty Estimate – Case #7

	ΔT [K]	**v_{avg} [m/sec]**
U_G	0.00824	0.00095
U_G (%S_1)	0.014	0.519

7.11 Conclusions for this Set of Simulations

- It seems that CFD software can also accommodate models with a reactor vessel that includes complex internal geometry along with previous complexities of variable fluid properties and power density.

- The results show that it is feasible to have an MSR that runs on natural circulation. However, pressure losses through the heat exchanger are not accounted for. Thus, the flow values are likely overstated.

- Using the previously determined difference in relative elevation between the reactor vessel and heat exchanger of 12 feet, a realistic reactor vessel internal structure can meet the design criteria of having a maximum ΔT of 139 °C.

8 Simulation of an Alternate MSR System Design

8.1 Abstract

This chapter provides:

- An alternate MSR system design, based on a reactor vessel with an external moderator/reflector, rather than one with internal moderator bars.
- A description of the analysis conducted, and ways to improve & refine the design.

8.2 Alternate Reactor System Design

The previous simulations had a reactor with moderator bars positioned inside the vessel. An alternate reactor design allows the fuel salt to partially serve as moderator. The reactor vessel is then surrounded by a "reflector," to enhance neutron utilization and keep the core in a critical state. Such a design, developed at the University of Idaho at Idaho Falls, is known as the Molten Salt Nuclear Battery™ (MSNB). Figure 8–1[101] shows the fluid system elements; i.e., reactor vessel (bottom center), discharge riser, connecting piping, upper annular heat exchanger, and lower annular downcomer.

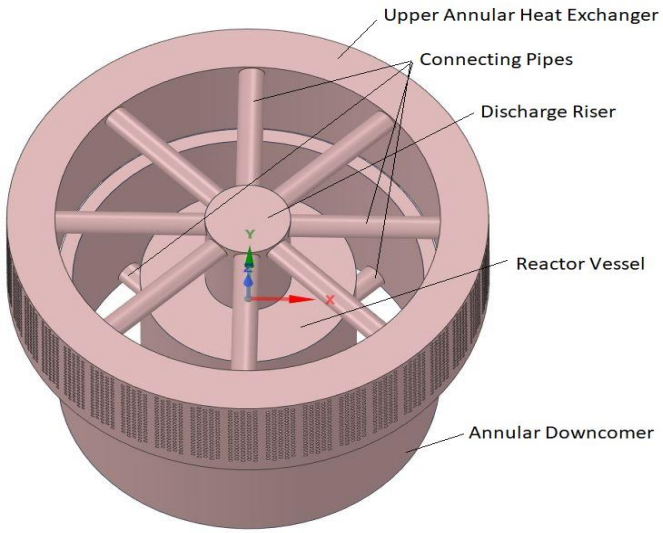

Figure 8–1 – MSNB Design

[101] MA Cardenas, University of Idaho, private communication (2019)

A one eighth section was developed for the CFD analysis, taking advantage of symmetry. Figure 8–2 shows the resulting 3D model. Note the relatively "thin" cross-section of the lower annular downcomer (see arrows in figure). Also, note that the heat exchanger portion of the model does not include any cooling tubes for extracting heat from the system.

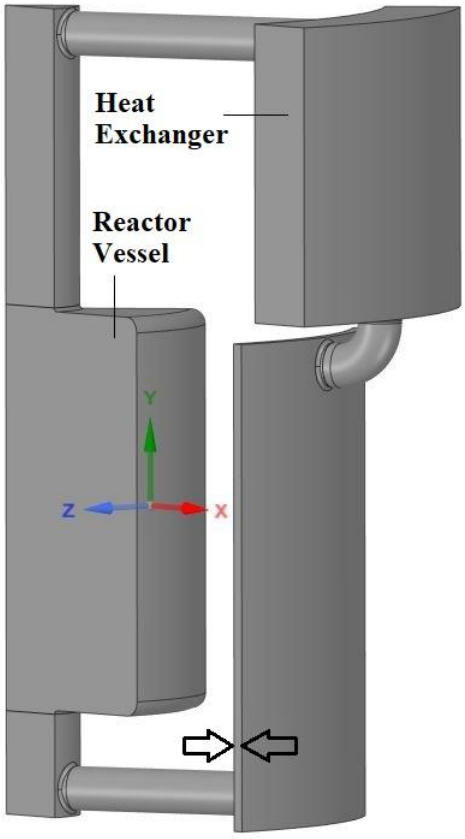

Figure 8–2 – Eighth-Section of Initial Reactor System Design

The reactor vessel is 1.35 m in diameter and 1.35 m high, for a nominal volume of 1.93 m^3, and aspect ratio of 1. The reactor vessel inlet & outlet risers are 0.5 m in diameter. All of the connecting pipes are 0.15 m in diameter. The relative height difference between the reactor vessel and heat exchanger is 47.01 inches (3.9175 ft. = 1.194 m). With a known (achievable) power density of 22.2 MW/m^3, the system should generate about 42.9 MW_t (14.3 MW_e), not considering friction losses.

A CFD analysis was conducted, using the same techniques and workflow sequence as before. At steady state, the temperature profile through the central plane is shown in Figure 8–3.

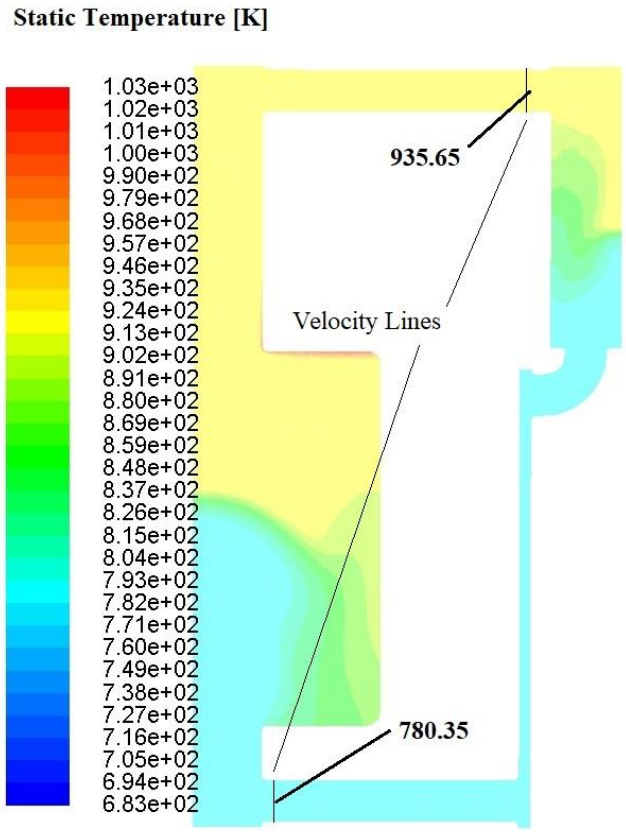

Figure 8–3 – MSNB – Steady State Temperature Profile

Velocity vectors through the central plane are shown in Figure 8–4. The highest velocities are in the pipes connecting the components. The thin cross-section of the lower annulus (downcomer) does not seem to be a limiting factor. It seems possible to refine the design to improve flow through these features. That is, the diameter of the connecting pipes could be increased, but this will increase the fuel salt volume somewhat.

Notice how flow in the reactor vessel circulates internally. There isn't a "flow-through" problem, even without having an internal baffle, which is a good thing.

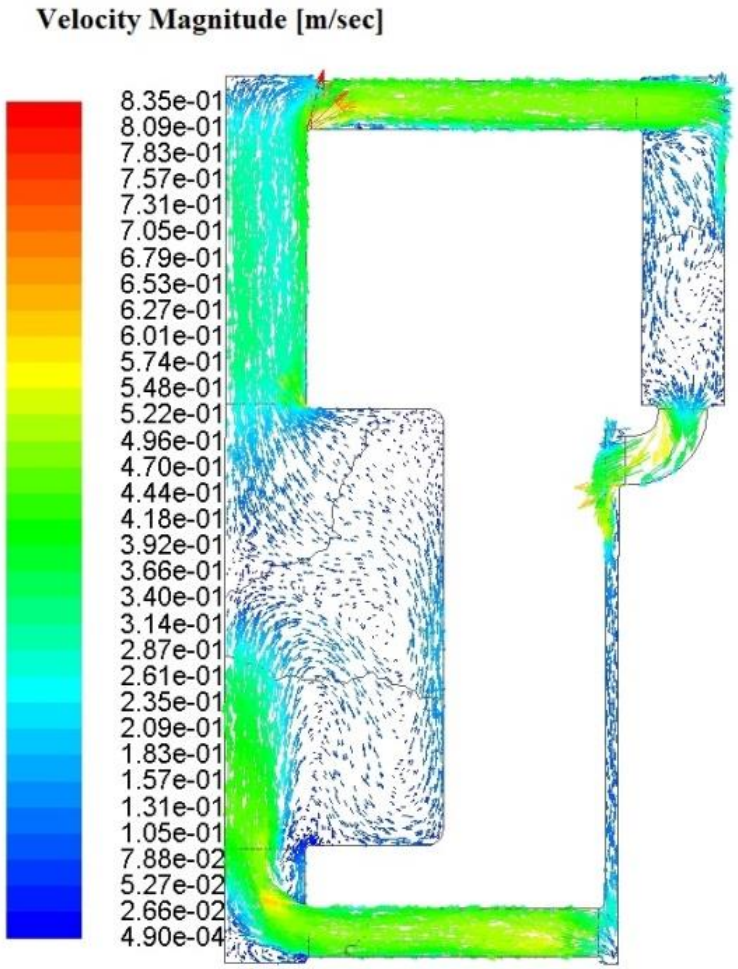

Figure 8–4 – MSNB – Velocity Vectors

Important results from the simulations include system temperatures. The recommended min & max temperatures (from Section 5.4.1 herein) are 797K and 936K, respectively, for an overall ΔT of 139K. CFD results show reactor inlet and outlet temperatures are 780K and 936K, respectively, for an overall ΔT of 156K. CFD values were obtained at the upper & lower connecting pipes, and they were used to check for convergence and calculate the power generated. However, as seen in Figure 8–3, there are regions in the reactor vessel where the temperature is even higher, and regions in the heat exchanger where it is even lower. Thus, some parts of the reactor vessel would likely suffer heat-related material degradation and some of the fluid in the heat exchanger would likely solidify.

As shown in Chapters 4 & 5 herein, increasing the relative height between the reactor vessel and heat exchanger increases the average velocity and decreases the overall ΔT. Thus, a critical and necessary refinement is to increase the relative elevation difference between the reactor vessel & heat exchanger. Recall that this model did not include any cooling tubes in the heat exchanger. Adding these features means that the pressure drop through an actual heat exchanger will be even greater. Thus, increasing the elevation difference is vitally important.

Using values for velocity & temperature at the reactor inlet & outlet, the thermal power generated by the system was calculated to be about 42 MW_t. As previously stated herein, the design goal was to generate $10MW_e$, such that 33.3 MW_t is needed. Thus, using the power density achieved in an actual MSR, the MSNB reactor vessel may be oversized.

The velocity profile in the connecting pipes is shown in Figure 8–5. As before, the average velocity of 0.4415 [m/sec] was determined by using a weighted average, based on the annular cross-section of the pipe. The profile is not strictly parabolic, as it would be for fully laminar flow. In fact, the Reynolds number is 20,600. For a relative roughness of 0.02 (as previously indicated), this indicates turbulent flow.

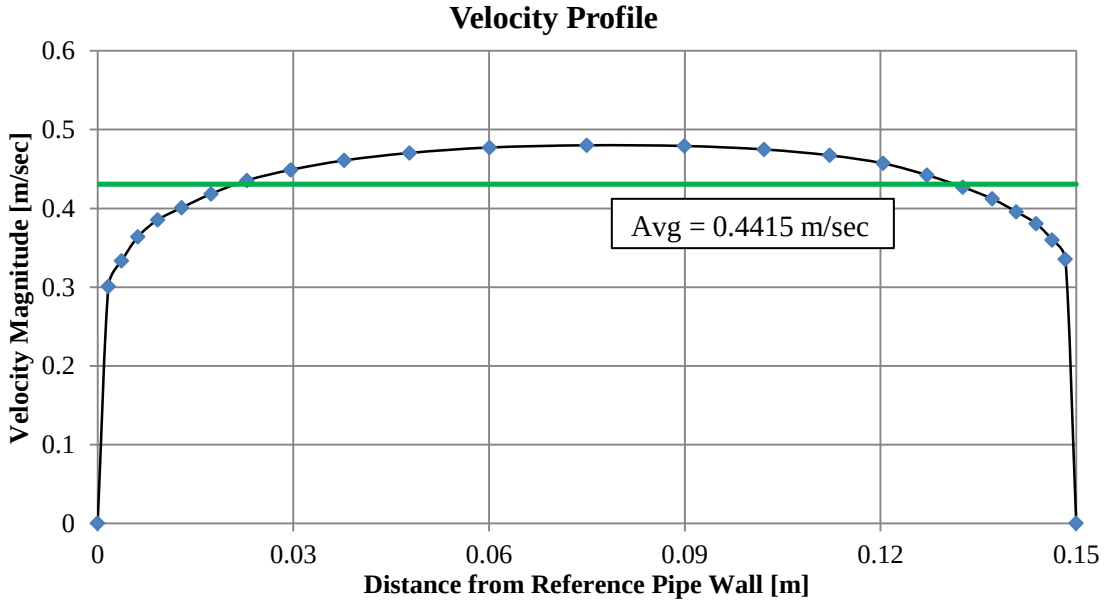

Figure 8–5 – Velocity Profile – Reactor Outlet Pipe

8.3 CFD-Specific Information

8.3.1 Mesh Evaluation – Resolving Boundary Layer

A plot of y+ values for the system components is shown in Figure 8–6. A total of 3,666 points exist for the reactor vessel wall. Of these, 3302 had y+ values ≤5 (90.07%). Thus, the mesh seems to be nominally able to capture boundary layer effects.

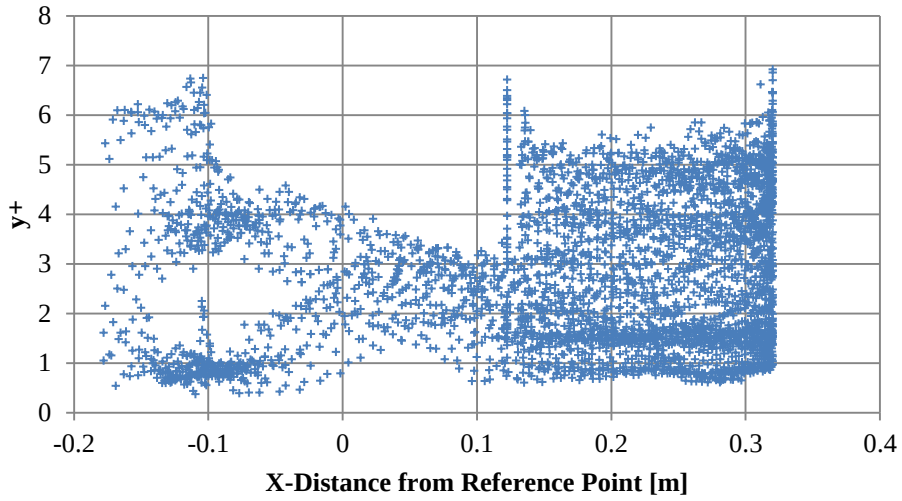

Figure 8–6 - y+ Values for Reactor Vessel Wall

8.3.2 Turbulence Model Evaluation

As before, results obtained using the k-ε turbulence model were compared with those using the k-ω SST model. The results, tabulated below, show no appreciable difference between the two. Thus, use of the k-ε model is valid. It is worthwhile to note that use of the k-ω model takes significantly more time per iteration. Further, it prolongs oscillations during the solution process; i.e., significantly more iteration is needed to achieve a steady state.

Parameter	k-ε Value	k-ω Value	% Difference
ΔT [K]	155.300	155.346	0.0295
v_{avg} [m/sec]	0.4415	0.4384	0.6906

8.3.3 V&V Analysis

As before, a basic verification analysis is presented to demonstrate the quality of results. There is only one case analyzed in this chapter, which will be evaluated using the Factor of Safety (FS) method.

8.3.3.1 Verification Basis Values

The same mesh refinement technique and refinement ratio was used as previous sections. The following table shows how this was satisfied, using the number of elements in each model as the basis. The table also includes the S_1, S_2 and S_3 CFD values for ΔT and v_{avg}.

Table 8-1 – Verification Basis Values

Mesh No.	**No. Elements**	**CFD Grid Designation**	**ΔT [K]**	**v_{avg} [m/sec]**
1 (Fine)	511,980	S_1	155.2972	0.4415
2 (Medium)	361,824	S_2	155.5522	0.4410
3 (Coarse)	255,942	S_3	156.5444	0.4360

8.3.3.2 Convergence Study

From the above data, one can obtain the FS method epsilon values (ε_{21} and ε_{32}) and solution ratio (R), as indicated in the following table.

Table 8-2 – Convergence Study Results – Case #7

Variable	**ΔT**	**v_{avg}**	**R (ΔT)**	**R(v_{avg})**
ε_{32}	0.25504	0.000512	0.25706	0.1018
ε_{21}	0.99216	0.005027		

Note that values for both ΔT and v_{avg} are $0 < R < 1$, indicating **monotonic convergence**.

8.3.3.3 Error Estimate

Next, the observed order of accuracy and error estimates are calculated, the results of which are given below. Recall that second-order accurate solution methods were used after numerous iterations, thus the theoretical accuracy (P_{th}) = 2.

Table 8-3 – Error Estimate

δ_{RE}	**ΔT [K]**	**v_{avg} [m/sec]**
	0.08824	0.00006

8.3.3.4 Uncertainty Estimate

Finally, the estimated (grid) uncertainty values are calculated, as shown below. Note that use of the FS method implies a 95% confidence factor.

Table 8-4 – Uncertainty Estimate

	ΔT [K]	**v_{avg} [m/sec]**
U_G	1.53	0.0023
$U_G(\%S_1)$	2.812	1.226

8.4 Conclusions for this Set of Simulations

- It seems that CFD software can be used to analyze realistic MSR designs, including the use of complex, temperature-dependent relations for actual fuel salts and variable power density.

- There are critical parameters that must be considered when designing an MSR driven by natural convection. The single most important one is the difference in relative elevation between the heat source and heat sink. Failure to do so will result in areas

of the reactor vessel that experience excessive thermal stress, and areas of the heat exchanger that clog up due to freezing (solidification) of the fuel salt.

9 Overall Conclusions & Suggestions for Future Study

The iterative solution methods employed by CFD make it an attractive option for analyzing power systems based on natural convection flow. The results of this research suggest that CFD can provide valuable engineering information to evaluate natural convection MSR designs. This is true even when designs include complex geometry and equations to simulate realistic reactor physics and behavior.

One unique aspect of simulations herein is the exclusive use of internal heat generation (specified as an energy source/power density) to model the reactor vessel, instead of an external surface heat flux. This closely resembles the type of MSR where the fuel is dissolved in the coolant/working fluid.

Another unique aspect for simulations with an actual fuel salt is the use of a newly-developed expression for a variable (temperature dependent) energy density, to reflect realistic MSR behavior. This makes the equations non-linear, and requires additional monitoring tools to evaluate solution convergence and determine steady-state conditions.

The results of Chapter 4 suggest that CFD can model natural convection flow to the extent necessary to support MSR design studies. The simulations therein used simple shapes and water as the working fluid. However, because the Boussinesq approximation was used, CFD results deviate from analytic values as the temperature difference increases. For this reason, use of the Boussinesq approximation is not recommended for evaluating realistic (practical) power plant designs.

In Chapter 5, a baffle was added to the simple cylinders to prevent flow-through. A real fuel salt was used as the working fluid, with a full set of physical parameter relations, rather than using the Boussinesq approximation. The variable energy source (density) relation was introduced. The CFD results closely match values from analytic methods.

Chapter 6 analyzes a newly built test rig. CFD results closely match values from analytic methods, and thus should provide a basis for comparison with experimental results, once they become available. However, the results show that the heat exchanger (cooler) has a very large pressure drop. Thus, one suggestion for future work is to increase the size of the cooler tubes. Note that the temperature difference is only 9° C, which is far less than that seen in a realistic (practical) power plant. Thus, another suggestion for future work is to increase the power rating of the heating element.

Chapter 7 shows that, in addition to complex fluid properties and variable energy density, CFD can also accommodate a complex MSR model, such as one which includes internal geometry in the reactor to represent moderator bars. Unfortunately, results therein are not directly comparable to those of Chapter 5, due to the increased diameter of the connecting pipe. Although the design goal for temperature range was achieved, it must be noted that adding cooling tubes in the heat exchanger will reduce flow somewhat.

Chapter 8 shows that CFD (when used with the previous techniques, fluid property relations and variable energy density) can evaluate other kinds of MSR designs. This includes the case when internal moderator bars are replaced with an external reflector. Note that the primary design variable is the relative difference in elevation between the reactor and heat exchanger. For the MSNB design analyzed therein, the elevation difference of 4 feet was insufficient to achieve the recommended temperature range. For future work, it is suggested that the relative elevation difference be increased and/or make the connecting pipe diameter. For a single design, several CFD cases could be developed, so as to optimize the relative height difference and pipe diameter, based on the motivation to minimize overall fuel salt volume.

This research used academic versions of software programs to obtain engineering solutions for natural convection MSRs and related experimental systems. While the results herein are not trivial, the software has limitations imposed on the number of faces, elements, and nodes that can be used in the model. Further, some features in the commercially available software

may be disabled. One option for future study is to use the full commercially available-software. This might enable/facilitate:

- Use of additional nodes, elements, etc., to better capture boundary layer effects.
- Use of well-rounded corners for reactor system components (vessels) and transitions from vessels to piping.
- Use of automated optimization routines, to minimize the required fuel salt volume, based on relative elevation difference between the vessels and the size of connecting pipes.

Once a specific system is identified as having met the design goals for temperature range, minimized fuel salt volume, etc., and its steady state parameters are known, use CFD to determine the transient behavior of the system. For example:

- What happens if the heat sink were suddenly removed? This would occur during a load rejection at the connected power generator, or when the heat extraction process was stopped.
- What happens if (for some reason) a slug of cold salt enters the reactor? Given the variable energy source relation, this would cause an increase in reactivity when compared to the steady state.

With this research as a starting point, hopefully many additional studies will be done, to help the development of MSRs as a source of much-needed energy around the world.

References

A. Technical Papers & Articles

Benes O, Konings RJM. 2012. Comprehensive Nuclear Materials, Volume 3 – Molten Salt Reactor Fuel and Coolant

Bettis, ES, Schroeder, RW, Cristy, GA, Savage, HW, Affel, RG, Hemphill, LF. 1957. The Aircraft Reactor Experiment – Design and Construction. Nucl. Sci. Eng. 2:804.

Cammi A, Luzzi L, Pini A. 2016. The Influence of Wall Thermal Inertia Over a Single-Phase Natural Convection Loop with Internally Heated Fluids, Chemical Engineering Science (submitted)

Cioncolini A, Iacovides H, Cooper D. 2014. Feasibility Study for Simple Molten Salt Reactor (unpublished)

Grimes WR, Blankenship FF, Keilholtz GW, Poppendiek HF, Robinson MT. 1958. Chemical Aspects of Molten Fluoride Reactors. Chapter 12 – Salt Fuels. Proceedings of 2nd UN International Conference on Peaceful Uses of Atomic Energy, 28:99-111

Ignatiev VV, Merzlyakov AV, Subbotin VG, Panov AV, Golovatov YV. 2006. Experimental Investigation of the Physical Properties of Salt Melts containing Sodium and Lithium Fluorides and Beryllium, Atomic Energy, 101(5):822-829

Kolmogorov AN. 1941. Local Structure of Turbulence in Incompressible Viscous Fluid for Very Large Reynolds Number

Kuron M. 2015. Three Criteria for Assessing CFD Convergence, The Engineer

Launder BE, Sharma BI. 1974. Application of the Energy Dissipation Model of Turbulence to the Calculation of Flow Near a Spinning Disc

Launder BE, Spaulding DB. 1973. The Numerical Computation of Turbulent Flows

LeBlanc D. 2010. Molten Salt Reactors: A New Beginning for an Old Idea, Nuclear Engineering and Design 240:1644-1656

Pratt & Whitney Aircraft Division. 1957. Circulating Fuel Core-Moderated Reactor (CMR), PWAC-186

Scarlat RO, Laufer RL, Blandford ED, Zweibaum N, Krumwiede DL, Cisneros AT, Anreades C, Forsberg CW, Greenspan E, Hu LW, Peterson PF. 2014. Design and Licensing Strategies for the Fluoride Salt-Cooled, High-Temperature Reactor (FHR) Technology, Progress in Nuclear Energy, 77:406-420

Serp J, Allibert M, Benes O, Delpech S, Feynberg O, Ghetta V, Heuer D, Holcomb D, Ignatiev V, Klooseterman JL, Luzzi L, Merle-Lucotte E, Uhlir J, Yoshioka R, Zhimin D. 2014. The MSR in Gen-IV: Overview & Perspectives, Progress in Nuclear Energy, 77:308-314

Toth LM, Del Cul G.D, Dai S, Metcalf DH. 1995. Molten Fluoride Fuel Salt Chemistry, American Institute of Physics Conference Proceedings, 346:617

Westfall C. 2004. Vision & Reality: The EBR-II Story. *Nuclear News*

Williams DF, del Cul GD, Toth LM. 2001. The Influence of Lewis Acid/Base Chemistry on the Removal of Gallium by Volatility from Weapons Grade Plutonium Dissolved in Molten Chlorides, Nuclear Technology, 136(3):367-370

B. National Laboratory Documents, Handbooks & Manuals

An Evaluation of the Molten Salt Breeder Reactor. 1972. WASH-1222

Cantor S, Cooke JW, Dworkin AS, Robbins GD, Thoma RE, Watson GM. 1968. Physical Properties of Molten Salt Reactor Fuel, Coolant and Flush Salts, ORNL-TM-2316

Catalog of Nuclear Reactor Concepts, ANL-7092 (1965)

DOE-HDBK-1019. 1993. Volume 1 of 2, Section NP-02

DOE-HDBK-1019. 1993. Volume 2 of 2, Sections EO-03 and NP-03

Gabbard CH. 1969. MSRE Thermal Convection Test – ORNL-MSR-69-25

Haubenreich PN. 1973. A Catalog of Dynamics Analyses for Circulating-Fuel Reactors, ORNL-MSR-73-7

Kasten PR, Bettis ES, Bauman HF, Carter WL. 1966. Summary of Molten Salt Breeder Reactor Design Studies, ORNL-TM-1467

Kerlin TW. 1967. ORNL Correspondence MSR-67-102

MacPherson HG. 1958. Molten Salt Reactor Program – Quarterly Progress Report, ORNL-2474

MacPherson HG. 1958. Molten Salt Reactor Program – Quarterly Progress Report, ORNL-2551

McMillan JH, Anthony CB, Guttmann K, Martin CP, Munier JL, Workey RD. 1953. A Reflector-Moderated, Circulating-Fuel Aircraft Reactor, ORNL CF-53-9-84

McWherter J. 1970. Molten Salt Breeder Experiment Design Basis, ORNL-TM-3177

Mills CB. 1952. The Fireball, A Reflector-Moderated Circulating-Fuel Reactor, ORNL Y-F10-104

National Physical Laboratory. 1981. Kaye & Laby Tables of Physical & Chemical Constants, Section 4.7.1

Reactor Physics Constants. 1963. Section 10. ANL-5800

Robertson RC. 1965. MSRE Design & Operations Report, Part I, Description of Reactor Design ORNL-TM-728

Robertson RC, Smith OL, Briggs RB, Bettis ES. 1968. Two-Fluid Molten-Salt Breeder Reactor Design Study, ORNL-4528

Robertson RC. 1971. Conceptual Design Study of a Single-Fluid Molten-Salt Breeder Reactor, ORNL-4541

Romie FE, Kinyon BW. 1958. A Molten Salt Natural Convection Reactor System, ORNL-CF-58-2-46

Rosenthal MW, Briggs RB, Kasten PR. 1969. Molten-Salt Reactor Program Semiannual Progress Report, ORNL-4396

Sohal MS, Ebner MA, Sabharwall P, Sharpe P. 2010. Engineering Database of Liquid Salt Thermo-physical and Thermo-chemical Properties, INL/EXT-10-18297

US Dept. of Energy. 2015. Quadrennial Technology Review, Chapter 4 – Technology Assessments

Williams DF. 2006. Assessment of Candidate Molten Salt Coolants for the NGNP/NHI Heat-Transfer Loop, ORNL/TM-2006/69

Wilson DW, McLain HA. 1972. Conceptual Thermal-Hydraulic Design of the MSBR Core. ORNL CF-72-11-8

Zasler J. 1958. Experimental 5 MW Thermal Convection Molten Salt Reactor, ORNL-CF-58-6-66

Zasler J. 1962. 576 MW_t Natural Convection Molten Salt Reactor Study, ORNL-TM-0269

C. Internet and On-Line Resources

Allen T. 2010. Molten Salt Database, http://allen.neep.wisc.edu/shell/index.php/salts, Nuclear Engineering and Engineering Physics Department, University of Wisconsin

chemistry.tutorvista.com

chem.libretexts.org, Chapter 21.7 – Nuclear Fission (2017)

http://phys.org/news/2011-05-nuclear-power-world-energy.html

http://www.livescience.com/39686-facts-about-thorium.html

http://www.world-nuclear.org/information-library/nuclear-fuel-cycle/introduction/physics-of-nuclear-energy.aspx

www.EngineeringToolBox.com/linear-expansion-coefficients-d_95.html

D. Textbooks

Cebici T, Smith AMO. 1974. Analysis of Turbulent Boundary Layers. First Edition. New York (NY): Academic Press

Hinze J. 1975. Turbulence. Second Edition. San Francisco (CA): McGraw-Hill

L'Annunziata MF. 1998. Handbook of Radioactivity Analysis. First Edition. San Diego (CA): Academic Press

Pletcher RH, Tannehill JC, Anderson DA. 2013. Computational Fluid Mechanics and Heat Transfer. Third Edition. Boca Raton (FL): CRC Press

Schlichting H . 1968. Boundary Layer Theory. Sixth Edition. New York (NY): McGraw-Hill

Wilcox D. 1998. Turbulence Modeling for CFD, First Edition. Glendale, (CA): Griffin Printing

E. Course Notes

T Xing. 2017. University of Idaho – ME550 - Computational Fluid Dynamics, esp. Lecture Notes for Session 17

F. Software Manuals & User Guides

Ignatiev VV, Feynberg O, Mezlyakov A. 2012. Progress in Development of MOSART Concept, ICAPP Proceedings, Paper 12394

G. Theses, Dissertations and Miscellaneous Documents

Francesco F. 2015. Development & Assessment of CFD Models for the study of Natural Circulation Dynamics [thesis]. [Milano (IT)]: Polytechnic University of Milan

Muharam Y. 2005. Detailed Kinetic Modeling of Oxidation & Combustion of Large Hydrocarbons [dissertation]. [Heidelberg (GER)]: Ruprecht Karls University

Qvist SA. 2013. Safety & Core Design of Large Liquid-Metal Cooled Fast Breeder Reactor [dissertation]. [Berkley (CA)]: University of California

Appendix A – Special Acknowledgements

Cardenas MA, University of Idaho; for the MSR design via private communication (June 2019)

Richards JD, University of Idaho; for details of the natural convection Test Rig (2019)